FENDER SYSTEM BEHAVIOR IN RANDOM SEAS

A Thesis

by

JAMES OFOEGBU

Submitted to the Office of Graduate Studies of
Texas A&M University
in partial fulfillment of the requirements for the degree of

MASTER OF SCIENCE

August 2008

Major Subject: Ocean Engineering

FENDER SYSTEM BEHAVIOR IN RANDOM SEAS

A Thesis

by

JAMES OFOEGBU

Submitted to the Office of Graduate Studies of
Texas A&M University
in partial fulfillment of the requirements for the degree of

MASTER OF SCIENCE

Approved by:

Chair of Committee,	John M. Niedzwecki
Committee Members,	Joseph H. Newton
	Billy Edge
Head of Department,	David V. Rosowsky

August 2008

Major Subject: Ocean Engineering

ABSTRACT

Fender System Behavior in Random Seas. (August 2008)

James Ofoegbu, B.Eng., Federal University of Technology Owerri, Imo State, Nigeria;

M.S., Texas A&M University

Chair of Advisory Committee: Dr. John M. Niedzwecki

Fendering systems are widely used in offshore installations for attenuating the effects of the impact energy of ships and barges in berthing or moored conditions. This study focuses on investigating current design practices and, developing a rational and functional approach to address random loading effects exerted on fendering systems. These loadings are often a consequence of combined wind, wave and current excitation as well as more controlled vessel motions.

Dimensional analysis is used to investigate the degree to which empirical design data can be collapsed and to provide an indication of the nonlinearity associated with the empirical data for fender sizing. In addition, model test data specifically measuring the normal fender force for a coupled mini-TLP/Tender Barge performed at the Offshore Technology Research Center (OTRC) model basin is used in this research investigation..

This data was characterized in terms of the typical statistical moments, which include the mean, standard deviation, skewness and kurtosis. The maxima and extreme values are extracted from the fender response data based upon a zero-crossing analysis and the results were studied in order to determine the underlying probability distribution function. Using selected parameter estimation techniques, coefficients of a best-fit two parameter model were determined. An illustrative example is presented and discussed that contrasts the deterministic and probabilistic models.

DEDICATION

This academic research study is dedicated to God for His mercy and to my family for their support and prayers

ACKNOWLEDGEMENTS

This research study was supported in part by the Texas Advanced Technology Program (C04-00174), the Texas Engineering Experiment Station (TEES) and the R.P. Gregory ’32 chair endowment. Each of these funding sources is gratefully acknowledged. Further, the data utilized in this thesis was made available as a result of a collaborative research program between the Offshore Technology Research Center (OTRC) and Statoil, Norway. The permission to utilize the data is gratefully acknowledged.

I also acknowledge my chair, Dr. John M. Niedzwecki for his immense contribution to this research work. Credit also goes to members of my advisory committee, Dr. Joseph H. Newton and Dr. Billy Edge for their commitment and effort in this research work and the classes I took under their tutelage. My appreciation also goes to Robert Dove, an engineer at Seaward/Trelleborg Marine Systems, for providing the fender catalogue and test performance data.

TABLE OF CONTENTS

Page

LIST OF FIGURES

Page

Page

Page

LIST OF TABLES

Page

NOMENCLATURE

C_b Block Coefficient

C_e Eccentricity Factor

C_m Virtual Mass Factor

C_s Softness Factor

C_c Berth Configuration Coefficient

D Fender diameter

ε Bandwidth

E_{ship} Energy Of Ship On Berthing

E_{fender} Energy Absorbed By Fender

f Frequency

K Radius Of Gyration Of The Ship

l Length Of Fender

m_i Spectral Moment Of The $i\,th$ Order

M Mass Or Displacement Of Ship

n Length Of Observation

R Distance Of The Point Of Contact From Center Of Mass

R_{fender} Fender Reaction Force

S_{XX} Spectrum

T_{crest} Mean Crest Period

$\overline{T}$ Mean Zero-crossing Period

V Approach Velocity Of The Ship Perpendicular To The Berth At The Moment Of Impact With The Fender

γ Angle Between Line Joining The Point Of Contact To The Center Of Mass And Velocity Vector

Δ Fender Compression In Meters

1. AN INTRODUCTION TO FENDER SYSTEMS

In the early years as marine transport slowly evolved, ports and terminals were built to receive small, lightly loaded vessels and ships with small drafts reflecting the shallow navigable channels through which they passed. Marine transport has grown to become an integral part of most nations' economy as it has also proved to be the most inexpensive way of moving heavy goods over very long distances. Today, navigation technology has vastly improved and has moved towards using bigger ships with deeper drafts. These ships include container cargo ships and LNG Tankers, whose displacements are in the order of thousands of dead weight tonnage (DWT). Naval architects have been successful in designing larger vessels that transport cargo at faster speeds across the ocean. Hence, ports and terminals need to be adequately designed for the berthing of these massive vessels without damage to the ship or the dock structure and often the ship channels must be dredged to accommodate these ships. On the other hand, very deep draft ships which are moored further from the terminal in deep water perhaps due to the near-shore shallow non-navigable channel are subject to sea waves resulting in increased concerns of ship motion response in the design of fendering systems.

1.1 Some Basic Fendering Systems

In moored conditions, fenders in combination with mooring lines (breast and spring lines) are utilized as station keeping systems to maintain minimum displacement from station for safe loading and unloading operations of products and cargo [1]. This is shown schematically in figure 1.1, where a large vessel is moored to a loading platform.

This thesis follows the style of Journal of Offshore Mechanics and Arctic Engineering.

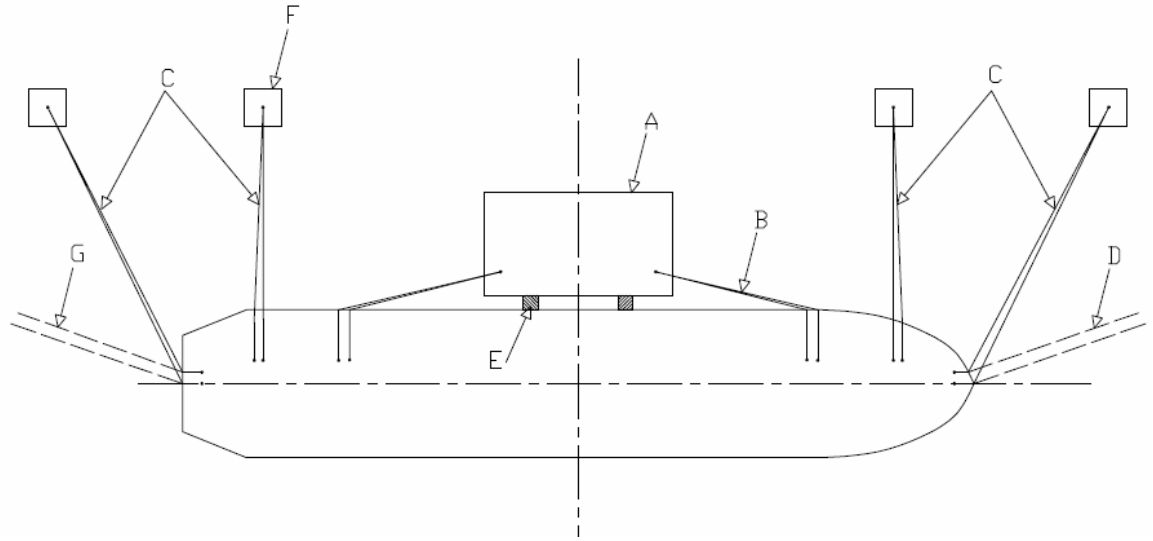

Fig.1.1 Layout of Dolphins, Fenders and Mooring Lines for Mooring Large Vessels by an Offshore Loading Platform. *A=Loading platform, B=Spring Lines, C=Breast Lines, D=Bow Lines, E=Fender Unit, F=Mooring Dolphin, G=Stern Lines [1].*

In both berthed and moored conditions, fenders have been utilized to reduce ship impact by absorbing the ship kinetic energy due to its motion. A wide variety of fender systems have been designed to undergo deflection/compression cycles and in turn produce a manageable reaction force. A fraction of this reaction force is imparted on the dock structure and the ship's hull and the remaining energy is dissipated in the fender. The overall design objectives are to achieve a reaction force that is less than an allowable lateral thrust on the dock platform and to produce a pressure less than the allowable hull pressure on ship hull contact area. The main parameters that influence the fender loads are associated with the configuration of the berthing facility (e.g., open or closed berth, depth of water at berth), the geometric characteristics and structural properties of the ship and fenders, the berthing procedures and conditions (e.g., speed of approach, mode of impact), and environmental forces (e.g., wind waves and current) [1].

Fender systems are also useful in the side by side mooring of an FPSO/Offloading Tanker or for various LNG/Terminal configurations. The resolution of the forces are often more complex and nonlinear due to the random nature of the wavefield than current design practice suggests.

Several applications of fender systems highlighted by notable authors have been selected and will now be briefly reviewed. Per Bruun [2] demonstrated that an adequately

designed tension mooring system combined with non-recoiling fenders could eliminate the need for breakwaters at offshore terminals. Breakwaters are constructed to protect harbors and shipping terminals primarily against wave conditions. Replacing breakwaters, which are expensive to construct and maintain, with tension mooring lines to limit excessive surge motion and non-recoiling fenders to absorb impact energy offers a viable design solution for some applications.

The need to address changing tidal levels at wharfs, ports and harbors has lead to the design and use of floating fenders. The significant variation of mean water level due to astronomical tidal changes at certain times during the year had rendered such harbors unsafe for berthing operations. The floating fender types can either be the full section cylindrical elastomeric fenders with chain connections at the ends hung from a quay side wall or vertically oriented hollow cylindrical fender sliding along an inner pile sleeve. Kirk [3] highlights the use of these vertically oriented fenders for passenger berths in the State of Alaska. This particular fender system is designed with a fender unit that floats up and down with the tide and the ship, allowing unattended line handling despite daily tidal height variations that exceed 8m (26ft). Further, the mooring lines from the ship can be secured to a metal cap at the top of each fender unit, allowing the ship to weathervane about the sleeved fender pile assembly.

Vessel impact on a fender-dolphin system results in both the compression of the fender locally and deflection of the piled dolphin globally, which is termed ‘flexible dolphin system’. A dolphin is a platform on pile clusters and could be designed to take the impact of the ship when docking and held against the broadside hull (*Breasting Dolphin*) or designed for mooring ships only (*Mooring Dolphins*). Louis [4] conducted a system-wide performance study on flexible steel dolphins concluding that the kinetic energy of the vessel is dissipated by a combination of compression in the fender units and bending in the dolphin piles. The equivalent stiffness of the structure includes the fender spring stiffness and the spring stiffness of the piles, which together are analyzed as a system of springs connected in series.

In a study conducted by Bradshaw, Baxter, Tsiatas, Marinucci, Ressler and Morgan [5], they compared the energy dissipation estimated using the kinetic energy method with the energy dissipation in a simple dynamic model of a fender pile impacted

by a berthing vessel. The kinetic energy method assumes that all the reaction force due to impact is applied to the vessel hull and pile. Using the dynamic model, they were able to show a reduction in the estimated forces in the pile by 25% due to 'system damping'. This demonstrated the over-conservatism in the kinetic energy method for practical designs.

The design criteria governing the selection of fender systems for different locations vary according to the factors considered by the design engineer. These factors include: the vessel's allowable hull pressure; allowable horizontal reaction force on dock/berth; fender maximum reaction force; stand-off distance between vessel and berth for loading/unloading operations; the design vessel; velocity of approach of vessel for both normal and abnormal conditions; vessel approach angle for both normal and abnormal conditions; the codes and standards to be used; fender spacing, design life of fender; friction coefficient during abrasion between fender and hull; safety factors to cover temperature effects, and tidal changes.

1.2 Fender Types and a Review of Current Design Practice

Fenders are classified according to their constituent material, form and energy absorbing mechanism. Elastomeric fender types are made of natural or synthetic rubber formed into various shapes that deflects when absorbing energy. Pneumatic fenders comprise a hollow rubber bag filled with air, which absorb energy when the enclosed air is compressed above normal air pressure. Foam-filled Fenders consist of a resilient closed cell block covered by a reinforced skin and undergoes compression during energy absorption. The buckling type fenders are manufactured in various geometric solid shapes with an attached frontal panel, which makes contact with the impacting hull. The solid shape component deflects elastically in order to absorb energy. The Figure 1.2 shows a pneumatic fender used at a ferry terminal at the Port of Houston, Figure 1.3 shows an elastomeric fender used at a large monopile berth, and Figure 1.4 shows the application of fenders on a Tension Leg Platform.

Fig 1.2 A Foam-filled Fender.

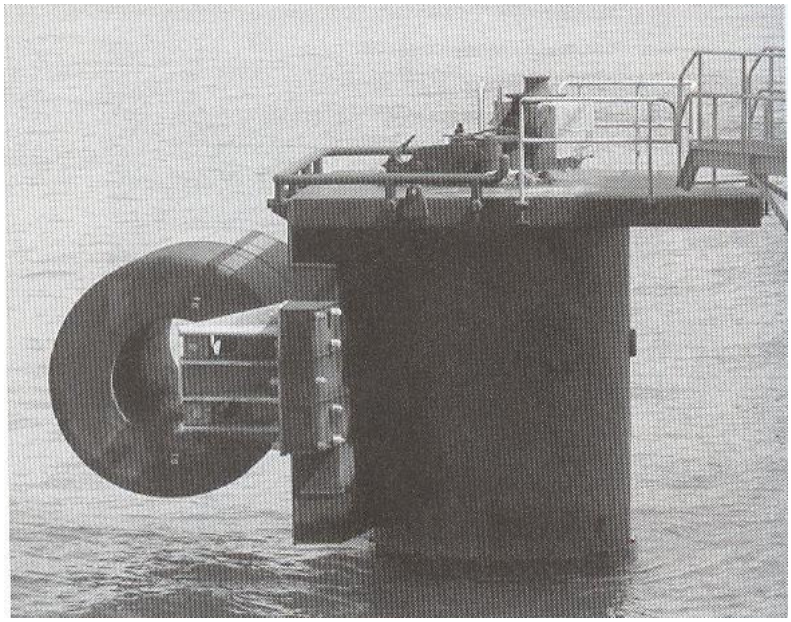

Fig 1.3 A Cylindrical Hollow Elastomeric Fender [6].

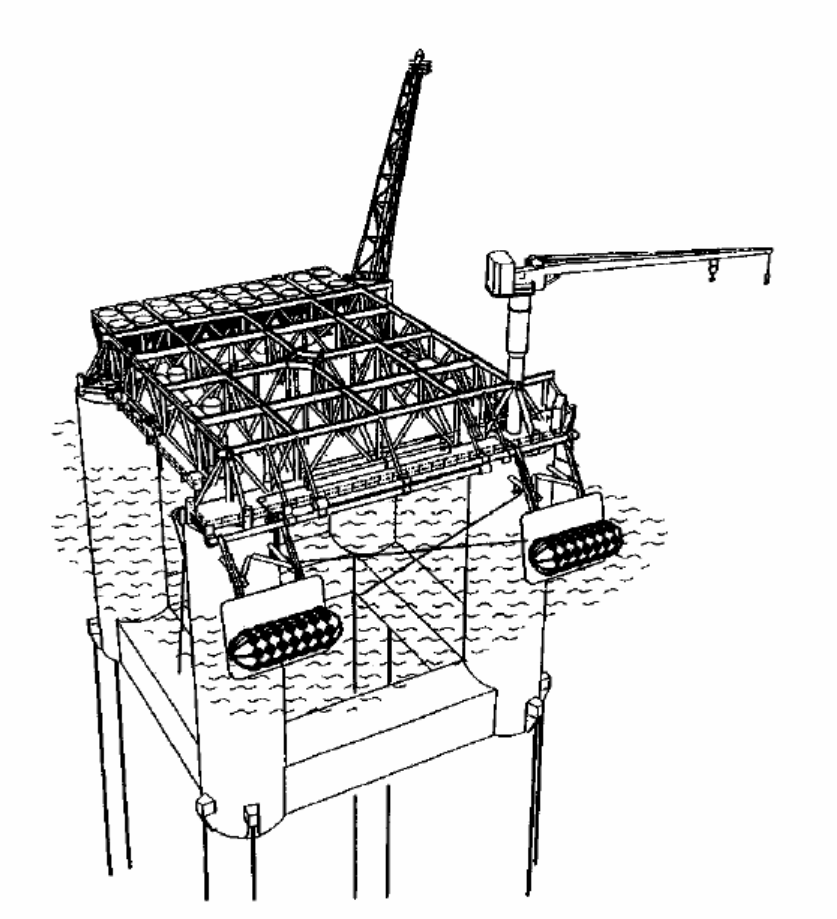

Fig 1.4 A TLP with Fender Units Attached [7].

The accurate determination of berthing energy is very critical to the design and selection of a fender system. Several methods are used in determining vessel berthing energy. These include, kinetic energy method, scale model tests, which are the basis for empirical methods and mathematical modeling methods [8]. The most common deterministic approach to fender design is the kinetic energy method, which seems to account for the major variables influencing vessel berthing. These variables are applied as correction factors to account for the size of vessel (displacement), design of the berth/dock and berthing conditions. Hence, the energy dissipated by the berthing vessel is obtained by multiplying the vessel's estimated total kinetic energy by these correction factors. These correction factors include: the eccentricity coefficient, which accounts for the rotation of the vessel during berthing; the virtual mass coefficient, which accounts for

a certain mass of water surrounding and moving with the vessel as it decelerates to stop; a berth configuration coefficient, which accounts for either an open-type or solid wall-type berth, where water being pushed by a berthing ship is displaced around the open-type berth or the water is compressed between the berthing ship and the solid wall berth causing a damping (energy loss) effect; the softness coefficient, this accounts for the fraction of energy loss due to the deflection of the vessel hull at the point of contact with the fender during berthing. This can be expressed in eqn. (1.1) [8].

$$E_{Ship} = \frac{1}{2} MV^2 \times C_e \times C_m \times C_s \times C_c \tag{1.1}$$

For soft fenders and small vessels, the softness factor C_s is generally taken as 1.0. For open type multi-piled quay or berth structures, the berth configuration coefficient C_c is conservatively taken as 1.0, while the virtual mass coefficient is obtained from eqn. (1.5). The eccentricity coefficient C_e is computed using eqn. (1.4) after block coefficient and ship's radius of gyration are deduced from eqn (1.2 and 1.3).

$$C_b = \frac{M}{hull\,length \times beam \times draft \times water\,density} \tag{1.2}$$

$$K = (0.19C_b + 0.11)L \tag{1.3}$$

$$C_e = \frac{K^2 + R^2 \cos^2 \gamma}{K^2 + R^2} \tag{1.4}$$

$$C_m = 1 + \frac{2D}{B} \tag{1.5}$$

As can be seen from eqn (1.1), the energy to be absorbed is a function of the square of the approach velocity. Hence, the determination of the velocity is one of the most important decisions in the design. The choice of the design velocity (velocity component normal to the dock) is based on ship displacement, site exposure and berthing procedure. Environmental aspects such as wind and current forces will influence. In practical situations, most vessels including the class of the ultra large crude carriers (ULCC) and very large crude carriers (VLCC) are brought into harbor with the assistance of tug boats. Figure 1.5 shows the approach velocity dependent on the ship displacement and navigation conditions.

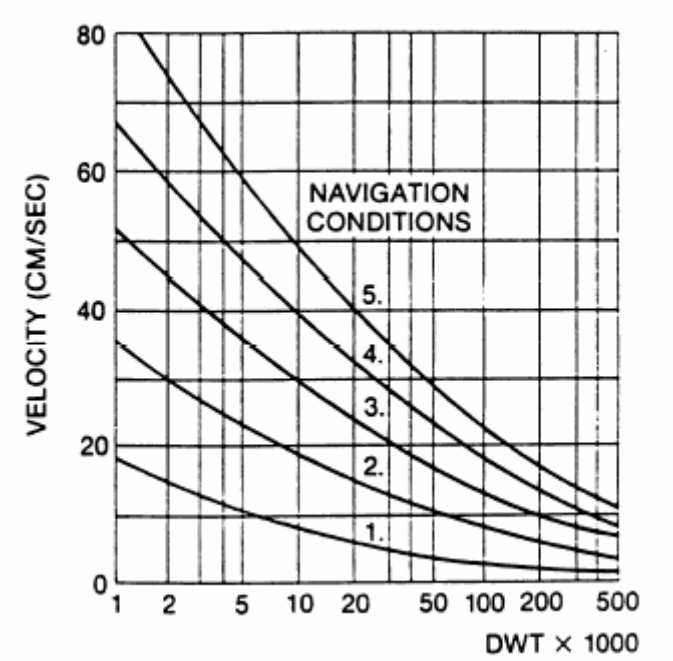

Fig 1.5 Design Berthing Velocity (mean value) as a Function of Navigation Conditions and Size of Vessel. *1=good berthing conditions, sheltered; 2=difficult berthing conditions, sheltered; 3=easy berthing conditions, exposed; 4=good berthing conditions, exposed; 5=difficult berthing conditions, exposed [9].*

The energy absorbed by the fender unit is obtained as the integral of its force-deflection function between zero and the deflection limit when the unit is compressed by the impacting vessel hull against the quay. This is given by eqn. (1.6).

$$E_{fender} = \int_0^{\Delta} R_{fender}(\Delta)\, d\Delta \tag{1.6}$$

Present fender design practice assumes that all berthing energy is absorbed by the fenders (E_{Ship}= E_{Fender}) especially when the berth/dock structure is considered fixed. Traditional fender selection procedure involves obtaining an allowable reaction force from the fore-mentioned computation and selecting an appropriate fender unit such that the fender deflection is within an acceptable range of rated percentage deflection of the fender size. Manufacturers of fenders provide technical catalogues showing performance curves for fender units. These curves are obtained as a result of rigorous testing program and indicate absorbed energy, reaction force and deflection limits in percentage of fender size (Diameter).

The reaction force to energy absorbed ratio (R/E_{fender}) describes an intrinsic property of the fender unit which makes it suitable and efficient for surface protection of vessel hulls [1]. A low reaction force to energy absorbed ratio implies the fender unit can absorb high impact energy within its elastic limits and dissipate low reaction force on the hull and berth surface. The allowable reaction force is also chosen in order to obtain contact pressure on the vessel hull within acceptable limits and mitigate damage to the dock structure. That is,

$$\frac{fender\ reaction\ force}{compressed\ fender\ contact\ area} < allowable\ hull\ pressure$$

The Table 1.1 can be used as a rough guide for selecting allowable vessel hull pressure. However, modern vessels are designed with higher strength steel plates with thinner thickness and wider spaced transverse stiffeners for their hulls. Consequently, this has reduced the allowable hull pressure of these massive vessels and made berthing design more complicated when planning and designing ports and docks.

Table1.1 Allowable Pressure on Vessel Hull Due to Fender Reaction Force [6].

Type of vessel	**Allowable Hull Pressure (KN/m^2)**
ULCC & VLCC	150 - 250
Tankers	250 - 350
Product & Chemical Tankers	300 - 400
Bulk Carriers	150 - 250
Post-Panamax Container Ships	200 - 300
Panamax Container Ships	300 - 400
Sub-Panamax Container Ships	400 - 500
General Cargo (un-belted)	300 - 600
Gas Carriers	100 - 200

1.3 Research Objective and Methodology

The design of fender systems has been basically a deterministic design process. In this research study, the implications of considering the excitation and response to be random processes will be investigated. This will require the introduction of probabilistic and statistical methods into the design process.

The first objective is to investigate current design practice for fender systems, identify key variables and develop dimensionless groups through dimensional analysis. Using these groups, dimensionless design curves for fender systems can be developed from the data presented by a manufacturer of fender components. This will be analyzed in an attempt to better understand the data available to designers.

Next, data from a model study of a coupled mini-TLP and a moored tender barge held against a fender system by breast lines will be investigated. The response of the fender system is a random time series output obtained from the experiments for selected load conditions. The objective is to statistically characterize the fender reaction data in order to understand its properties. Also, the relationship between the excitation or forcing sequence and the fender response mechanism is investigated.

Maxima and extreme values extracted from the fender response data, using the zero-crossing analysis, will be studied to determine the underlying probability distribution function describing it. Using selected parameter estimation techniques, coefficients of a best-fit function will be produced for use by the designer to select fender systems meeting specific probability of exceedence criteria.

2. DETERMINISTIC ANALYSIS OF FENDER SYSTEMS

The force-deflection performance curves for various fender system components are provided by the manufacturers for the design engineer. The information provided is either in a tabular or graphical form and is typically based upon empirical studies, which are performed to relate the applied force to the fender element deflection and absorbed energy. A rated maximum percentage deflection of the fender size (i.e. diameter or height) is often assigned to these units to guide designers. Typically, this limit is in the range of 55% - 65%.

In this section, an effort is made to recast the design information typically provided by the manufacturer into a more compact form using dimensional analysis. Besides compacting the information, it allows one to investigate the consistency of the data provided, obtain a sense of the variability of the data and degree of non-linearity of the various fender elements used in developing a fender system. More specifically, attention is focused upon the degree of consistency and non-linearity of the design data provided for relating the reaction force, deflection and energy absorption for various sizes of the fender element selected.

2.1 Identification of Key Variables

In order to visualize the mini-TLP and tender barge configuration of interest, a series of sketches are presented in Figures 2.1 and 2.2. They illustrate the head and sea conditions that were tested in the OTRC model basin and idealization of the coupling and fender force measurement systems. Note the fore and aft breast lines were added for the coupled system design. Since each body had its own mooring system, it was also possible to release the breast lines and measure the loads on the fender system for uncoupled bodies in close proximity.

The sketches presented in Figure 2.2 identify some of the key geometrical variables that should be considered for this two-body system. The information presented in Table 2.1 contains a compendium of geometric, fluid and dynamic variables that capture the essence of the fender design problem. Of course, depending on the particular application, this list may vary.

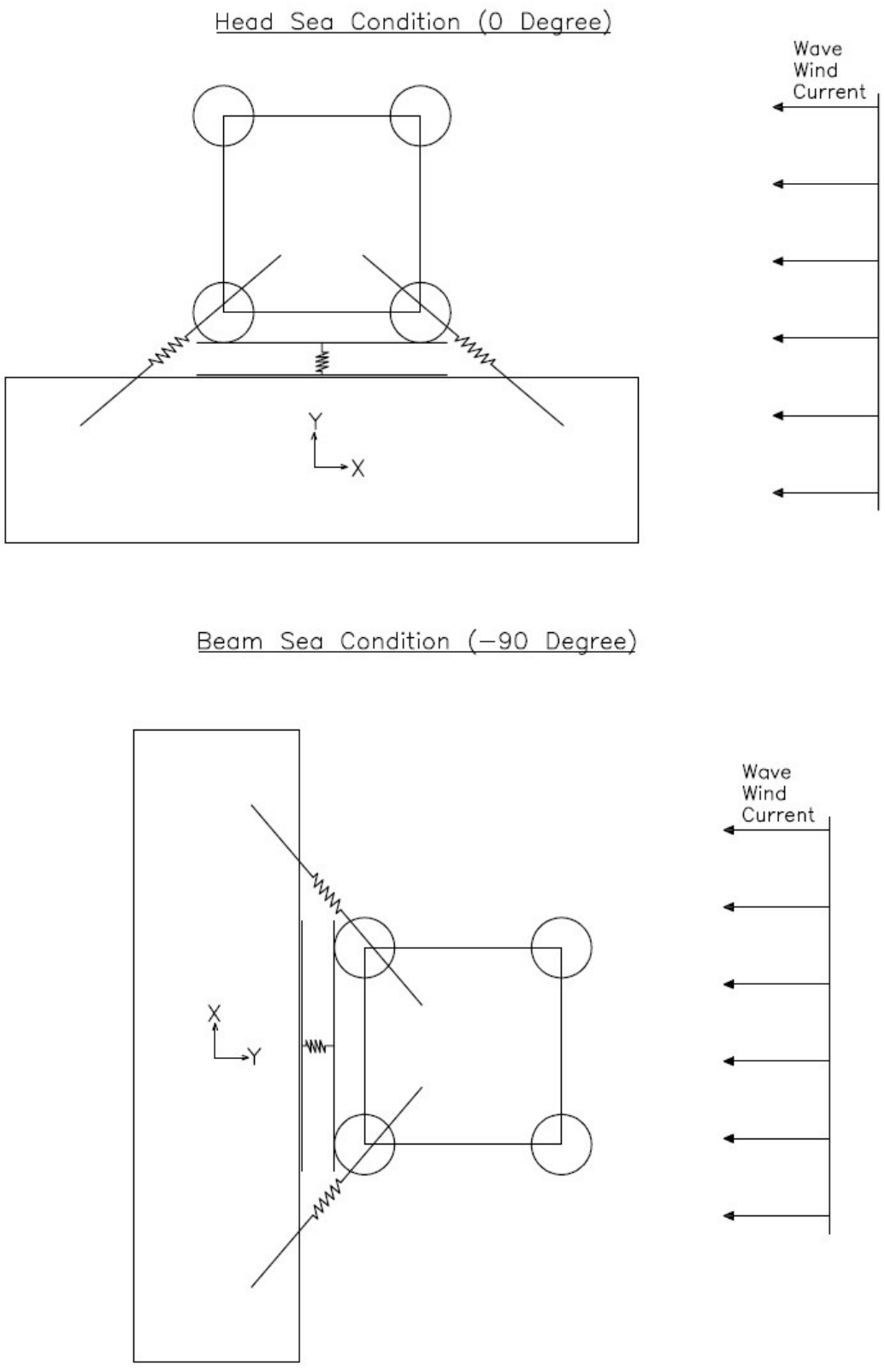

Fig 2.1 Definition Sketch of Mini-TLP/Tender Barge System and Loading Sequence.

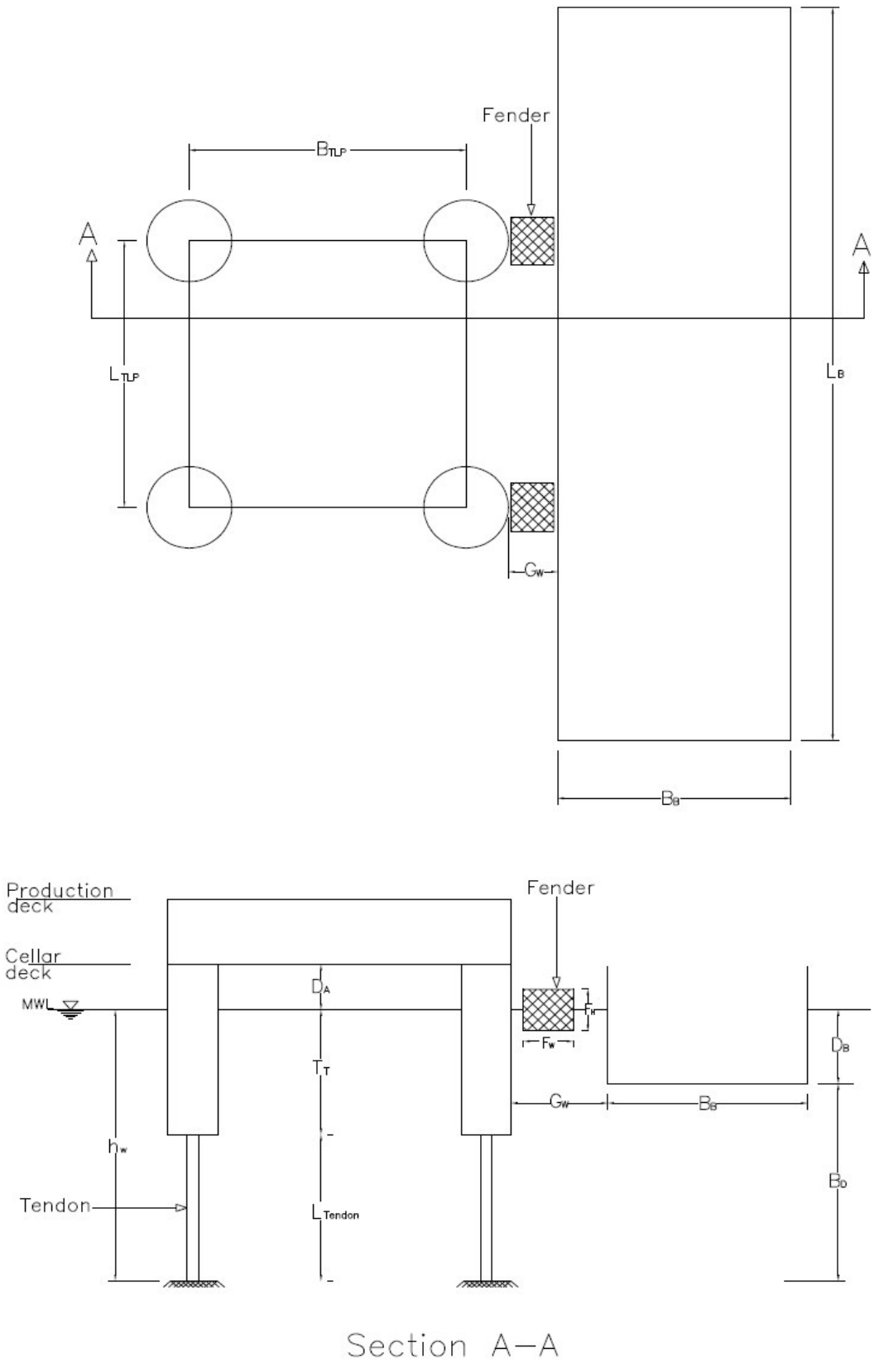

Fig 2.2 Sketch Showing Geometric Variables for Dimensional Analysis.

Table 2.1 Key Variables, Symbols, Definition and Fundamental MLT Units.

No.	Symbol	Description	MLT
1	L_{TLP}	Length of TLP	L
2	T_T	Draft of TLP	L
3	D_A	Airgap of TLP	L
4	L_{Tendon}	Length of Tendon	L
5	L_B	Length of Barge	L
6	B_B	Beam of Barge	L
7	D_B	Draft of Barge	L
8	B_D	Barge Bottom Clearance	L
9	Δ	Fender Compression	L
10	G_W	Separation Distance	L
11	h_w	Water Depth	L
12	H	Wave Height	L
13	T_p	Wave Period	T
14	V	Approach Velocity	LT^{-1}
15	ρ	Density	ML^{-3}
16	g	Gravitational Acceleration	LT^{-2}
17	M_{TLP}	Displacement of TLP	M
18	M_B	Displacement of Barge	M
19	M_O	Momentum	MLT^{-1}
20	E	Energy Absorbed	ML^2T^{-2}
21	F	Fender Reaction Force	MLT^{-2}

2.2 Development of Dimensionless Groups

In order to develop the dimensionless parameters for the variable list presented in table 2.1 one can utilize a variant of the Buckingham Pi Theorem [10]. For this analysis, the repeating variables are selected to be;

ρ – Density – Mass scale = ML^{-3}

Δ – Fender compression – Length scale = L

g – gravitational acceleration – Time scale = LT^{-2}

The total number of variable is 21 and the number of repeating variable is 3 leading to the expectation of 18 dimensionless variables of interest gives pi variables. This can be expressed as seen in equation 2.1 and 2.2

$$f\left(\Pi_1,\Pi_2,\Pi_3,\Pi_4,...\Pi_{15}\right)=0 \tag{2.1}$$

$$f\left(\frac{F}{\rho g \Delta^3},\frac{E}{\rho g \Delta^4},\frac{M_B}{\rho \Delta^3},\frac{M_{TLP}}{\rho \Delta^3},\frac{M_O\sqrt{\Delta}}{\rho \Delta^{3\frac{1}{2}}\sqrt{g\Delta}},\frac{L_B}{\Delta},\frac{B_B}{\Delta},\frac{L_{TLP}}{\Delta},\frac{D_A}{\Delta},...,\frac{G_W}{\Delta}\right)=0 \tag{2.2}$$

Of course, there are many variations that can be considered. In this study, given the manufacturer's design curves are available, this analysis was used to guide the interpretation of that data to a dimensionless form.

2.3 Interpretation of Design Performance Curves

The flowchart presented in Figure 2.3 was developed in order to capture the basic issues and procedure a design must consider. One can see that a variety of procedures leading to a compacted deterministic approach require a series of simplifying assumptions. It is interesting that apparently even the most basic concepts of maxima or combined effects of wind, waves and currents are left to the designer to address when interpreting the data on force, absorbed energy and fender deflection.

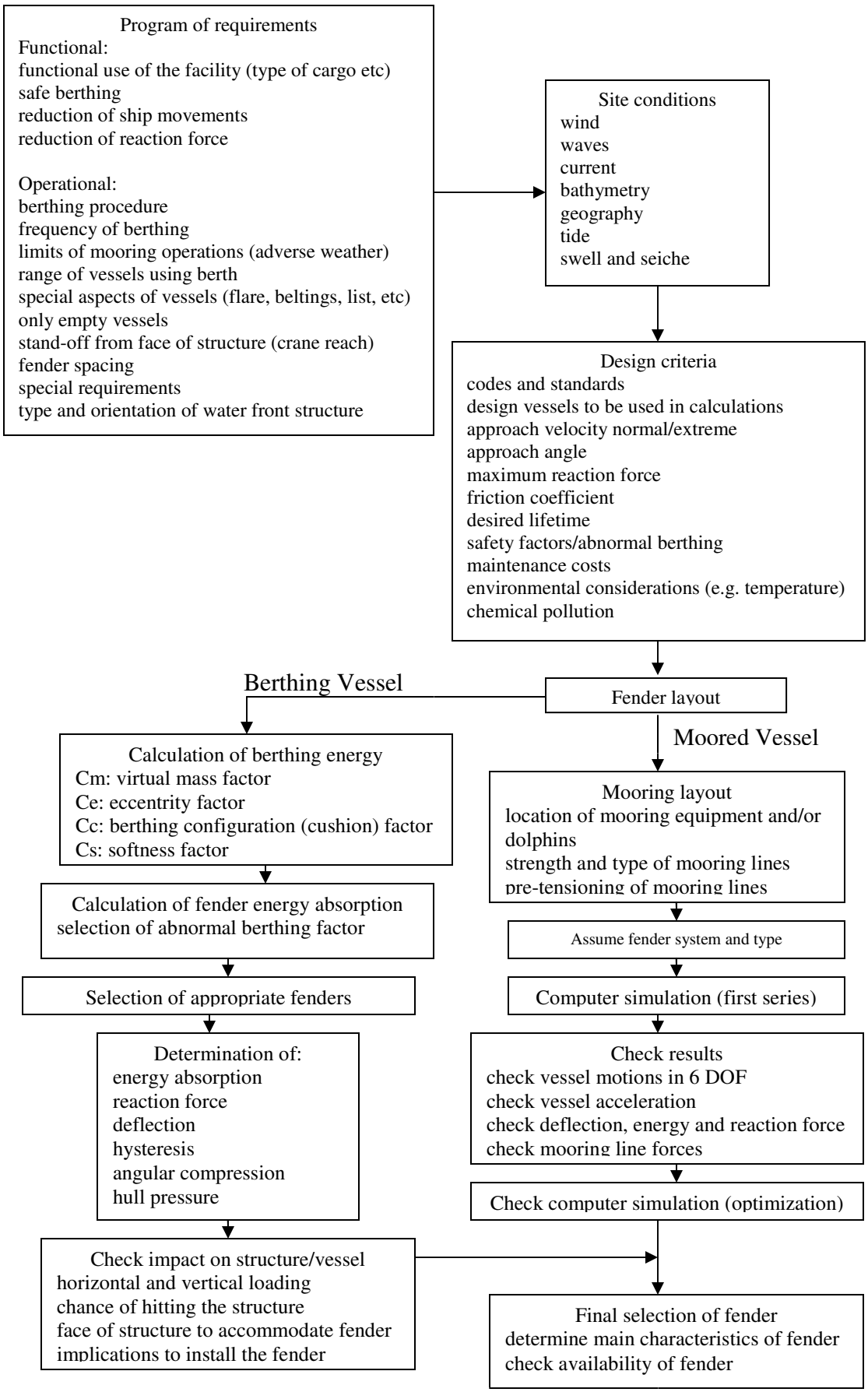

Fig. 2.3 Flowchart of Design Steps [2].

In this study, a specific fender type has been selected for analysis. This dimensional performance curves for a 3m (10ft) diameter elastomeric fender are shown in Figure 2.4 as plots of energy absorbed against percentage deflection and reaction force transferred against percentage deflection for different lengths. The performance curves, which are a product of static load laboratory tests, are also available for foam-filled fenders, Super-cone buckling fenders and Unit element V-shaped buckling fenders.

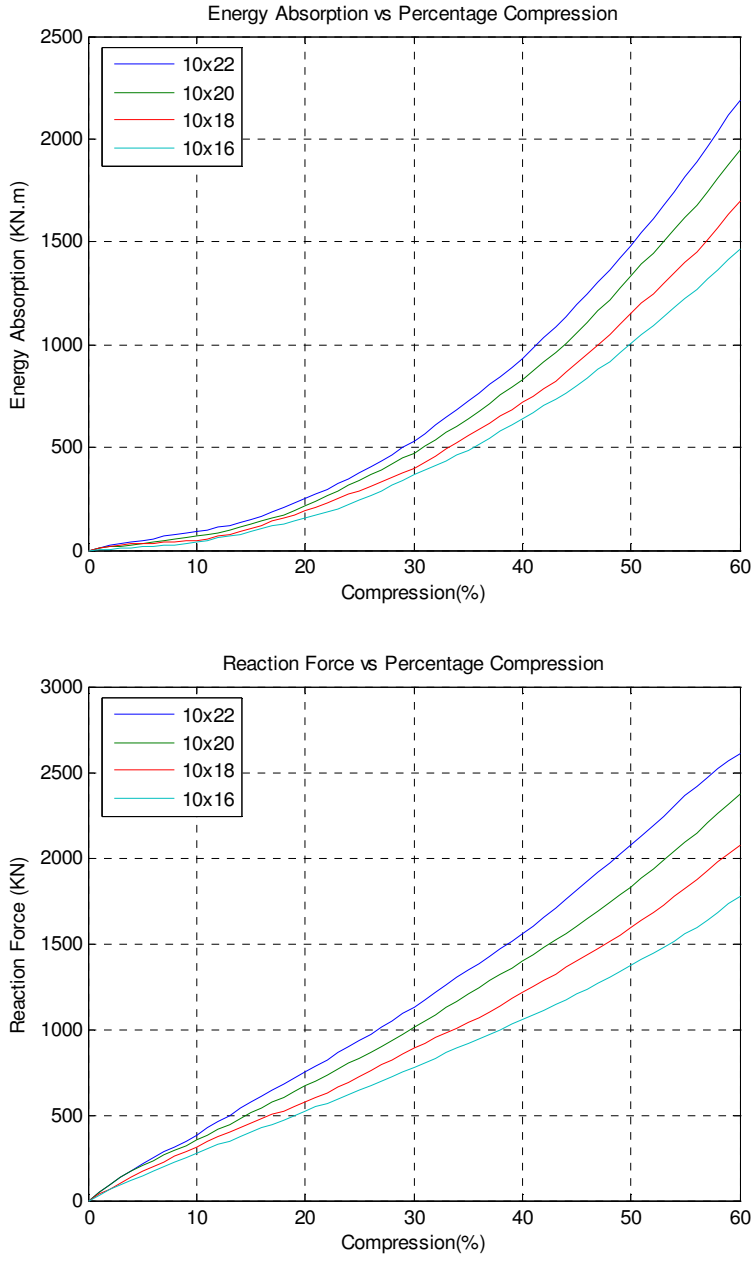

Fig. 2.4 Performance Curve for 3.048m (10ft) Diameter Elastomeric Fender [6].

A closer study of these curves showed that for the elastomeric fenders, the curves of energy absorbed showed a bit of non-linear behaviour with increasing deflection compared to the reaction force curve, which was fairly linear with increasing deflection. However, the reverse is the case for the super cone buckling fender and unit element buckling fender, where the reaction force curves exhibit high nonlinearity even within the prescribed 60% deflection range of the fender unit size. This observed linear and nonlinear behavior for the two related variables of the fender (absorbed energy and reaction) over similar deflection ranges is seen as an important property that affects its response, especially when exposed to the impact of random load excitations.

Furthermore, non-linearity was also studied by examining the ratio of reaction forces $\left(\frac{F_2}{F_8}, \frac{F_4}{F_8}, \frac{F_8}{F_8}, \frac{F_{10}}{F_8}\right)$ against percentage deflection and ratio of absorbed energy $\left(\frac{E_2}{E_8}, \frac{E_4}{E_8}, \frac{E_6}{E_8}, \frac{E_8}{E_8}, \frac{E_{10}}{E_8}\right)$ against percentage deflection shown in figure 2.5. The ratios of these variables are given for selected fender diameters against the 2.44m (8ft) diameter fender. Note that the fender force subscripts were chosen to correspond to the sample of elastomeric data which was presented in imperial not SI units. The plot of ratio of reaction forces shows the uniform linearity of fender reactions across all percentage deflections. This suggests that for selected sizes of elastomeric fender systems, there is little variability in the linear behavior for fender reaction across a range of percentage deflection values. However, this is not exactly the same for the ratio of fender absorbed energy. Although there is little variability for the smaller diameter fenders, the ratio of the 3.048m (10ft) diameter fenders drops sharply between 0% – 15% deflections and remains linear for greater deflections.

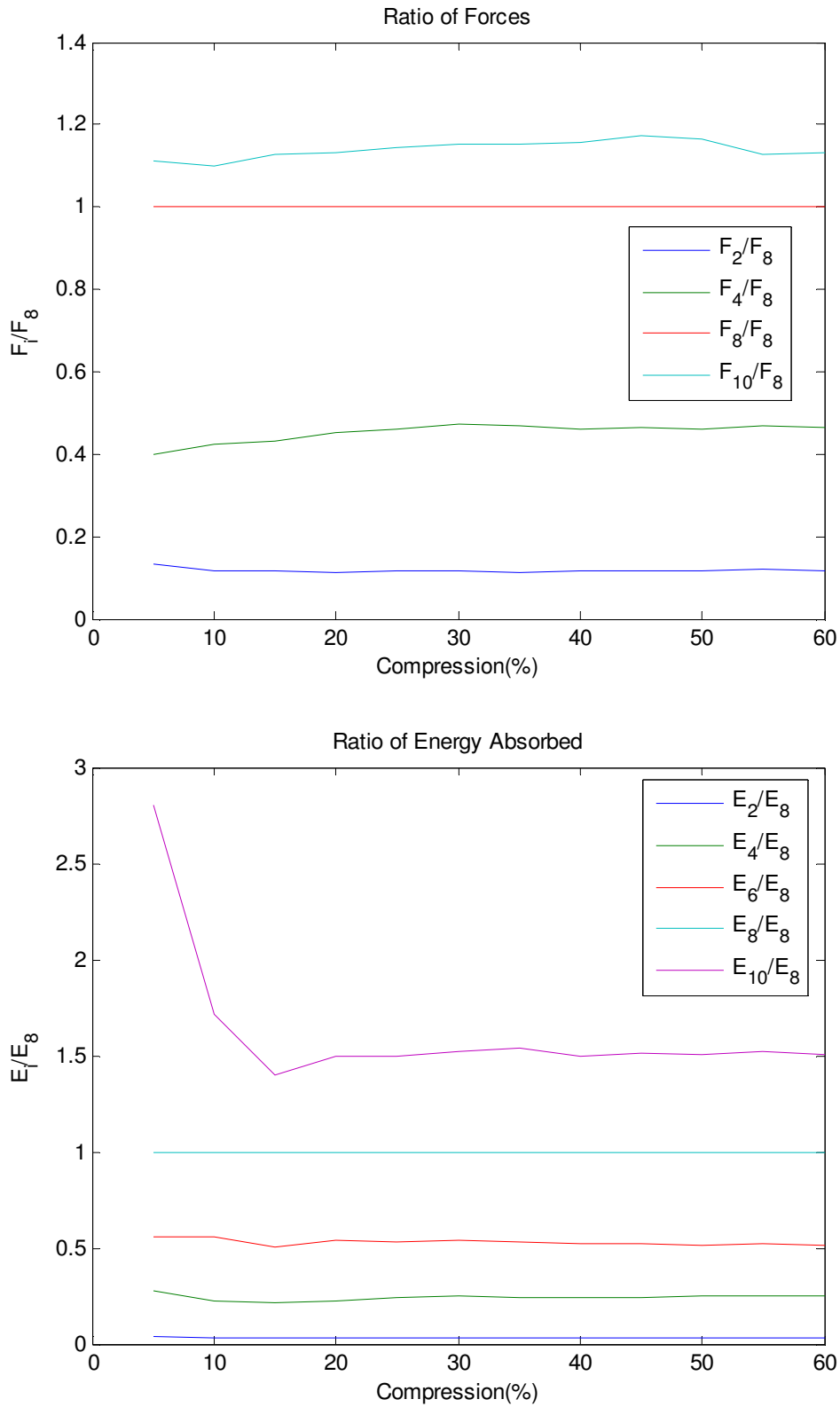

Fig. 2.5 Test of Linearity on Performance Data.

2.4 Recasting of Design Curves

The dimensionless expressions obtained from dimensional analysis in Section 2.3 are used in recasting the performance curves. It is then presented in a compact format for the designer's use. Equation 2.3 shows the transformation equations used for recasting the design curve. The diameter of the fender is represented by D. Note that while normalized absorbed energy, normalized reaction force and normalized deflection terms relevant to our study have been selected from the terms in equation 2.2, the effect of other terms considered are held constant. This is because our simplification does not take their variability into account.

$$f\left(\frac{F}{\rho g D^3}, \frac{E}{\rho g D^4}, \frac{\Delta}{D}\right) = 0 \tag{2.3}$$

On these recasted plots shown in Figure 2.6, the arguments of equation 2.3 are plotted such that the normalized absorbed energy and normalized reaction force are plotted on the vertical axis while the normalized deflection is plotted on the horizontal axis. For each diameter a family of curves is shown for different fender lengths using equation 2.4, where D_{max} and l_{max} are the maximum diameter and maximum length.

$$\frac{D \times l}{D_{\max} \times l_{\max}} \tag{2.4}$$

The recasted curve for the 3m (10ft) diameter elastomeric fender is shown in figure 2.6 while the recasted curves for the 1.8m (6ft) and 2.4m (8ft) diameter elastomeric fender is shown in Appendix A3.

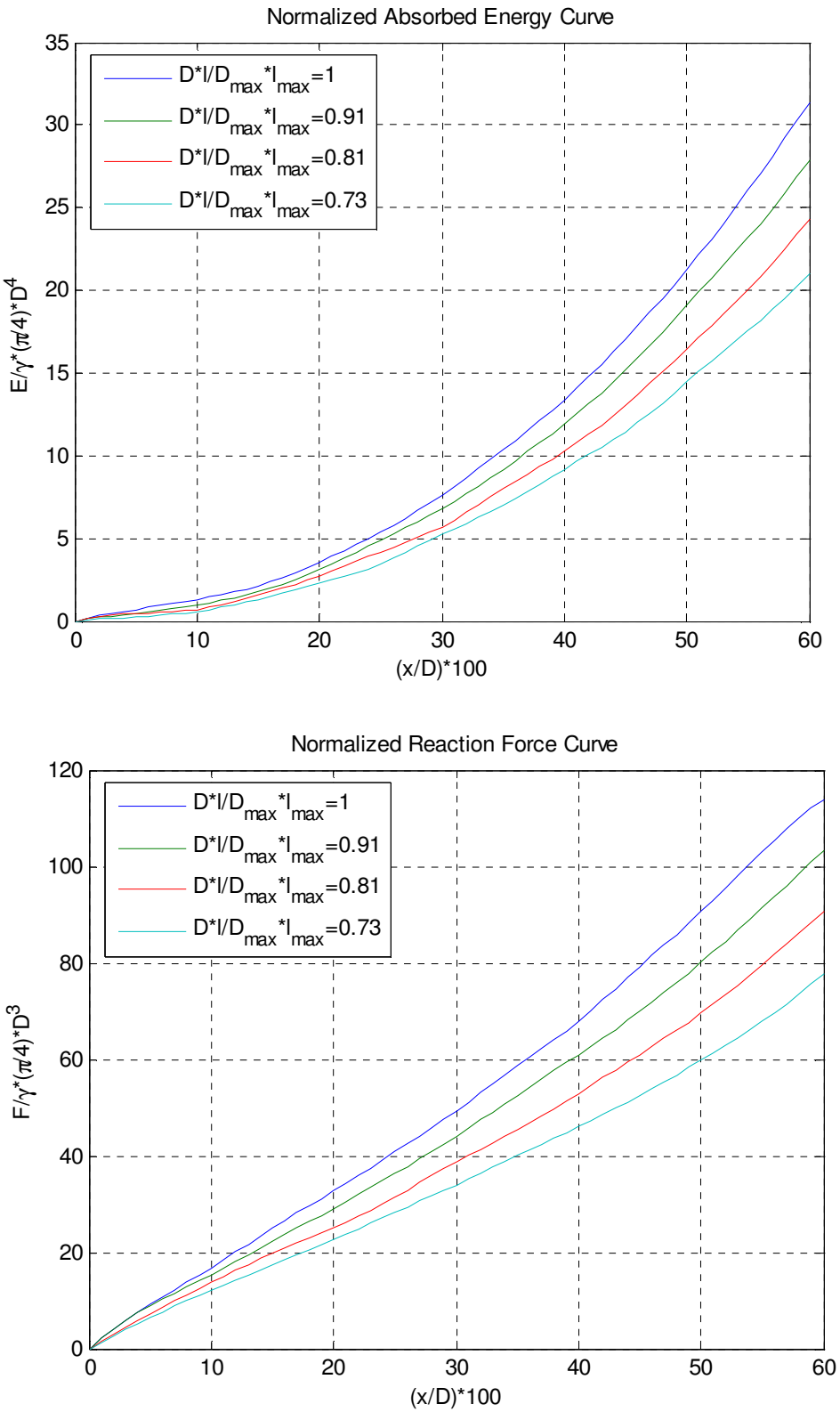

Fig 2.6 Normalized Performance Curve for 3.048m (10ft) Diameter Elastomeric Fender.

A verification of the result obtained using the above curves was carried out by solving backwards to see how close we are to obtaining the original values. Details of this exercise are presented in Section 2.5, where a selected case has been shown in detail. A summary of the result obtained for other cases are tabulated in Table 2.2, which shows the percentage deviations at a glance. The manufacturer (Seaward/Trelleborg), who supplied the test data, maintained an accuracy range of ±15% during the test program from which the performance curves were developed.

Our investigation yielded results within this prescribed range for the 0.914m (3ft) DIA, 1.83m (6ft) DIA and 2.44m (8ft) DIA fenders while some wide divergence from the ±15% were observed especially for the 0.61m (2ft) DIA and certain parts of the 3.048m (10ft) DIA fenders. The wide variation observed could be attributable in part to the variables selected when performing the dimensional analysis. The local fender geometric variables considered for normalizing the absorbed energy and reaction forces do not seem to be sufficient to capture the entire process. Considering the 'hysteresis' effect in rubber, if variables defining the material property were also considered in normalizing the functions, then the percentage inaccuracy would have been further reduced. Hence, in the effort to collapse the design performance curves, we observed a fair degree of variability, which would suggest that more variables might be needed to better characterize the empirical data for design.

This conclusion would be consistent with the limited dimensional analysis that was performed. An addition source of error was introduced in reading the original design curves and converting them to dimensionless plots. Every attempt was made to minimize this source of error but nevertheless it could not be eliminated as the original data was not available for use in this study.

2.5 Example

Select 2x10 fender size, and substitute the values of its length and diameter into Equation 2.4.

$$\frac{2\times10}{2\times10}=1.0$$

Assuming impact energy of 44.2KN.m acts on the selected fender unit, this will result in a deflection of 60% of Diameter and fender force of 273.4KN when traced on the absorbed energy/deflection curve of the 2x10 curve.

The same absorbed energy value is input in the normalized Equation 2.5 from the 3.048m (10ft) DIA Seaguard Plots of Figure 2.6.

$$\frac{E}{\gamma\left(\pi/4\right)D^4}=\frac{44.2\times1000}{1030\times\left(\pi/4\right)\times\left(10\times12\times0.0254\right)^4}=0.633 \qquad (2.5)$$

Reading off the result obtained from the curve of $\frac{D\times L}{D_{\max}\times L_{\max}}=1.0$ in Figure 2.6, a deflection of 4.33% of fender diameter is obtained. Extending a line from this point of deflection value to the reaction curve of the 3.048m (10ft) DIA fender and reading off on the vertical axis indicates a dimensionless value of 8.16, which when equated to its parent Equation 2.6, the fender force can be calculated.

$$\frac{F}{\gamma\left(\pi/4\right)D^3}=\frac{F}{1030\times\left(\pi/4\right)\times\left(10\times12\times0.0254\right)^3}=8.162 \qquad (2.6)$$

$$F=186.96KN\neq273.4KN$$

Hence the Percentage difference = -31.6%. Table 2.2 shows the percentage difference of the above analysis for several combinations of fender diameters (in feet), i.e. a combination of the fender diameters on the top row against fender diameters in the first column.

Table 2.2 Percentage Deviations for Verification of Results from the Recast Dimensionless Plots.

	2x10	3x10	4x10	6x10	8x10	10x10
2x10	0	-5.02	-19.43	-11.9	-22	+49.6
3x10	+5	0	-15.47	+2.1	-10.5	+56.83
4x10	+19.16	+7.2	0	+7.48	+2.39	+11.58
6x10	+10.85	-1.53	-8.48	0	-5.32	+3.18
8x10	+16.5	+4.74	-4.32	-0.55	0	+8.98
10x10	-31	-7.01	-12.06	-8.86	-8.37	0

3. ANALYSIS OF EXPERIMENTAL DATA

Due to stochastic nature of environmental loadings on offshore structures, fender systems for such offshore applications also respond randomly while converting impact energy to reaction forces. Using an experimental model, we shall investigate their response to different load cases (wind, wave and current) and headings for a coupled mini-TLP/Tender Barge.

3.1The Mini-TLP/Tender Barge Experiment

The mini-TLP/Tender Barge experiment was conducted at the Offshore Technology Research Center (OTRC) model basin by Dr. Tiegen (MARIN) and Dr. Niedzwecki (Texas A&M University). Table 3.1 shows the environmental design characteristics.

Table 3.1 Design Environmental Characteristic for Target Location.

Parameter	Value
Significant Wave Height (H_s)	4.0m
Peak Period (T_p)	16.0sec
Peakedness Factor (γ)	2.0
Current Velocity (V_c)	0.95m/s
Wind Velocity at Z_0=10m	25.65m/s
Wind Velocity at Platform reference height Z_r=17.2m	27.41m/s
Water depth	1000m

The model mini-TLP/Tender Barge was built to a scale ratio of 1:62 and tested for typical West Africa environmental conditions. The design seas were modeled using a single peaked JONSWAP wave spectrum model with a significant wave height of 4 meters, a peak period of 16 seconds and a peak enhancement factor of 2. The design wind speed at deck elevation was 27.4 m/s and the near surface current velocity was 0.95 m/s. Instrumentation for the experiments included four wave probes for measuring wave elevations, wind meter for measuring wind speed, current meter for measuring orthogonal components of current velocity. Also, load cells were used to account for the weight

effect of the topside on mini-TLP and supplies on Tender Barge, lasers and tracking camera devices for measuring motions of the bodies, springs and shear cells to measure tensions in risers, mooring lines and fender. During the experiment, the fender system connecting the two bodies was adapted to a single bar protruding from the mini-TLP with compression springs at the end and measurements taken using attached shear cell equipment. The model breast lines were calibrated to a spring constant of 33.97N/m and the fender system calibrated to a spring constant of 25.92N/m. Also, a 10m (161.3mm model scale) stand-off distance for the prototype between the two bodies was maintained during the experiment. Two heading conditions of 0^o and -90^o for environmental loads of wind, wave, current and their combinations were set up during the testing. Output time series of fender reaction was obtained from the experiment at a sampling rate of 0.252sec for a typical 3hr duration, which yielded a realization of 42,105 data points for each load condition and heading.

In practice, this two body connection moored side by side is favored due to the limited storage space on the mini-TLP, so the barge is used to store produce, supplies and provide accommodation for the crew while the mini-TLP performs either drilling or production-type activities. The choice of the site offshore West Africa was as a result of its friendly metocean criteria, which is the mild fully developed swell waves in that area.

Tables 3.2 and 3.3 show the prototype and model geometric properties, center of gravity, weight and natural periods. Figure 3.1 is a picture of the experimental setup at the OTRC.

Table 3.2 Prototype and Model Mini-TLP Properties [11].

Parameter	Prototype	Model (1:62)
Draught (m)	28.50	0.460
Column diameter (m)	8.75	0.141
Column separation distance (m)	28.50	0.460
Pontoon height (m)	6.25	0.101
Pontoon width (m)	6.25	0.101
Deck clearance (m)	10.00	0.161
Center of gravity [X] (m)	0.00	0.000
Center of gravity [Y] (m)	0.00	0.000
Center of gravity [Z] (m)	27.04	0.436
Displacement (t)	10320	0.0271
Number of tethers	8	4
Number of risers	12	12
Natural period in surge/sway (s)	133	140
Natural period in yaw (s)	121	101
Natural period in pitch (s)	4.9	4.9
Natural period in heave (s)	2.6	2.6

Table 3.3 Prototype and Model Tender Barge Properties [11].

Parameter	Prototype	Model (1:62)
Draught	3.7	0.060
Overall length	91.5	1.476
Length at water line	89.4	1.442
Width	27.5	0.444
Length of flat part of barge bottom	72.9	1.176
Center of gravity [X] (m)	0.0	0.0
Center of gravity [Y] (m)	0.0	0.0
Center of gravity [Z] (m)	6.8	0.110
Displacement (t)	8533	0.0349
Number of mooring lines	8	4
Total vertical pretension on mooring lines	101	0.000415

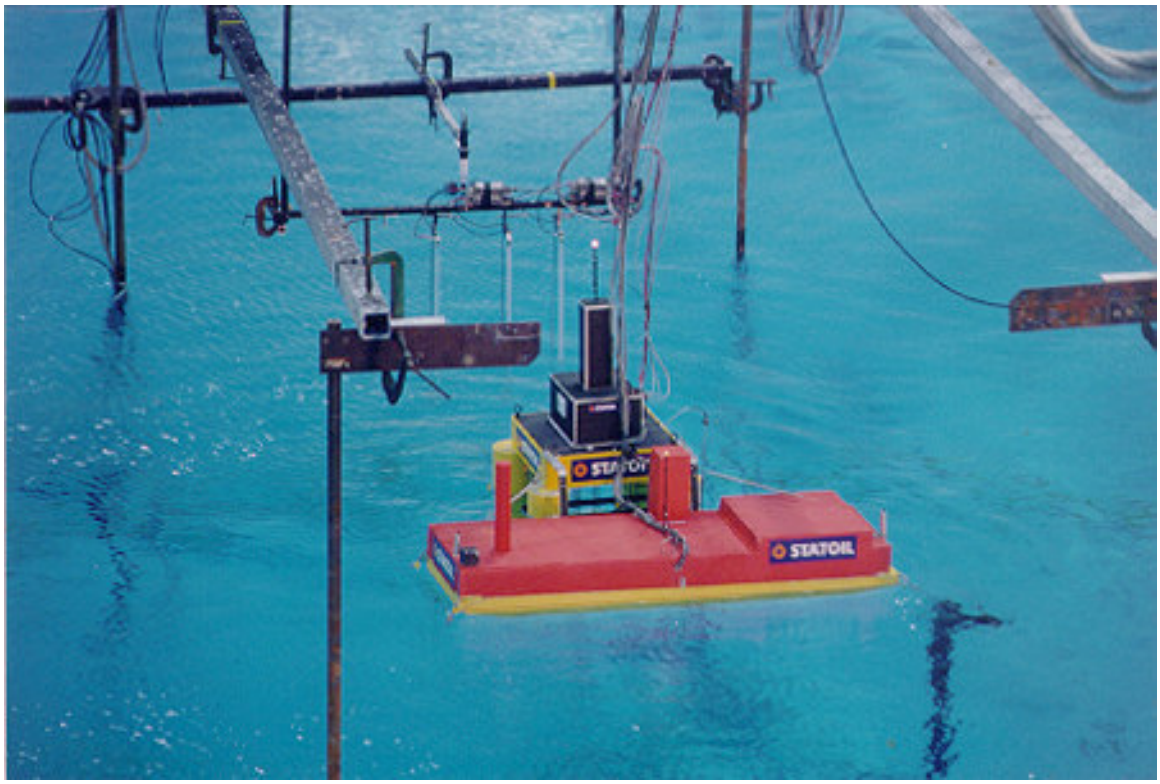

Fig 3.1 Coupled Mini-TLP and Tender Barge at OTRC Wave Tank During Model Testing.

During the experiment, the following measurements were made and shown as time series plots; wave elevation, current velocity in X and Y axis, wind speed, wave runup elevation on Mini-TLP, wave elevation between the two bodies, offset distance between the two bodies, tension in each Mini-TLP tendon, tension in each riser, tensions in each spring line, tension in Tender Barge mooring lines, fender reaction forces, accelerations of Mini-TLP in three coordinate axis, and accelerations of Tender Barge in three coordinate axis. Also response of the mini-TLP and Tender Barge were also measured as time series of motions in 6 degree of freedom as following; surge at CG of both bodies, sway at CG of both bodies, heave at CG of bodies, roll, pitch, and yaw.
Despite measurements been made for both coupled and uncoupled cases, our emphasis in this study will be on the coupled cases, because the two bodies encounter considerable impacts when coupled. Table 3.4 shows the load cases and directions being investigated.

Table 3.4 Environmental Load and Direction.

Load	Heading
Wind	0 Deg
Wave	0 Deg, -90 Deg
Current	0 Deg
Wind + Wave + Current	0 Deg, -90Deg

3.1.1 Procedure

The fender reaction force obtained from the experimental data is provided as a function of time, F(t). While the fender performance curves (Reaction Force and Absorbed Energy), as used in current design practice, are typically supplied as a function of percentage deflection, F(%Δ) and E(%Δ). The performance curves for 3.048m (10ft) Dia 6.71m (22ft) long elastomeric fender was curve-fit with a polynomial equation using the least square method in MATLAB. This was used as the basis for transforming the time series plots of the fender reaction force to a time series of the percentage deflection as a function of time, %Δ(t) and absorbed energy as a function of time, E(t). Figure 3.2 shows this in a flowchart.

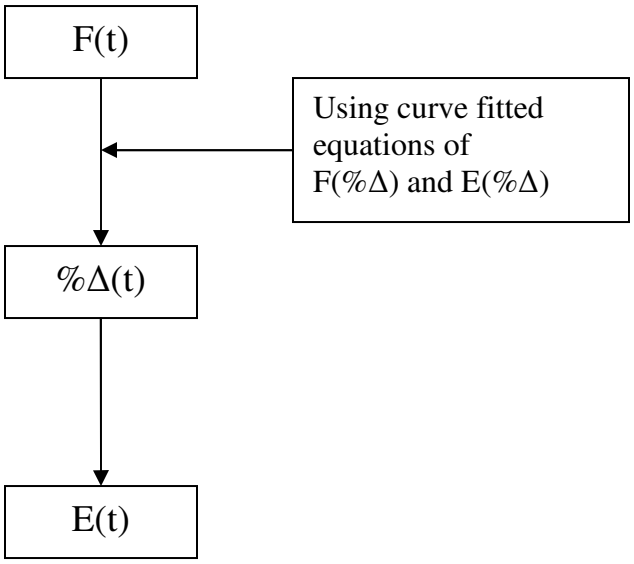

Fig. 3.2 Flowchart of Transformation of Functions.

3.1.2 Analysis of Results

Referring to Figure 2.1 and considering the size of the prototype mini-TLP column, it was assumed that four 3.04m (10ft) Dia fender units attached to each of the two mini-TLP columns facing the barge and absorbing the impact would be needed. Assuming an equal distribution of the loading, the fender reaction time series from the experiment was scaled down using a scale ratio 1:8 to obtain data for one fender unit. The

effect of varying the number of fender units per column on the statistics of the outputs could also be studied.

Figures 3.3 to 3.8 illustrates the fender reaction time series from the experiment and outputs of the transformation, which are the fender deflection time series and absorbed energy time series for the first 2000 datapoints for all the load cases and headings investigated in this research study.

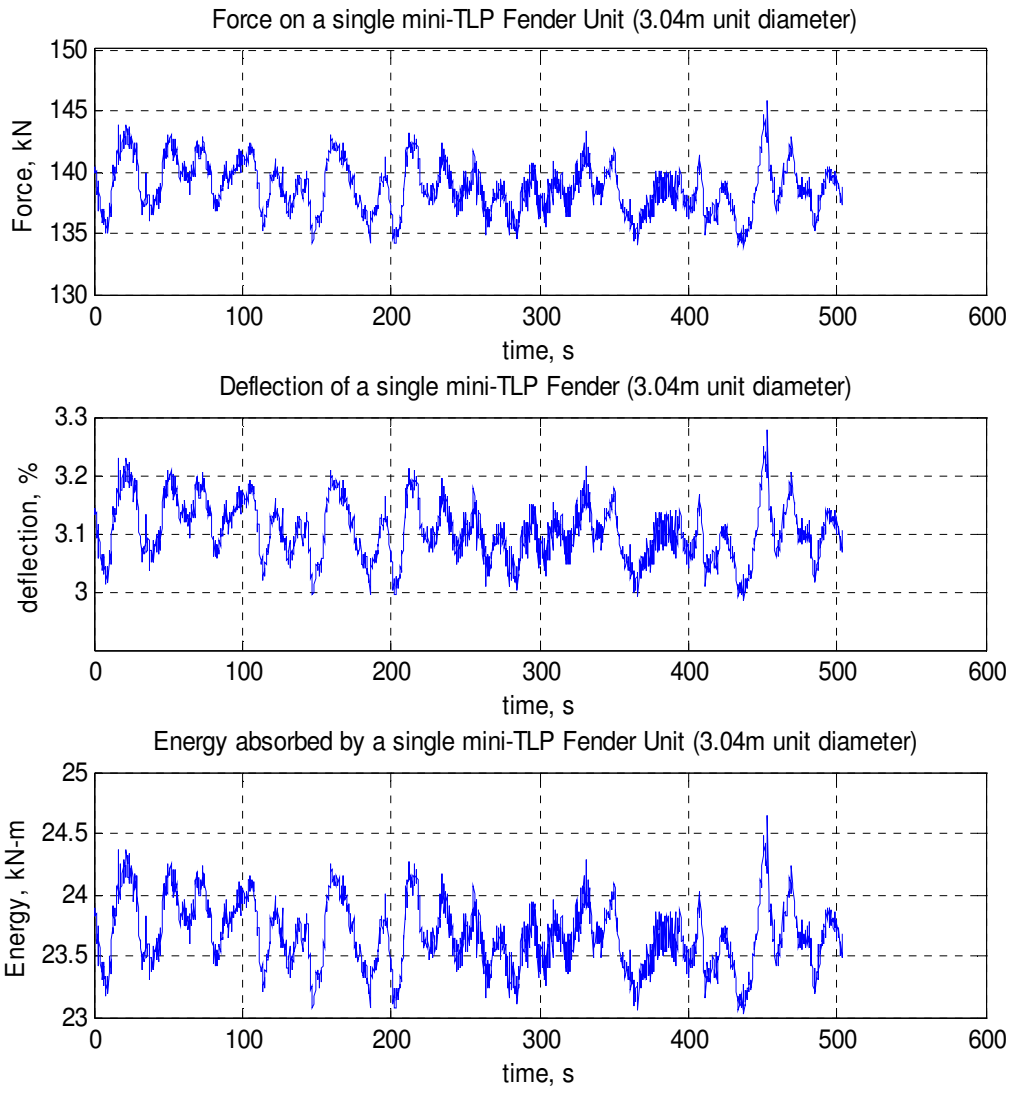

Fig 3.3 Time Series of Reaction Force, Deflection and Absorbed Energy for Wind Only at 0 Deg Heading (Case 1).

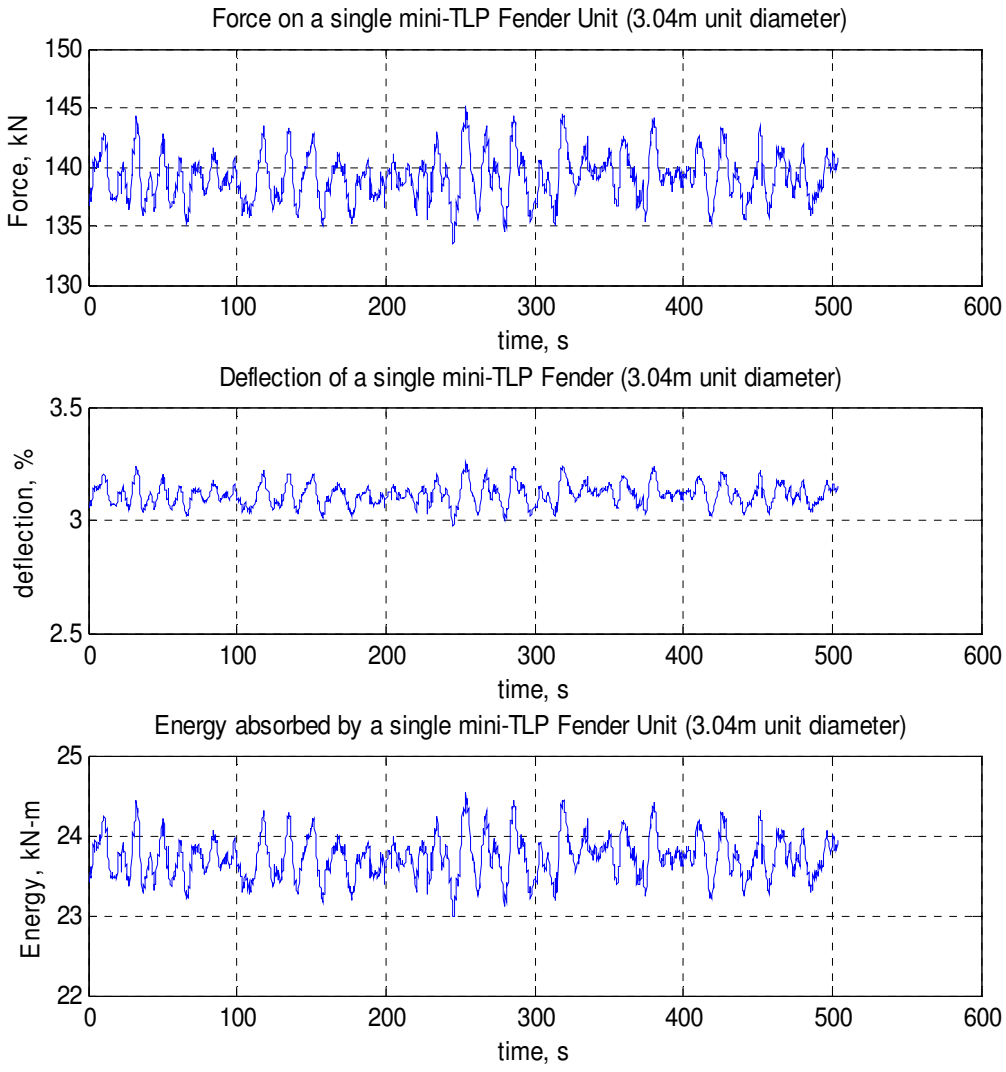

Fig 3.4 Time Series of Reaction Force, Deflection and Absorbed Energy for Wave Only at 0 Deg Heading (Case 2).

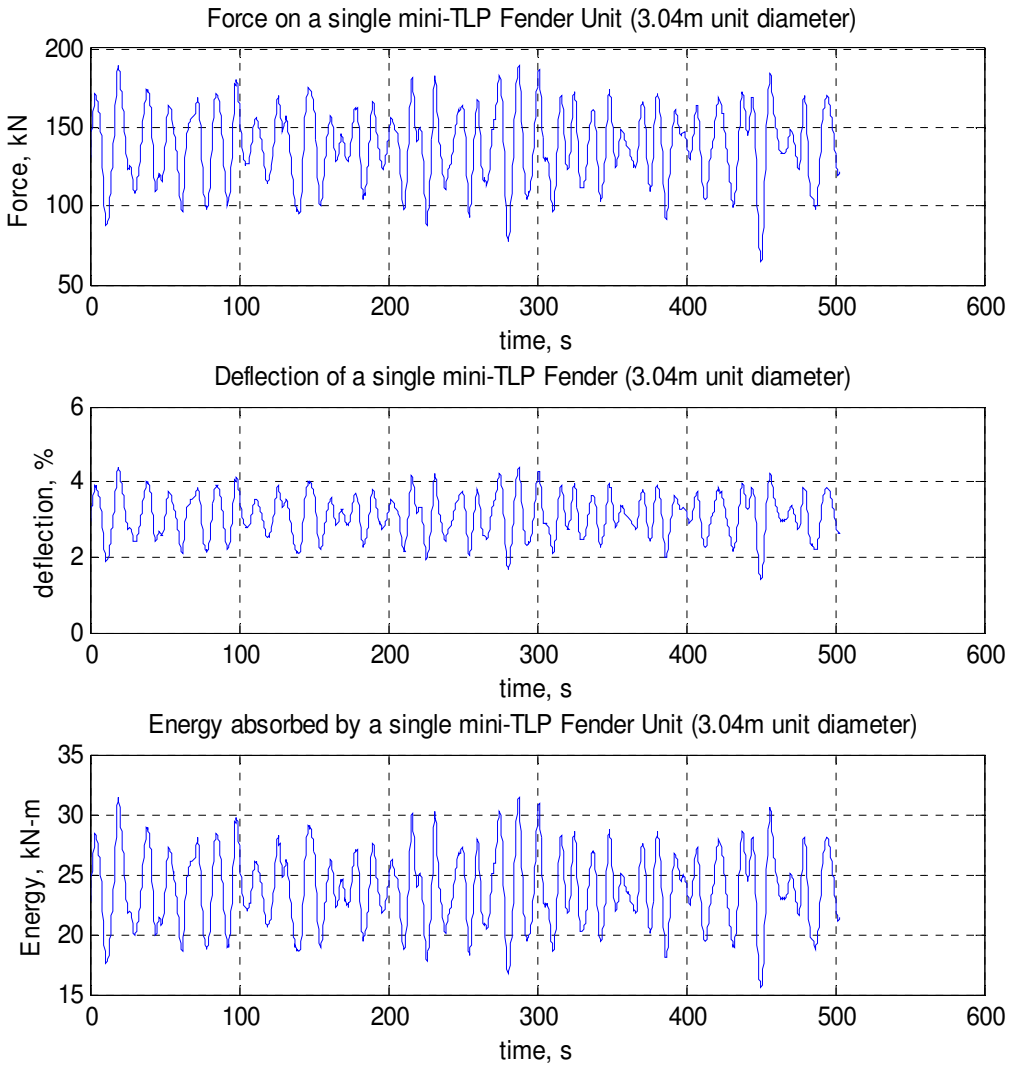

Fig 3.5 Time Series of Reaction Force, Deflection and Absorbed Energy for Wave Only at 90 Deg Heading (Case 3).

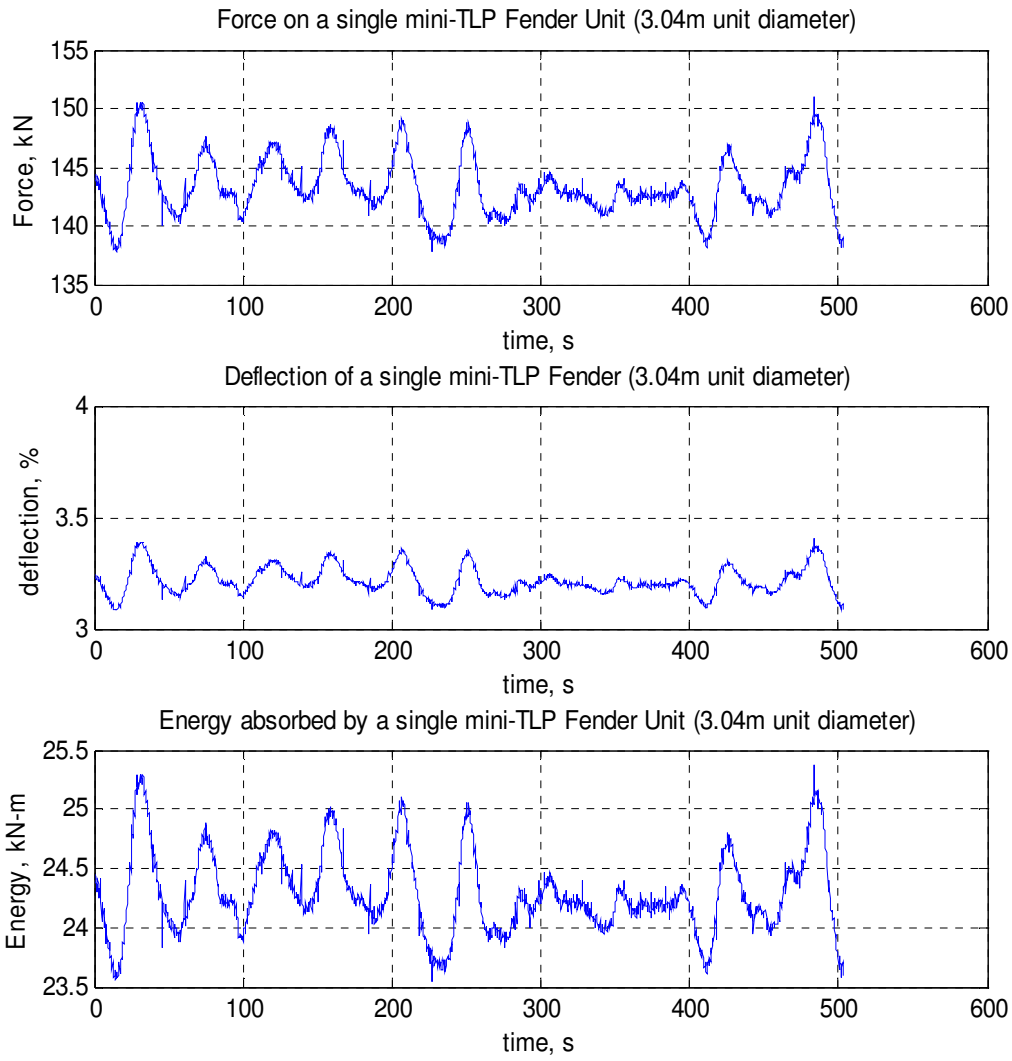

Fig 3.6 Time Series of Reaction Force, Deflection and Absorbed Energy for Current Only at 0 Deg Heading (Case 4).

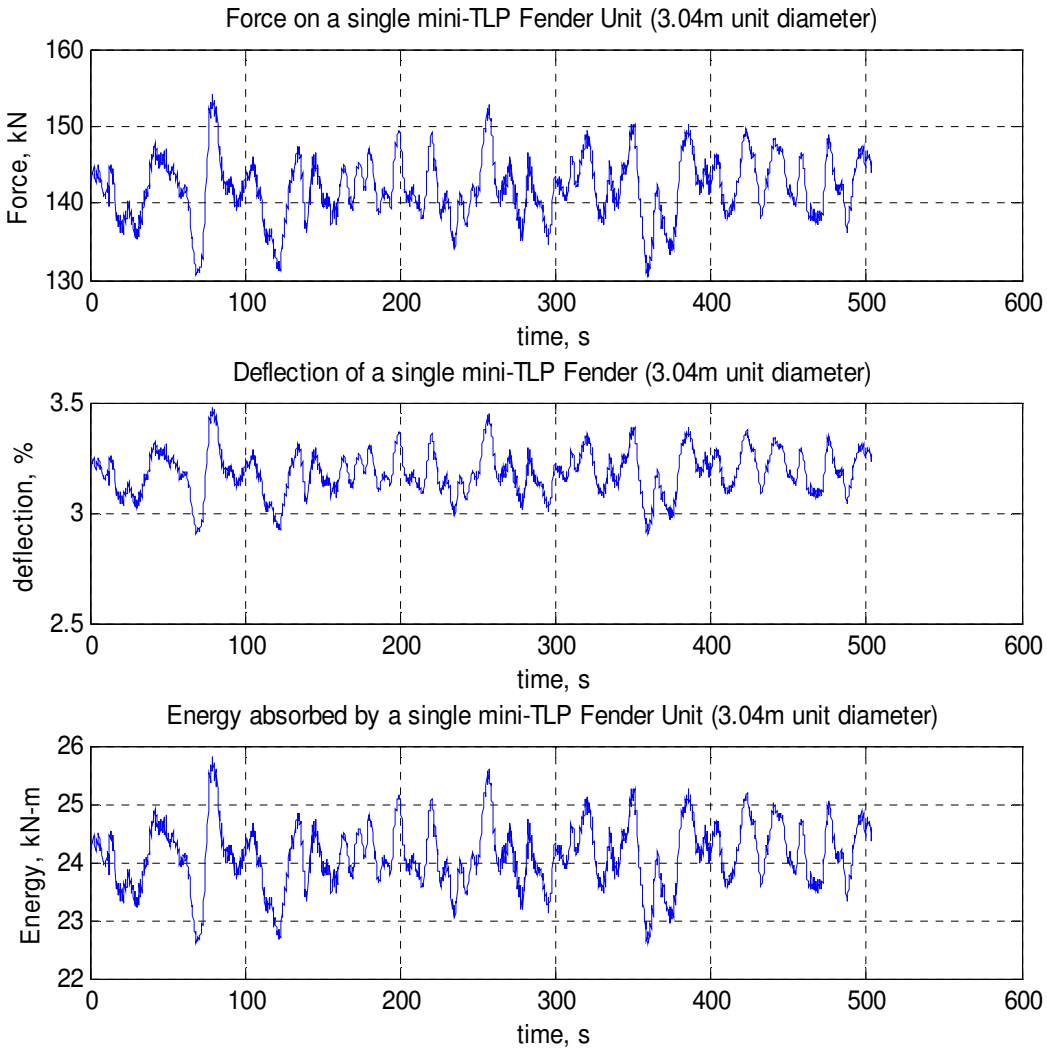

Fig 3.7 Time Series of Reaction Force, Deflection and Absorbed Energy for Wind + Wave + Current at 0 Deg Heading (Case 5).

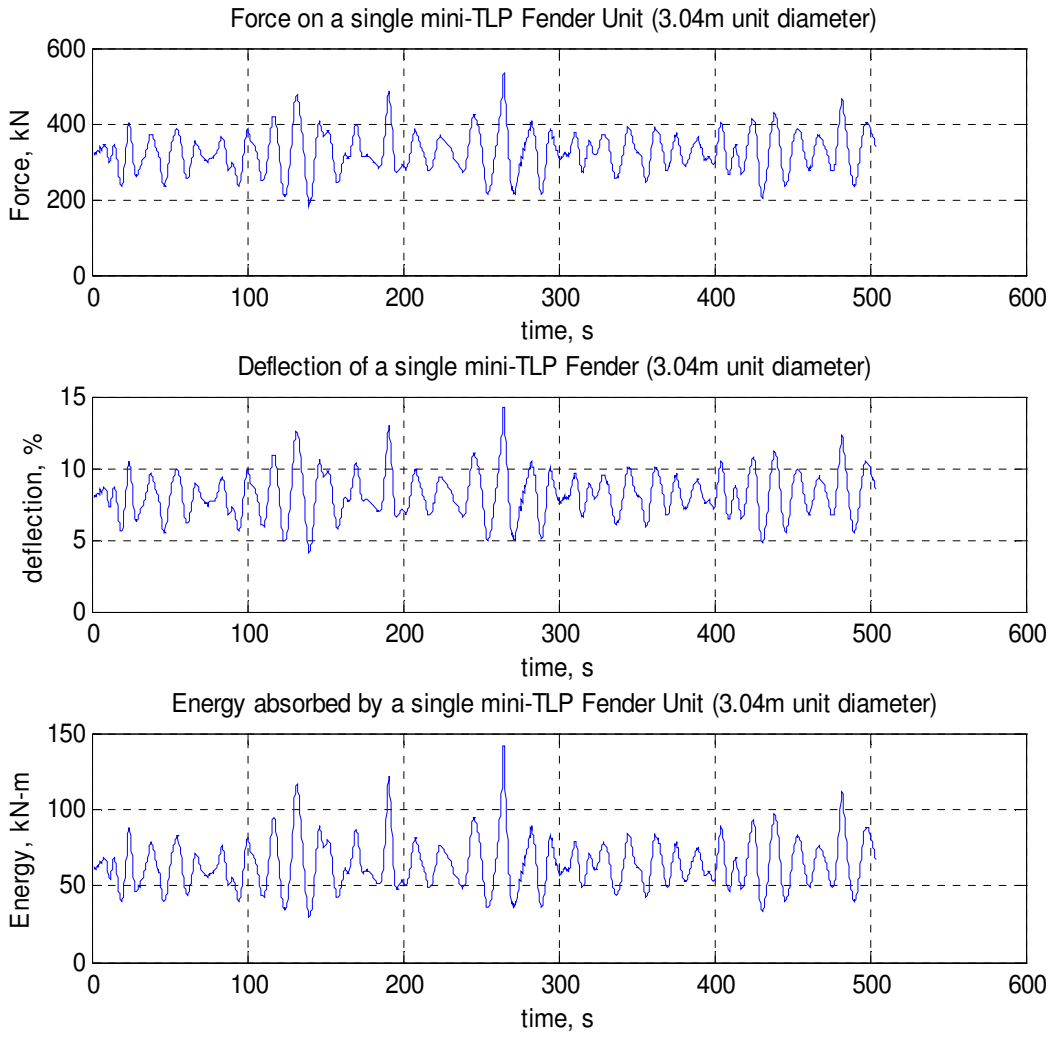

Fig 3.8 Time Series of Reaction Force, Deflection and Absorbed Energy for Wind + Wave + Current at 90 Deg Heading (Case 6).

The data presented in these figures illustrate the random nature of the measured time series and the estimated deflection and energy absorption characteristics. Initially, the data will be characterized in terms of the typical statistical moments, which include the mean, standard deviation, skewness and kurtosis. More specifically,

(i) Maximum and Minimum Values: - these describe the highest and lowest values in the data.

(ii) Measures of Central Value: - these give measures of the mean, median and mode of the distribution. The mean is also referred to as the first central moment or expectation of a continuous random variable X with a probability density function $f_X(x)$.

$$E[X] = \mu_x = \int_{-\infty}^{\infty} x f_x(x)\, dx \tag{3.1}$$

(iii) Measures of Dispersion: - these include variance, standard deviation and coefficient of variation. The variance indicates the dispersion or spread of the data from the mean, while the standard deviation is the square root of the variance and has the same unit as the mean. Mathematically, the variance is referred to as the second central moment of a random variable X with a probability density function $f_X(x)$.

$$Var[X] = \int_{-\infty}^{\infty} (x-\mu_x)^2 f_x(x)\, dx \tag{3.2}$$

$$\sigma_x = \sqrt{Var[X]} \tag{3.3}$$

$$COV(X) = \frac{\sigma_x}{\mu_x} \tag{3.4}$$

The coefficient of variation indicates the amount of uncertainty or randomness of the random variable and as a dimensionless quantity relates the degree of dispersion of the random variable to the mean.

(iv) Skewness: - the symmetry of the distribution about its mean is measured by the skewness, which is represented mathematically by the third central moment of a continuous random variable X. The skewness coefficient is obtained by normalizing the skewness by cube of the standard deviation. A skewness coefficient of zero indicates the distribution is symmetric about the mean, a negative indicates the distribution is

asymmetric and skewed to the right of the mean while a positive indicates an asymmetric distribution skewed to the left of the mean.

$$skewness = \int_{-\infty}^{\infty} (x-\mu_x)^3 \, f_x(x)\, dx \qquad \lambda_1 = \frac{skewness}{\sigma^3} \tag{3.5}$$

(v) Kurtosis: - this is a measure of the peakedness of the distribution with respect to a normal distribution and is mathematically represented by the fourth central moment of a continuous random variable X. A value of 3 indicate its peak is same as a normal distribution, a value less than 3 indicates a mild peak while a value greater than 3 indicates a sharp peak.

$$kurtosis = \int_{-\infty}^{\infty} (x-\mu_x)^4 \, f_x(x)\, dx \qquad \lambda_2 = \frac{kurtosis}{\sigma^4} \tag{3.6}$$

In the tables that follow, Tables 3.5 to 3.12, the statistical characteristics of the fender reaction forces that were measured in the experiments for the various environmental conditions and model headings are shown. Additionally, the estimated characteristic fender deflection and energy absorption are presented.

Table 3.5 Parameters for Wind Only, 0 Deg Heading (Case 1).

	Minimum	Maximum	Mean	Standard Deviation	COV	Skewness	Kurtosis
Fender Reaction (KN)	129.42	147.25	138.66	2.2	0.02	-0.042	3.12
Fender Deflection (%)	2.88	3.31	3.10	0.05	0.02	-0.032	3.12
Energy Absorbed (KN.m)	22.46	24.84	23.66	0.29	0.01	-0.005	3.11

Table 3.6 Parameters for Wave Only, 0 Deg Heading (Case 2).

	Minimum	Maximum	Mean	Standard Deviation	COV	Skewness	Kurtosis
Fender Reaction (KN)	127.75	152.19	139.42	2.89	0.02	0.17	3.17
Fender Deflection (%)	2.84	3.43	3.12	0.07	0.02	0.19	3.18
Energy Absorbed (KN.m)	22.25	25.53	23.77	0.39	0.02	0.22	3.20

Table 3.7 Parameters for Wave Only, 90 Deg Heading (Case 3).

	Minimum	Maximum	Mean	Standard Deviation	COV	Skewness	Kurtosis
Fender Reaction (KN)	27.13	276.28	137.88	26.44	0.19	0.08	3.28
Fender Deflection (%)	0.59	6.74	3.10	0.64	0.21	0.20	3.39
Energy Absorbed (KN.m)	12.50	49.54	23.80	3.58	0.15	0.57	4.07

Table 3.8 Parameters for Current Only, 0 Deg Heading (Case 4).

	Minimum	Maximum	Mean	Standard Deviation	COV	Skewness	Kurtosis
Fender Reaction (KN)	133.60	154.56	143.46	2.29	0.02	0.28	4.08
Fender Deflection (%)	2.98	3.49	3.22	0.06	0.02	0.30	4.09
Energy Absorbed (KN.m)	22.99	25.88	24.31	0.31	0.01	0.34	4.14

Table 3.9 Parameters for Wind + Wave + Current, 0 Deg Heading (Case 5).

	Minimum	Maximum	Mean	Standard Deviation	COV	Skewness	Kurtosis
Fender Reaction (KN)	123.29	159.44	142.48	4.73	0.03	-0.01	3.12
Fender Deflection (%)	2.73	3.61	3.20	0.12	0.04	0.02	3.12
Energy Absorbed (KN.m)	21.69	26.59	24.19	0.64	0.03	0.07	3.12

Table 3.10 Parameters for Wind + Wave + Current, 90 Deg Heading (Case 6).

	Minimum	Maximum	Mean	Standard Deviation	COV	Skewness	Kurtosis
Fender Reaction (KN)	60.85	339.95	161.61	24.44	0.15	0.31	4.40
Fender Deflection (%)	1.32	8.58	3.68	0.62	0.17	0.47	4.77
Energy Absorbed (KN.m)	15.18	67.18	27.14	3.78	0.14	0.97	6.94

Table 3.11 Parameters for Wind + Wave + Current, 0 Deg Heading (Barge Not Moored, Realization 1).

	Minimum	Maximum	Mean	Standard Deviation	Skewness	Kurtosis
Fender Reaction (KN)	61.32	239.00	149.32	20.77	-0.16	3.57
Fender Deflection (%)	1.33	5.70	3.37	0.51	0.05	3.55
Energy Absorbed (KN.m)	15.22	40.94	25.28	2.93	0.25	3.71

Table 3.12 Parameters for Wind + Wave + Current, 0 Deg Heading (Barge Not Moored, Realization 2).

	Minimum	Maximum	Mean	Standard Deviation	Skewness	Kurtosis
Fender Reaction (KN)	65.77	246.8	151.43	21.35	-0.06	3.46
Fender Deflection (%)	1.42	5.92	3.42	0.53	0.05	3.48
Energy Absorbed (KN.m)	15.62	42.63	25.59	3.06	0.34	3.72

Upon examination of these parameters that characterize the time series, several trends were noted. The kurtosis values, especially for the Wind+Wave+Current 90 Deg heading case and Current only 0 Deg case, reflects probability density functions that have sharp peaks when compared with a normal distribution. The 90 Deg heading load cases show the greatest deviation or spread of data about the mean with also the largest amount of randomness. However, this amount of randomness from the COV seems to be more varied for the three variables investigated compared to the 0 Deg heading load cases, which seems to be almost constant over the three variables investigated. Although the magnitude of the skewness is very close to zero, the effect of wind loading only on the fender systems skews the distribution slightly to the right of the mean. Hence, the distributions could be approximated to being symmetrical except the Wind+Wave+Current 90 Deg case. It is also observed that despite the orientation of the two body system in the Wave only 90 Deg heading load case, the Wave only 0 Deg load case has a higher distribution mean for the variables. The reverse is noticed when the Wind+Wave+Current 90 Deg heading case is compared to the Wind+Wave+Current 0 Deg heading case. This is attributed to the shielding effect of the mini-TLP on the tender barge.

In the determination of the underlying distribution function appropriate for the model test results, the data will be plotted on normal probability graph. On visual

examination, we are able to determine how closely the normal probability distribution function describes our output random variables. This graphical approach is preferred to other methods like the Chi-Square Test and the Kolmogorov-Smirnov (K-S) Test, because the visual examination gives a clearer picture of how the data aligns or deviates from the ideal normal distribution over the whole range of data, while test above give a number which is a general representation of the entire data. Figure 3.9 to 3.15 shows the normal probability plots for all load cases and heading.

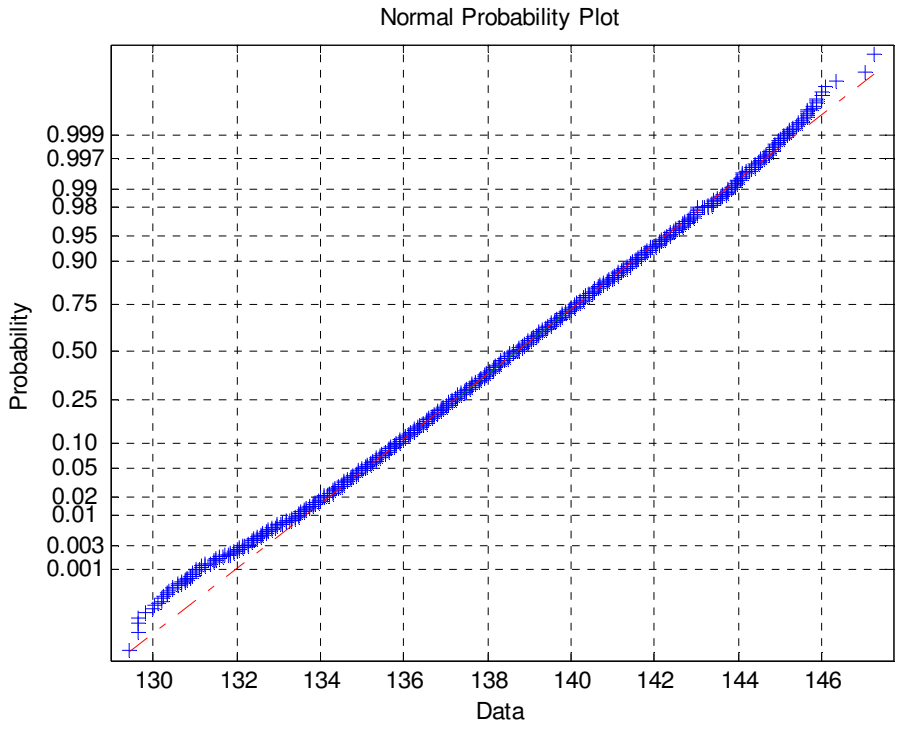

Fig 3.9 Normal Probability Plot for Wind Only 0 Deg Heading (Case 1).

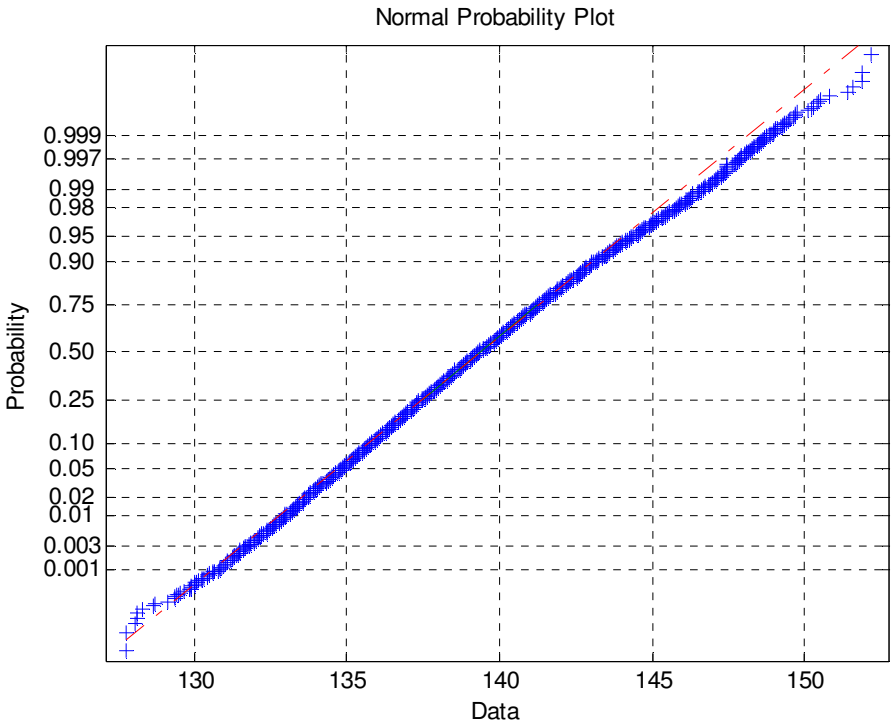

Fig 3.10 Normal Probability Plot for Wave Only 0 Deg Heading (Case 2).

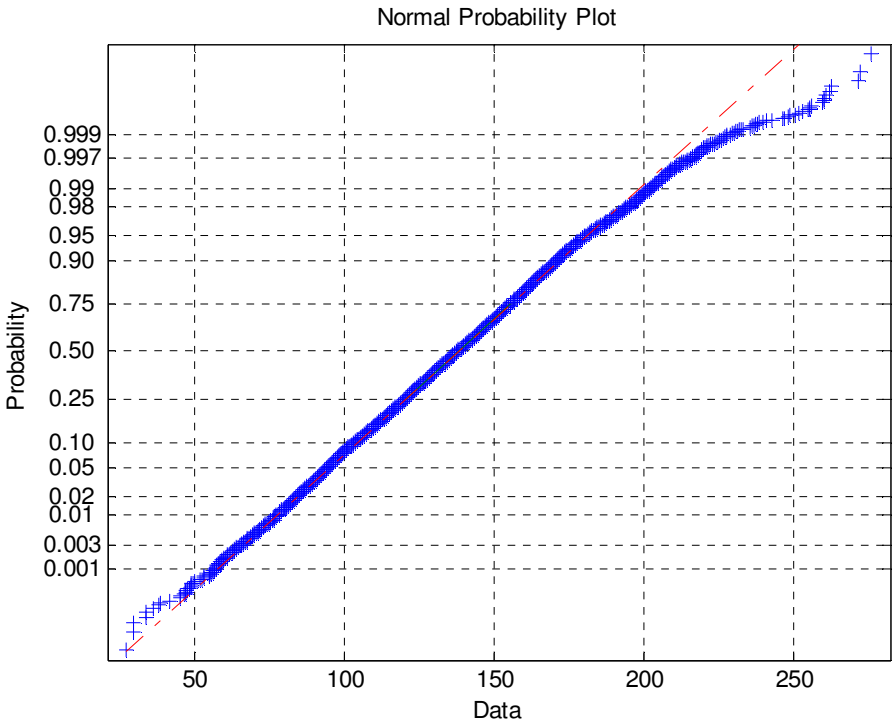

Fig 3.11 Normal Probability Plot for Wave Only 90 Deg Heading (Case 3).

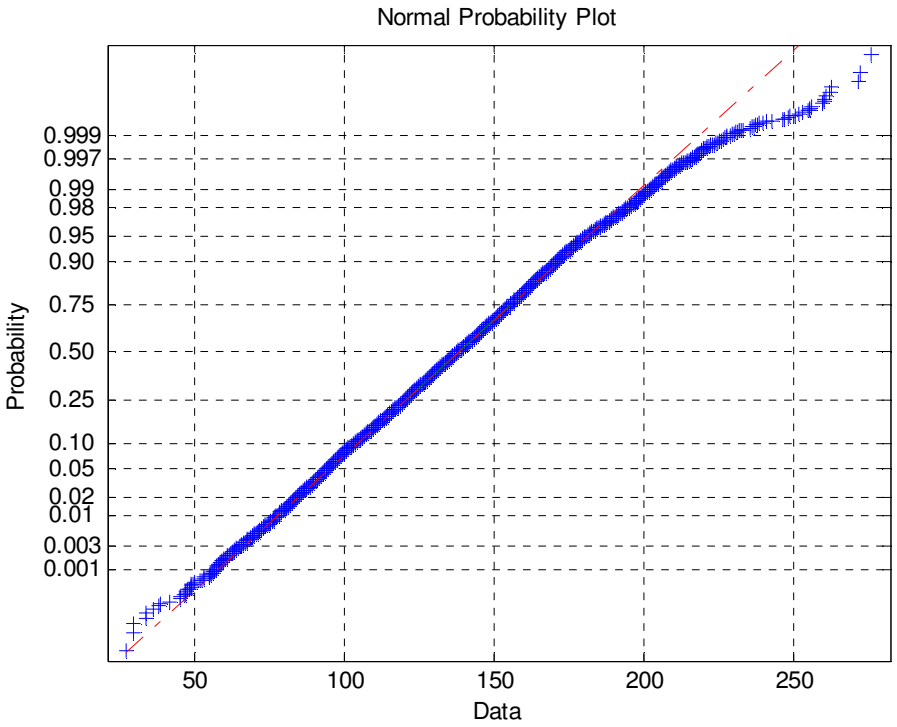

Fig 3.12 Normal Probability Plot for Current Only 0 Deg Heading (Case 4).

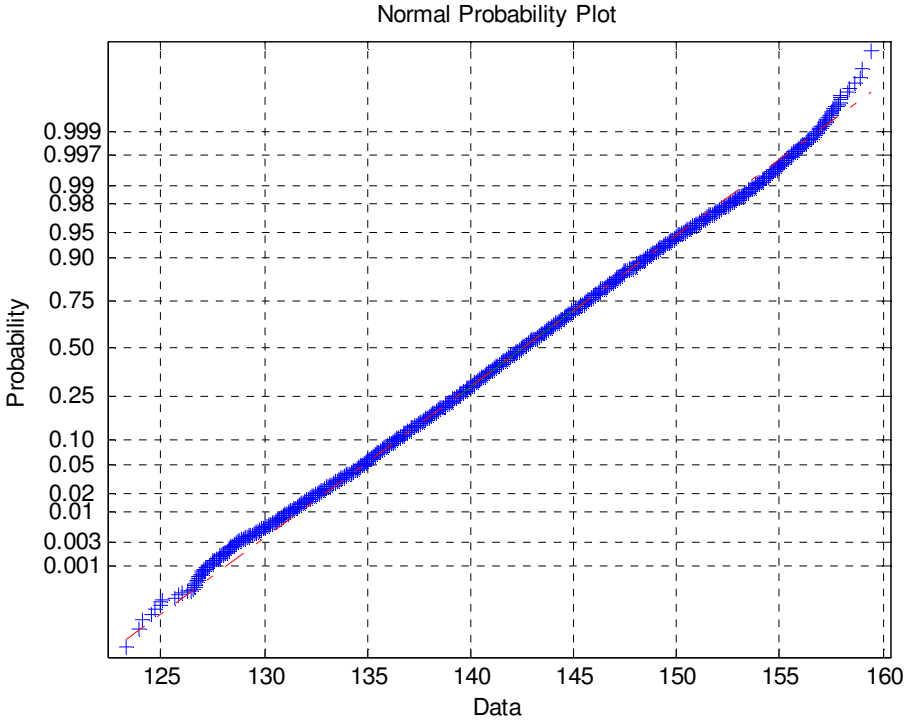

Fig 3.13 Normal Probability Plot for Wind+Wave+Current 0 Deg Heading (Case 5).

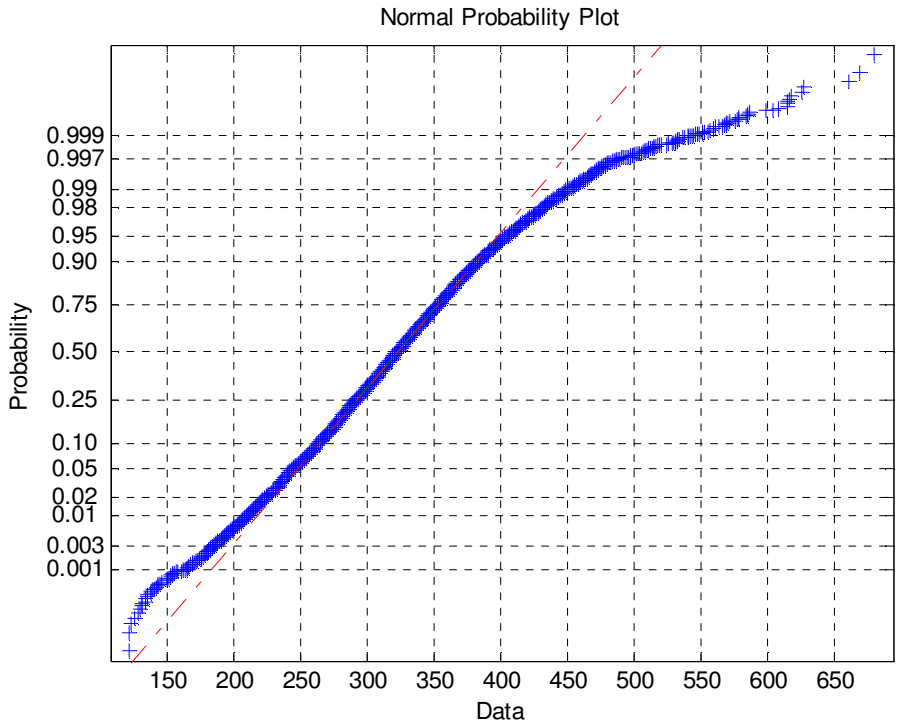

Fig 3.14 Normal Probability Plot for Wind+Wave+Current 90 Deg Heading (Case 6).

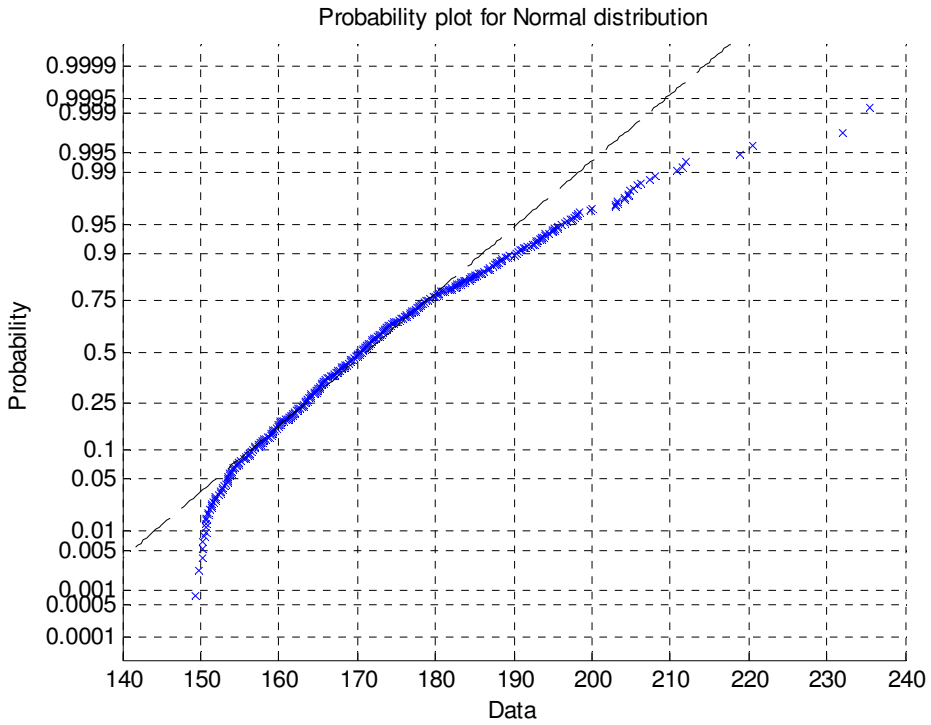

Fig 3.15 Normal Probability Plot for Wind+Wave+Current 0 Deg Heading (Barge Not Moored, Realization 1).

The Table 3.13 presents at a glance the observations on the fender response when plotted on a normal probability paper. Its deviation from the normal probability line could be described as either 'fair' or 'good' for close deviations. However, very wide deviation from the normal probability line could be described as either '+off' (deviations above the line) or '-off' (deviations below the line).

Table 3.13 Deviation of the Fender Response from the Normal Probability Fit Line.

	$\theta = 0^o$ **Case 1**	$\theta = 0^o$ **Case 2**	$\theta = 0^o$ **Case 4**	$\theta = 0^o$ **Case 5**	$\theta = -90^o$ **Case 3**	$\theta = -90^o$ **Case 6**
Low end tail fit	+ off	fair	+off	good	+off	+off
High end tail fit	+ off	-off	-off	good	-off	-off
Middle region fit	good	good	good	good	good	fair

It is observed that the fender response fits the normal probability distribution for Case 5 in the upper, lower and middle regions of the data. On comparison with the same load combination in the -90 degree heading, the fit to the normal distribution line seem to be fair in the middle region and widely deviated in the upper and lower tail regions. In general, almost all of the cases have a close fit to the normal distribution line for fender response data in the middle region. Also, the upper and lower extreme value data for all the cases, except case 5, deviate from the normal probability line. This shows that the extreme value fender response data exhibit non-Gaussian behavior.

The most common load case an offshore facility is exposed to on a day to day basis is a combination of wind, waves and current. In the -90 Deg heading, the fender responses are generally higher for the above combination, as seen in Table 3.10. Hence, it is observed that fender response in case 6 exhibits the largest deviations at the upper extreme values and a not-too-good fit to the normal distribution line in the middle region. This study has in effect shown the behavior of the fender response under single and uncoupled loadings, although that may not exist in reality.

4. INTERPRETATION OF RANDOM PROCESSES

In the design of engineering systems subject to random excitation, the intent is to be able to design such systems to withstand anticipated extremes. Here the focus is to design a fender system that would be able to survive extreme conditions that would test the deflection and energy absorption capabilities given the nature of the random loading. Figure 4.1 shows a segment of the measured fender force time series noting the locations of the maximum and minimum values.

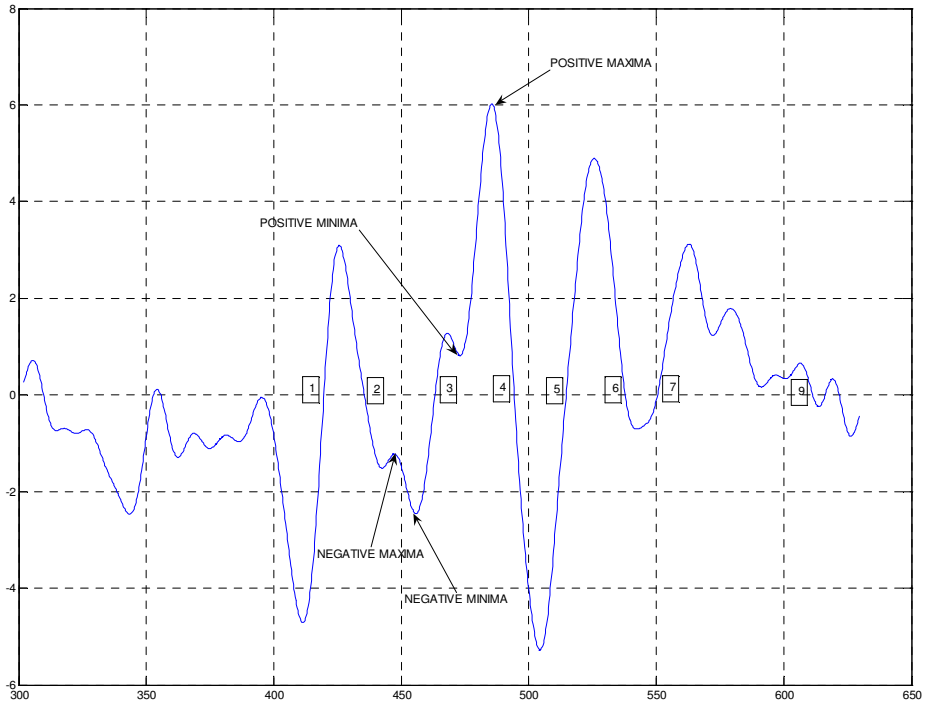

Fig. 4.1 Points of Extreme Values (Maxima) and Minima in a Sample of the Measured Fender Force Time Series.

A narrow-banded time series signal is characterized by a single peak or trough that occurs in a half cycle, while a wide-banded time series signal can contain multiple peaks in a half cycle. The time series presented in Figure 4.1 indicates a wide-banded process as multiple peaks occur in half cycles between points 3-4 and points 7-9. Each of the time series data from the experiment exhibits multiple peaks between half cycles. In order to study the extreme value statistics, a method will be applied to extract the extreme

values (positive maxima) within each half cycle above the mean line. The negative minima data points are also another set of extreme values, which is useful in other engineering applications but will not be utilized in this study. Various probability density distribution function are used to describe extreme values in a data set and include the weibull distribution, the rayleigh distribution and the gumbel distribution. [12]

A method for identifying cycles in a time series record and subsequently obtaining the extreme value from the data set is called *the zero crossing analysis method.* Using this method, the peak values between an up-crossing and down-crossing point for a prescribed level crossing were obtained. The extreme value was evaluated as the maximum peak value within the appropriate half cycle. Utilizing this method to analyze the fender reaction response time series data, the algorithm was coded in MATHLAB to perform this analysis. An example of the process is presented in Figure 4.2. The level crossing was specified as the process mean value, the extreme value for the half cycle is selected as peak 2 since it is greater than peak 1.

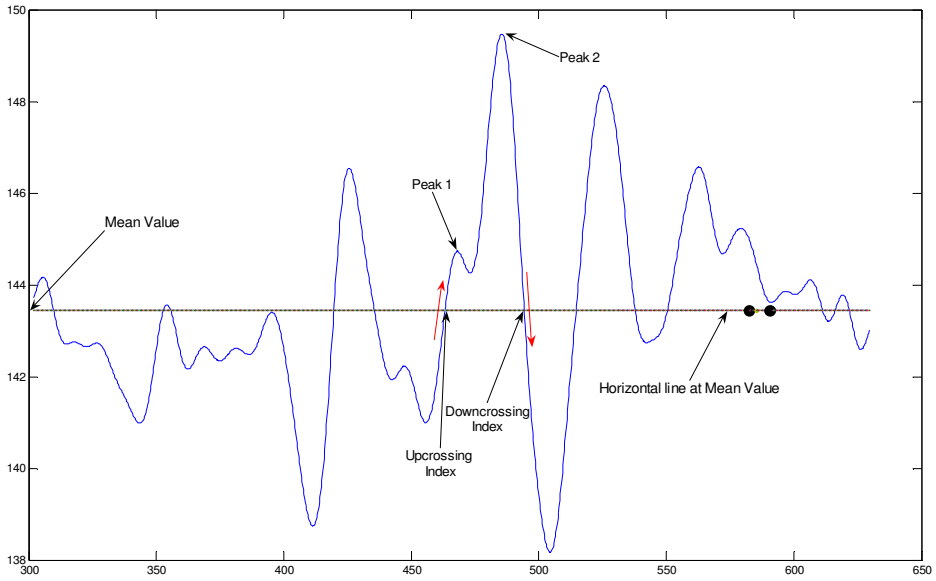

Fig. 4.2 Zero-crossing Analysis to Obtain the Extreme Values.

The raw data was filtered before the zero crossing analysis was carried out. Filtering was performed on the response reaction time series in order to remove high frequency noise in the data. A Butterwort filter algorithm available in MATHLAB was

utilized in this study. It was specified to be a low pass digital filter cutting off cycles with frequency higher than 20Hz (or periods lower than 0.05secs). The effect of the filter is observed when comparing Figure 4.3 with Figure 4.2. In the signal processing of the experimental data, noise appears as high frequency oscillation which overlay the data and hence is smoothed out in regular practice while retaining the nature of the original data.

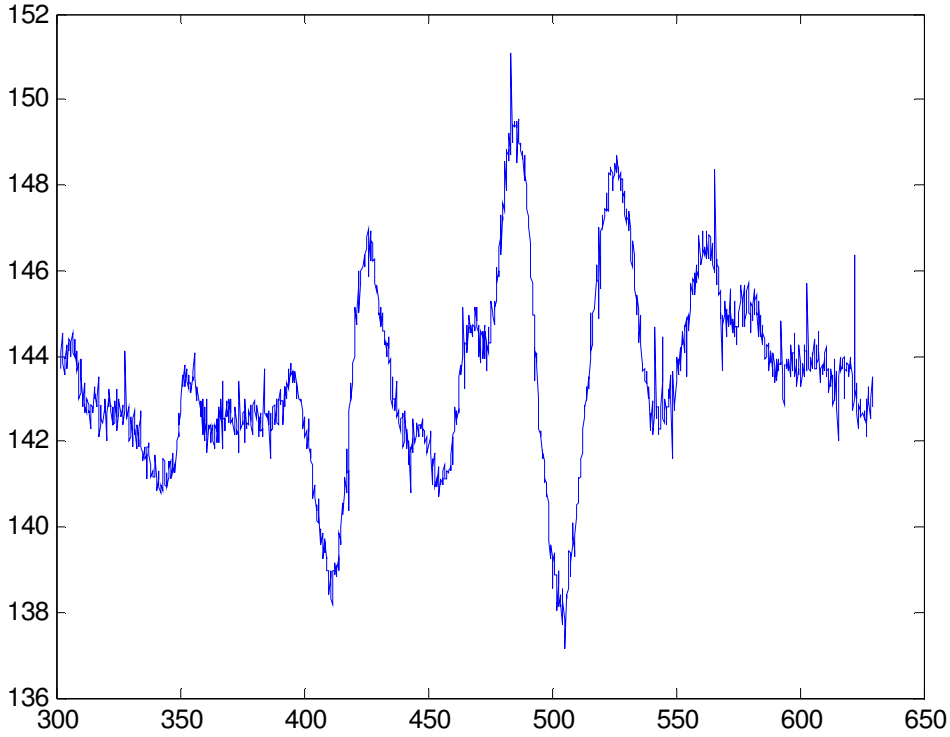

Fig. 4.3 The Unfiltered Raw Data.

4.1 Characterizing the Extremes of the Measured Fender Force

Statistical characterization of the extremes of the measured fender forces were evaluated for each load case. Since the extreme value data is a random variable, determining its underlying probability distribution and parameters is of considerable interest. To this end, the extreme value data for each case considered was plotted on the probability paper for various established probability distributions in order to understand the nature of the data.

Figures 4.4 through 4.11 present a comparison of the probability plots for the various data sets investigated. These graphs compare the normal, log-normal, exponential, rayleigh, weibull and extreme value distribution for the various data set. The following eight data sets are examined:

1. Fender reaction for 0 Deg Current Only
2. Fender reaction for 0 Deg Wave Only
3. Fender reaction for 0 Deg Wind Only
4. Fender reaction for 0 Deg Wind+Wave+Current
5. Fender reaction for 90 Deg Wind Only
6. Fender reaction for 90 Deg Wind+Wave+Current
7. Fender reaction for 0 Deg Wind+Wave+Current, Barge not moored (Realization 1)
8. Fender reaction for 0 Deg Wind+Wave+Current, Barge not moored (Realization 2)

It is observed that overall, the Rayleigh distribution, which is part of the weibull family of distribution, appear to provide a reasonably good fit to the data. Thus, given the standard deviation of the data, a reasonable estimate of the fender could be obtained. This information is summarized in Table 4.1, which shows how each probability distribution function describes each case for both the low tail and high tip. The descriptor ‘ + off ’ means the data is below the fit line and ‘ – off ’ means the data is above the fit line. When the wind and wave conditions dominate for head seas, the Rayleigh distribution gives a closer fit, while for combined load in beam sea, more scatter is observed. Hence the idea to characterize the data is in order.

Table 4.1 Summary of the Distribution Fits on Figure 4.4 to Figure 4.8.

	$\theta = 0^o$ **Case 1**	$\theta = 0^o$ **Case 2**	$\theta = 0^o$ **Case 3**	$\theta = 0^o$ **Case 4**	$\theta = -90^o$ **Case 5**	$\theta = -90^o$ **Case 6**
Normal						
Low end tail fit	+ off	+ off	+ off	+ off	+ off	+ off
High end tail fit	+ off	+ off	fair	good	+ off	+ off
Log-Normal						
Low end tail fit	+ off	+ off	+ off	+ off	fair	fair
High end tail fit	+ off	+ off	fair	good	+ off	+ off
Exponential						
Low end tail fit	ok	ok	ok	ok	ok	ok
High end tail fit	- off	- off	- off	- off	- off	- off
Rayleigh						
Low end tail fit	+ off	good	good	ok	good	good
High end tail fit	+ off	good	- off	ok	good	+ off
Weibull						
Low end tail fit	+ off	+ off	+ off	+ off	+ off	+ off
High end tail fit	+ off	+ off	+ off	+ off	+ off	+ off
Extreme Value						
Low end tail fit	+ off	+ off	+ off	+ off	+ off	+ off
High end tail fit	+ off	+ off	+ off	+ off	+ off	+ off

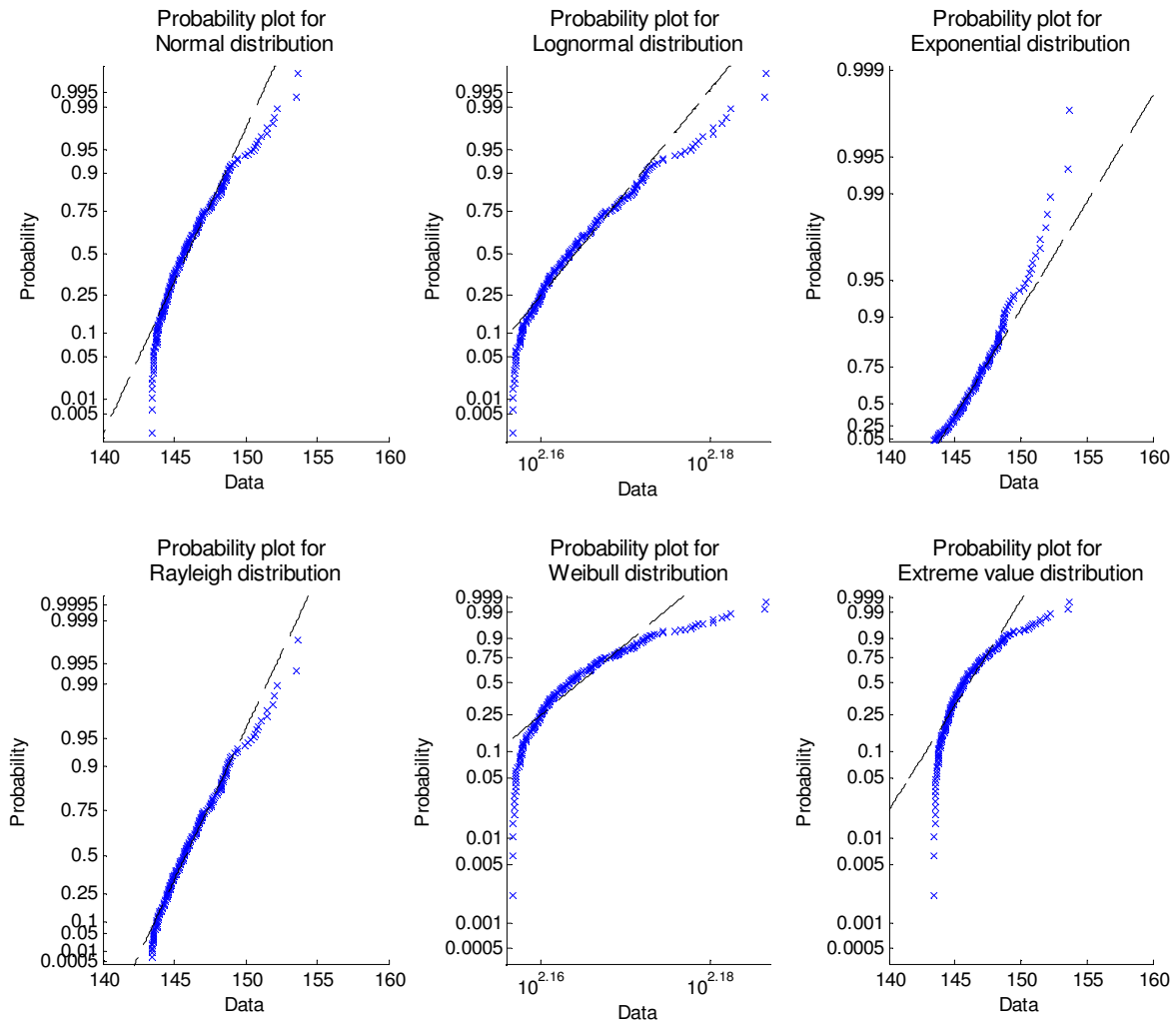

Fig. 4.4 Extreme Value Probability Plot for Case 1 (0 Deg Current Only of Fender Reaction).

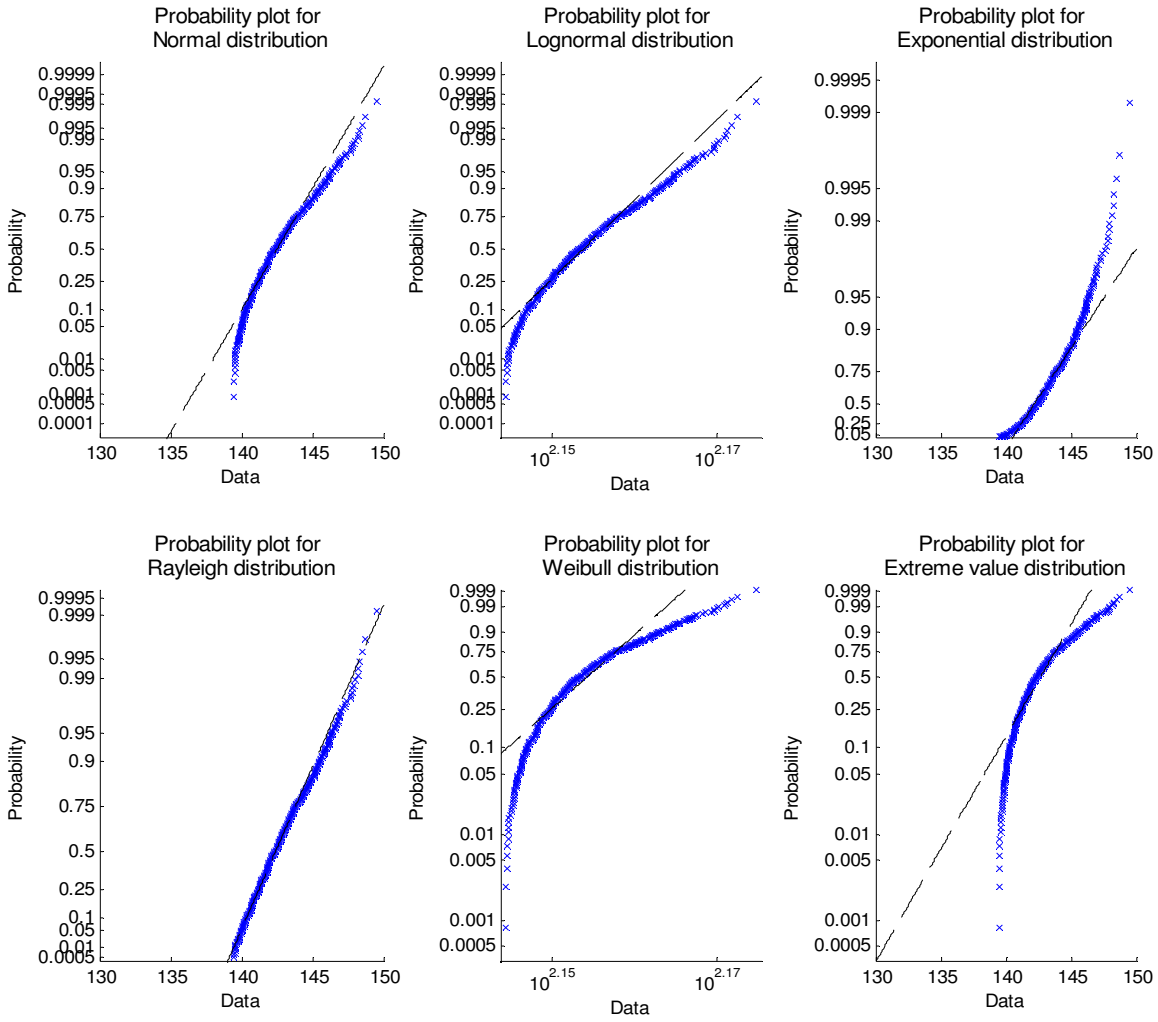

Fig. 4.5 Extreme Value Probability Plot for Case 2 (0 Deg Wave Only of Fender Reaction).

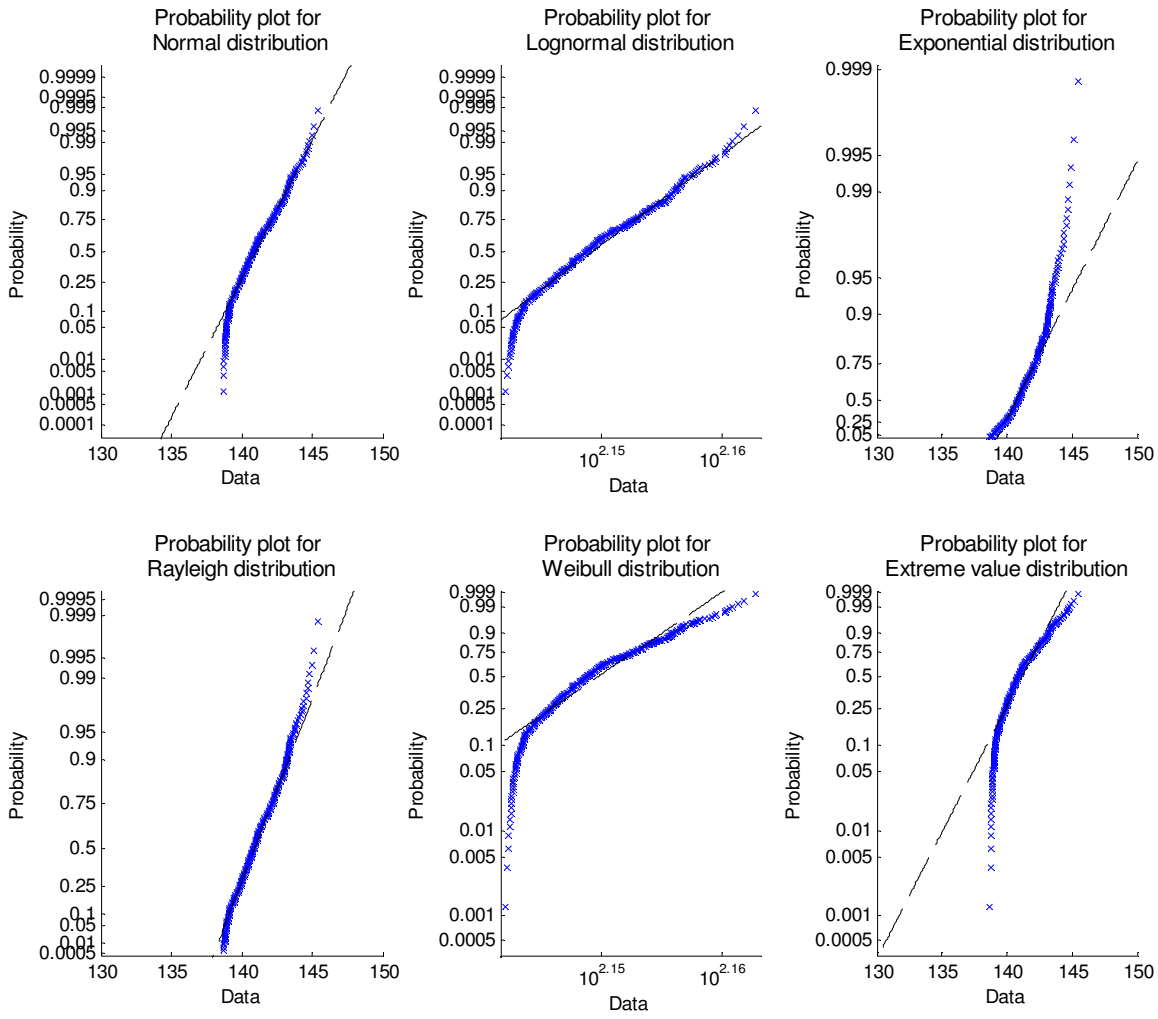

Fig. 4.6 Extreme Value Probability Plot for Case 3 (0 Deg Wind Only of Fender Reaction).

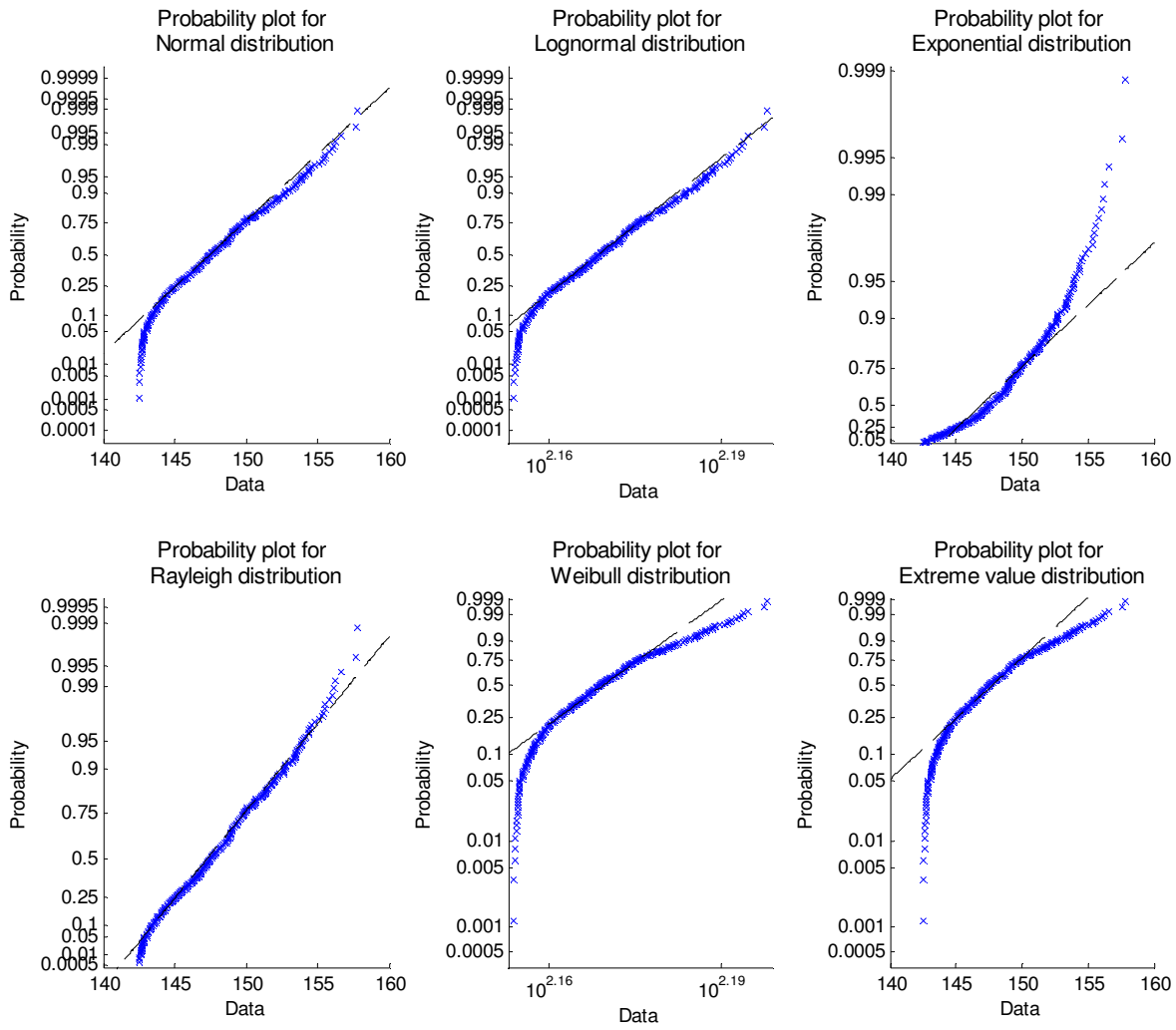

Fig. 4.7 Extreme Value Probability Plot for Case 4 (0 Deg Wind+Wave+Current of Fender Reaction).

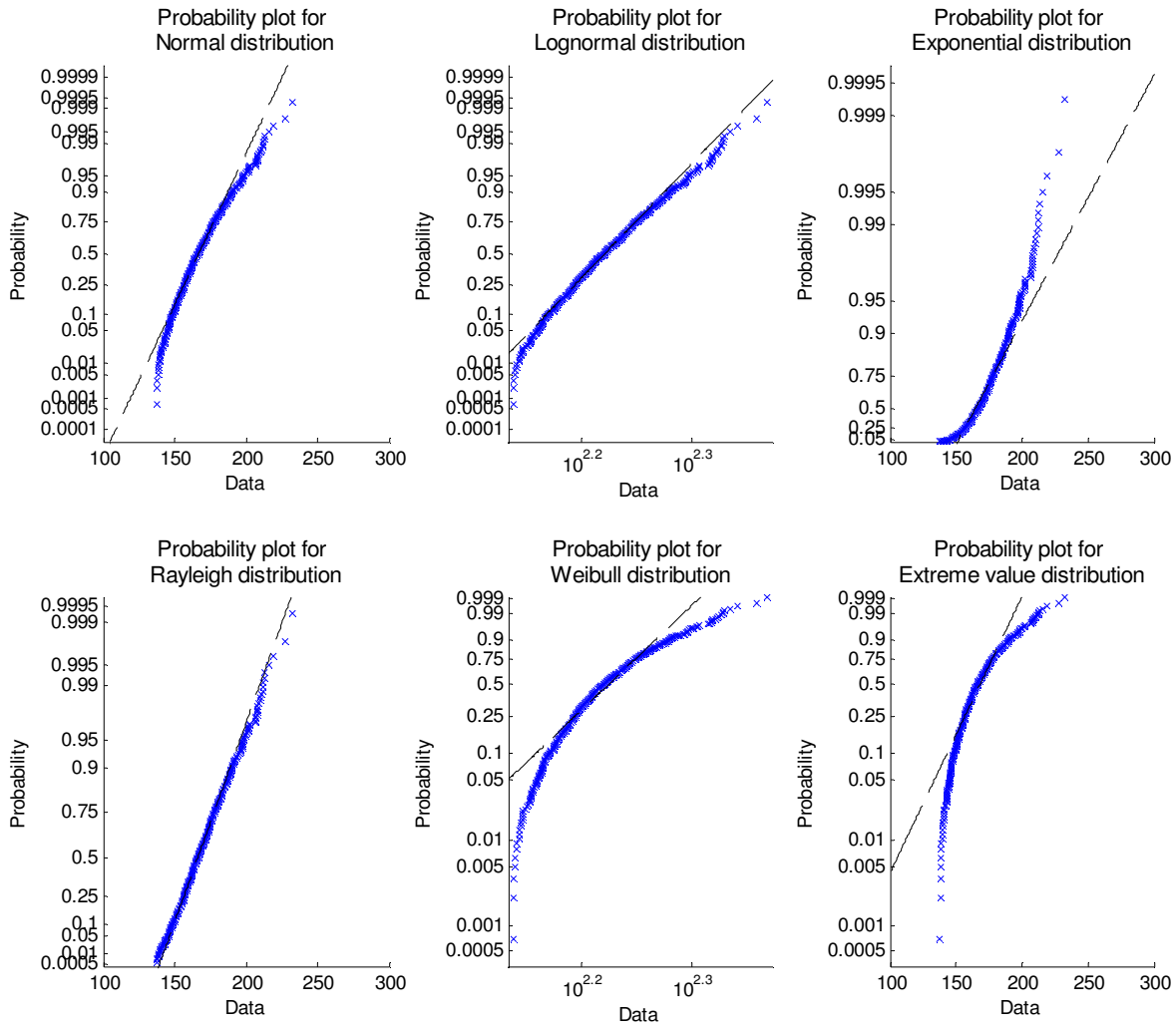

Fig. 4.8 Extreme Value Probability Plot for Case 5 (90 Deg Wind Only of Fender Reaction).

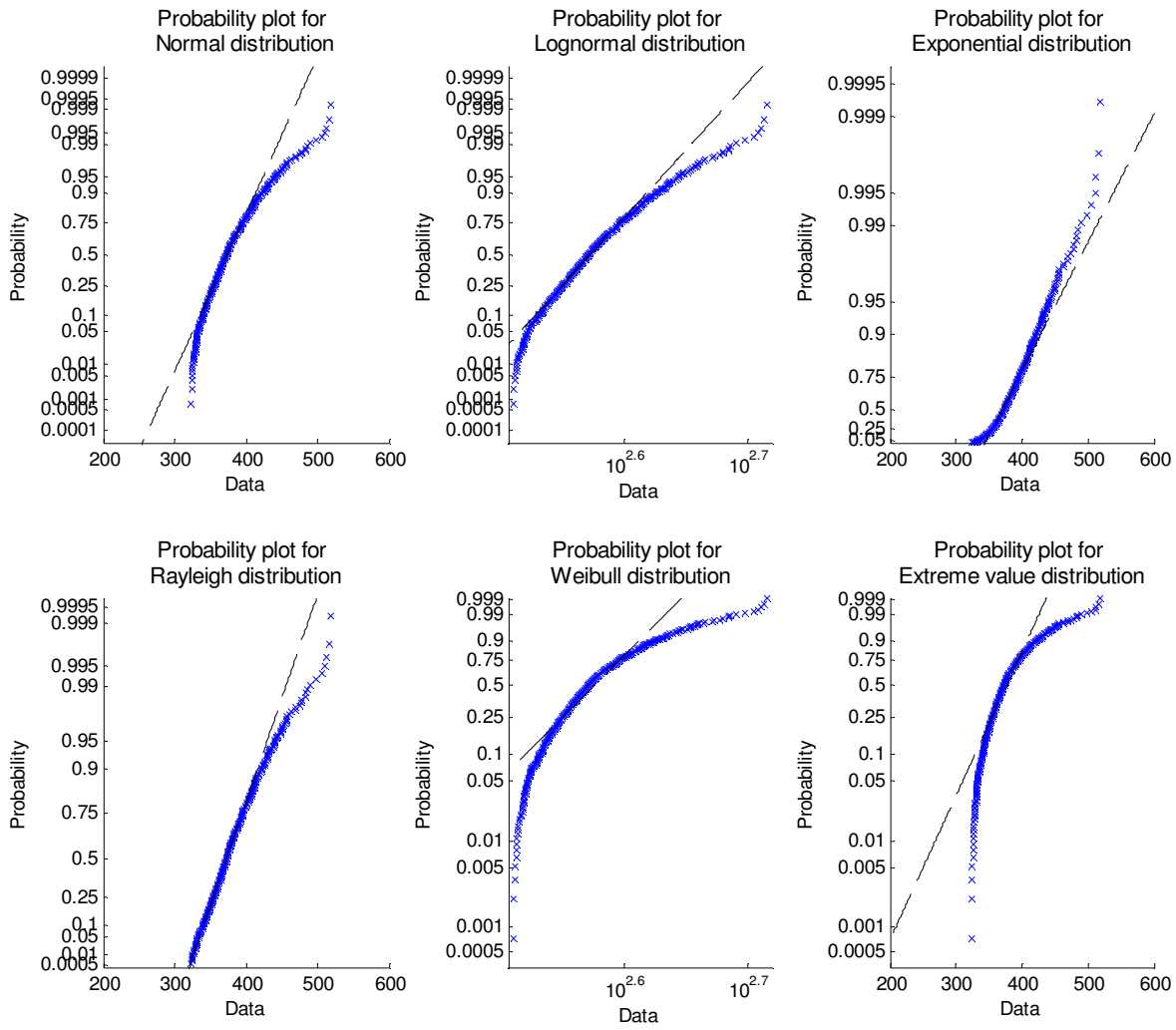

Fig. 4.9 Extreme Value Probability Plot for Case 6 (90 Deg Wind+Wave+Current of Fender Reaction).

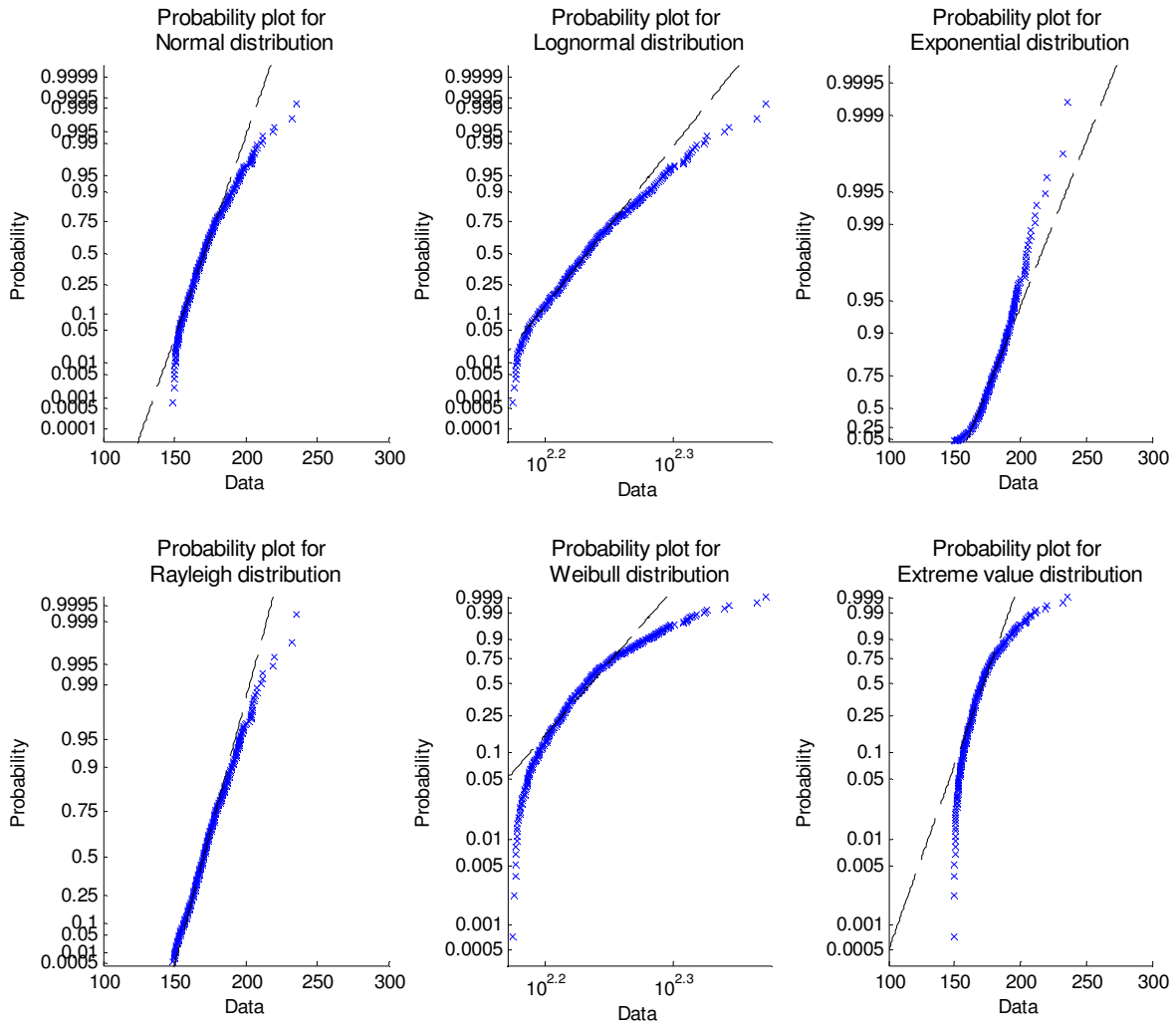

Fig. 4.10 Extreme Value Probability Plot for Case 7 (0 Deg Wind+Wave+Current, Barge Not Moored, Realization 1) of Fen. Rctn.

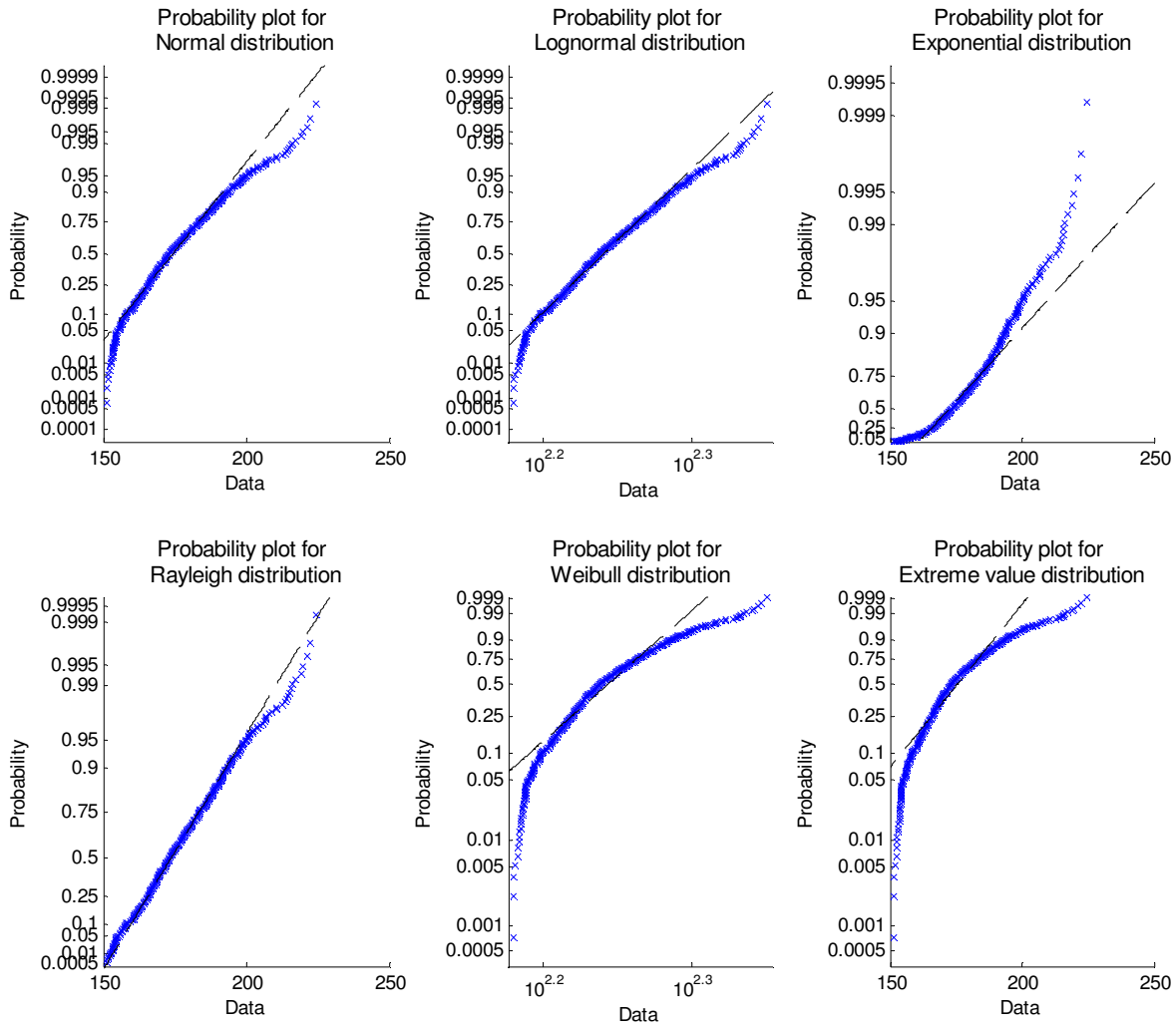

Fig. 4.11 Extreme Value Probability Plot for Case 8 (0 Deg Wind+Wave+Current, Barge Not Moored, Realization 2) of Fen. Rctn.

4.2 Ochi's Most Probable Extreme Values

Previous work by Michel Ochi [12] in random waves on the estimation of extreme wave height and sea state derived the probable extreme value for a non-narrow band random process. This was based on the assumption that the wave height (amplitude) obeyed a Rayleigh distribution probability law. Hence, if the probability density function of the extreme value for a given number of cycles is plotted, the modal value, which coincides with the peak, is called the *most probable extreme value* or *characteristic value*. This was expressed by Ochi [12] as,

$$\overline{y}_n = \sqrt{2\ln\left(\frac{2\sqrt{1-\varepsilon^2}}{1+\sqrt{1-\varepsilon^2}}n\right)}\sqrt{m_0} \tag{4.1}$$

where ε is the bandwidth parameter of the spectrum, n is the number of cycles, m_0 is the zeroith spectral moment, $\overline{y}_n$ is the most probable extreme value, T_s is the time record length of a realization of data and $\overline{T}_z$ is the mean zero crossing period. Normalizing the most probable extreme value, $\zeta_n = \overline{y}_n \big/ \sqrt{m_0}$ and converting the number of cycles to time, $n = T_s \big/ \overline{T}_z$, equation 4.1 is transformed to equation 4.2.

$$\zeta_n = \sqrt{2\ln\left(\frac{2\sqrt{1-\varepsilon^2}}{1+\sqrt{1-\varepsilon^2}}.\frac{T_s}{\overline{T}_z}\right)} \tag{4.2}$$

As previously noted, this formulation is applicable to non-narrow banded random processes, where the solution above is for bandwidth less than 0.9 (i.e. $\varepsilon < 0.9$). Given this condition and considering that the order of magnitude of the factor $\left(\frac{2\sqrt{1-\varepsilon^2}}{1+\sqrt{1-\varepsilon^2}}\right)$ is very low, it is mostly negligible. This proves that the probable extreme value is a function of the number of observation n irrespective of the bandwidth parameter ε for a non-narrow banded process.

The *risk parameter* α was introduced by Ochi [12] to equation 4.2 as a modification to account for the probability of the probable extreme value being exceeded especially given a large record length. The risk parameter is always much less than 1

(i.e. $\alpha \ll 1$). Typically values of α ranging between 0.01 and 0.05 are used for practical marine applications. Equation 4.3 shows the probable extreme value for a wide banded random process.

$$\zeta_n = \sqrt{2\ln\left(\frac{2\sqrt{1-\varepsilon^2}}{1+\sqrt{1-\varepsilon^2}}.\frac{T_s}{\alpha \bar{T}_z}\right)} \tag{4.3}$$

The various parameters used for computing probable extreme value for normalized fender reaction for risk parameters $\alpha = 1$ and $\alpha = 0.01$ for all load cases and headings are presented in Table 4.2. The value of $\alpha = 1$ corresponds to the original form first presented by Davenport [13].

Figures 4.12-4.18 shows plots of probability of exceedence curves for all load cases indicating the probable extreme values that were tabulated in Table 4.2 for the same risk parameters. The risk parameter $\alpha = 0.01$ was chosen as a more stringent exceedence probability criterion and in most ocean application cases it could be replaced by $\alpha = 0.05$ exceedence probability criteria [12]. The probability of exceedence is plotted on a vertical logarithm axis against the standardized normal variate of the extreme value data on a normal scale horizontal axis. From the exceedence curves, it is observed that in several cases the experimental data is not of sufficient length. More specifically, there are not enough data points in these plots to closely predict the theoretical most probable extreme values for risk parameter $\alpha = 0.01$.

Table 4.2 Parameters for Computing the Probable Extreme Value.

Load Case and Heading	ε	$\sqrt{1-\varepsilon^2}$	$\sqrt{m_0}$	$T_s\,(hr)$	T_Z (sec)	$\alpha = 1$	$\alpha = 0.01$
						ζ_n	ζ_n
0 Deg Current Only	0.85	0.53	2.08	3	44.37	3.204	4.413
0 Deg Wave Only	0.51	0.86	1.98	3	17.22	3.567	4.684
0 Deg Wind Only	0.72	0.69	1.52	3	26.54	3.408	4.563
0 Deg Wind + Wave + Current	0.71	0.70	3.39	3	25.10	3.426	4.577
90 Deg Wave Only	0.37	0.93	16.28	3	15.01	3.617	4.721
90 Deg Wind + Wave + Current	0.41	0.91	33.61	3	15.28	3.609	4.716
0 Deg Wind + Wave +Current (Barge not moored, Realization 2)	0.47	0.88	21.35	3	15.58	3.599	4.708

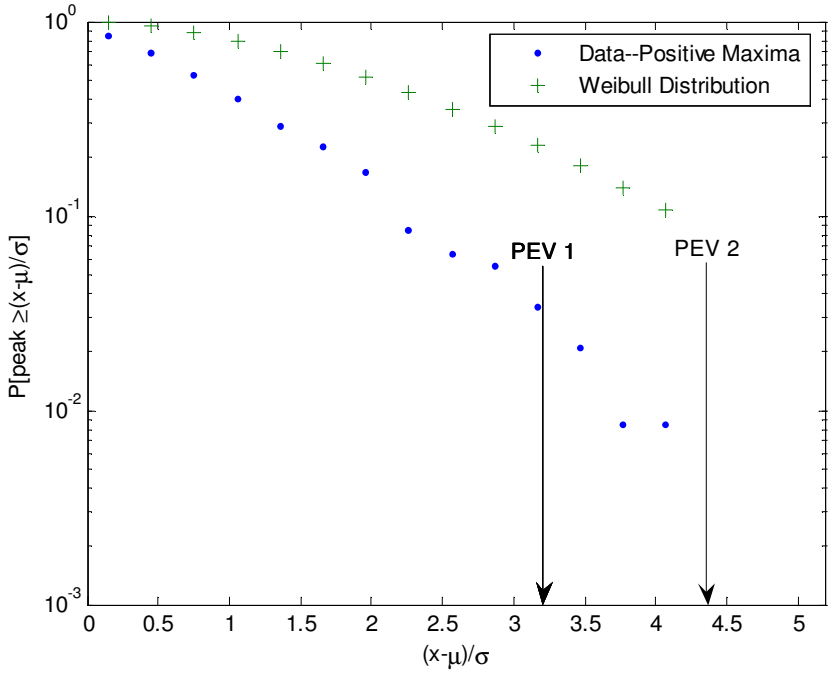

Fig 4.12 Probability of Exceedence of Extreme Value for Case 1, Showing Theoretical Most Probable Extreme Values PEV 1 and PEV 2 for $\alpha = 1$ and $\alpha = 0.01$

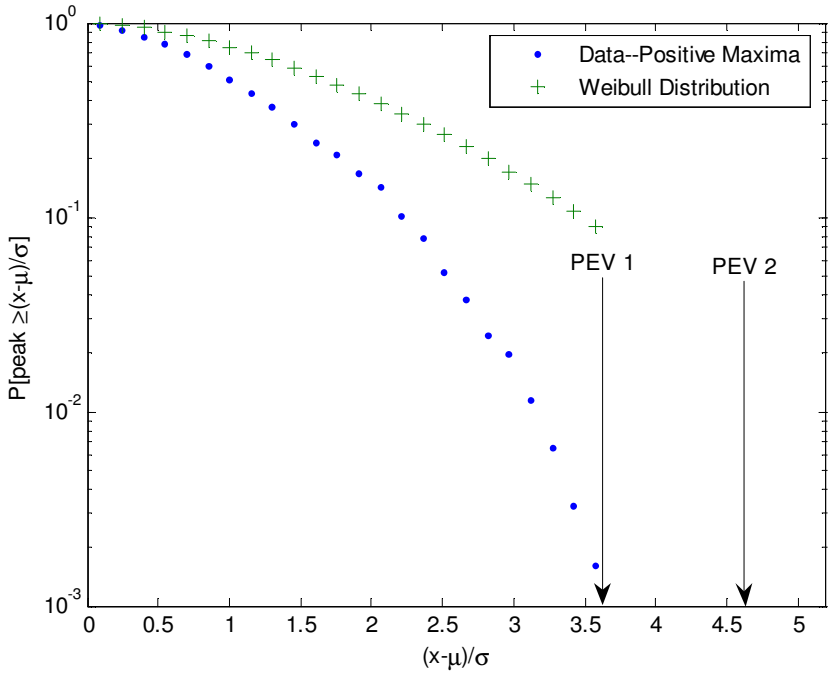

Fig 4.13 Probability of Exceedence of Extreme Value for Case 2, Showing Theoretical Most Probable Extreme Values PEV 1 and PEV 2 for $\alpha = 1$ and $\alpha = 0.01$

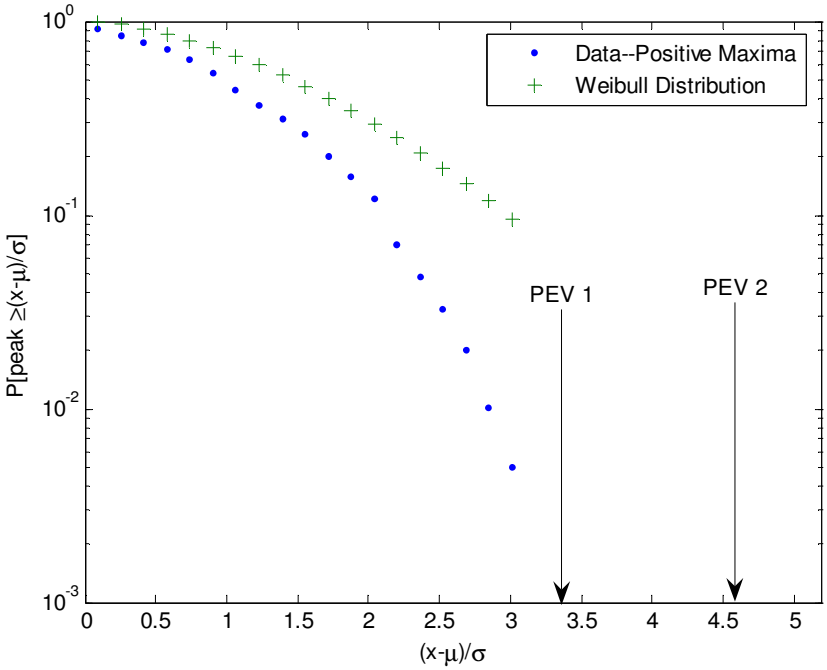

Fig 4.14 Probability of Exceedence of Extreme Value for Case 3, Showing Theoretical Most Probable Extreme Values PEV 1 and PEV 2 for $\alpha = 1$ and $\alpha = 0.01$

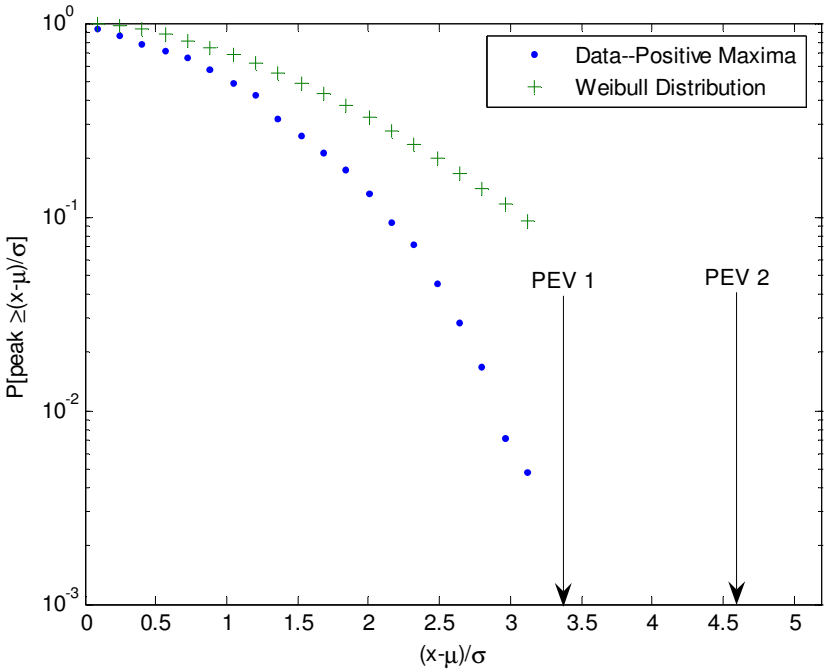

Fig 4.15 Probability of Exceedence of Extreme Value for Case 4, Showing Theoretical Most Probable Extreme Values PEV 1 and PEV 2 for $\alpha = 1$ and $\alpha = 0.01$

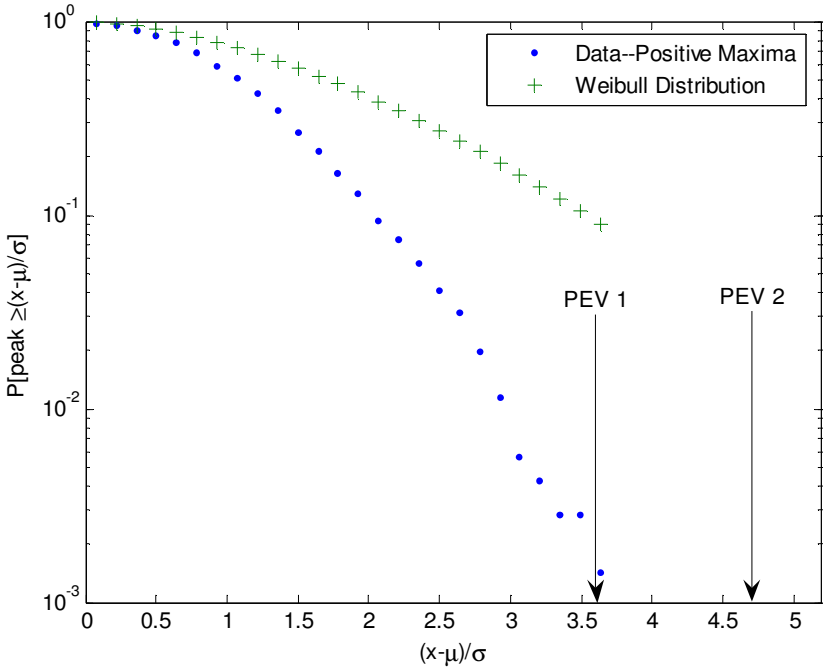

Fig 4.16 Probability of Exceedence of Extreme Value for Case 5, Showing Theoretical Most Probable Extreme Values PEV 1 and PEV 2 for $\alpha = 1$ and $\alpha = 0.01$

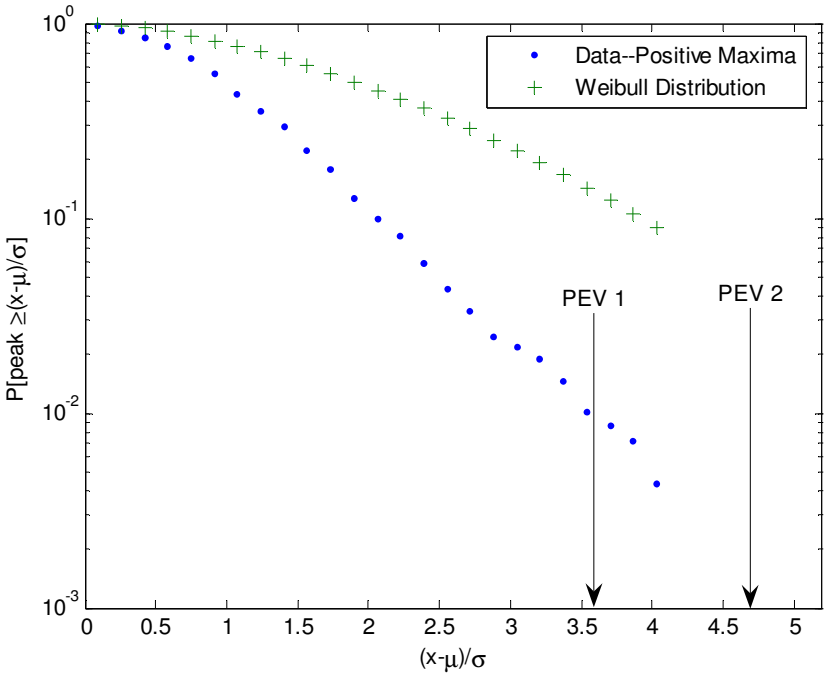

Fig 4.17 Probability of Exceedence of Extreme Value for Case 6, Showing Theoretical Most Probable Extreme Values PEV 1 and PEV 2 for $\alpha = 1$ and $\alpha = 0.01$

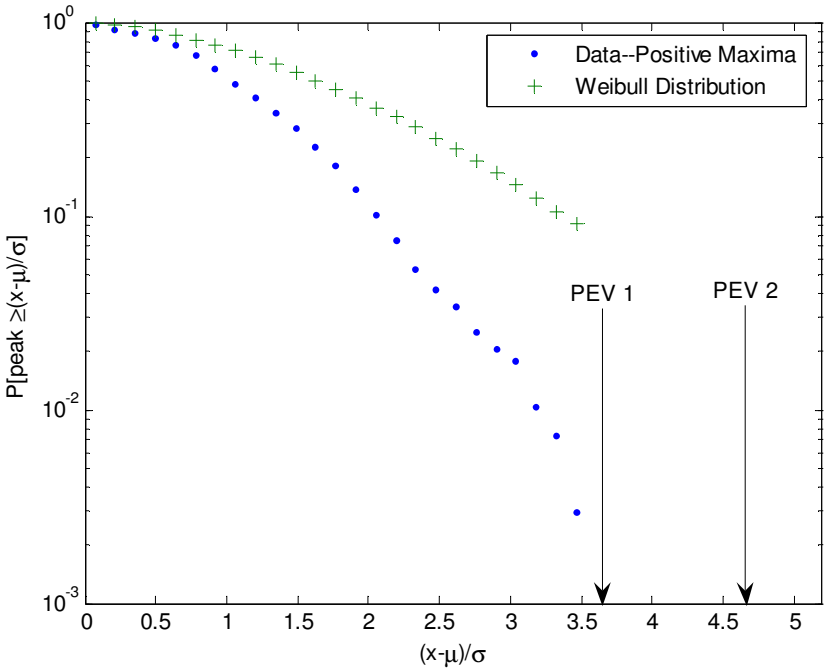

Fig 4.18 Probability of Exceedence of Extreme Value for Case 7, Showing Theoretical Most Probable Extreme Values PEV 1 and PEV 2 for $\alpha = 1$ and $\alpha = 0.01$

4.3 Comparison of Spectral Bandwidth

Another investigation undertaken in the course of this research was to compare the energy content in the environmental forcing to the energy content in the response of the fender system. This in effect would create a picture of how the energy is 'spread' in the frequency domain between the forcing mechanism and the response mechanism. The bandwidth parameter ε, which is computed from the spectrum, gives approximate information of the energy content of the system being measured where $\varepsilon = 0$ means the process is narrow-banded and $\varepsilon = 1$ means the process is wide-banded. However, Ochi [19] re-stated 'that although the parameter ε does not necessarily represent a measure of the energy spreading of a spectrum, it plays a convenient role in further development of the theory'.

Difficulties were encountered while trying to compute ε numerically from the spectrum by evaluating moments, especially the fourth moment m_4, because of the power associated with the frequency.

Bandwidth

$$\varepsilon = \sqrt{1 - \frac{m_2^2}{m_0 m_4}} \tag{4.4}$$

Spectral moments

$$m_4 = \int_0^\infty f^4 S_{XX}(f)\,df \tag{4.5}$$

$$m_2 = \int_0^\infty f^2 S_{XX}(f)\,df \tag{4.6}$$

Hence the following simplification below was adopted in computing ε;

$$\varepsilon = \sqrt{1 - \frac{m_2^2}{m_0 m_4}} = \sqrt{1 - \left(\frac{m_2}{m_0} . \frac{m_2}{m_4}\right)} = \sqrt{1 - \frac{T_{crest}^2}{\bar{T}_z^2}} \tag{4.7}$$

given, mean crest period = $T_{crest} = \sqrt{\frac{m_2}{m_4}}$ (4.8)

mean zero-crossing period = $\bar{T}_z = \sqrt{\frac{m_2}{m_0}}$ (4.9)

Table 4.3 shows these computed parameters for the comparison of the bandwidth ε between the forcing function and the fender response function. In both headings under

the wave only loading, the excitation and the fender response could be interpreted as been closely narrow banded. However the bandwidth parameter for the fender response is a little higher than for its corresponding excitation in the 90 Deg heading while there is a substantial difference in the 0 Deg heading. The other single load cases in the 0 Deg heading, which comprise the current and wind show a strong wide banded bandwidth behavior between the excitation sequence and the fender response. Interestingly, the bandwidth parameter for the fender response is lower than its corresponding excitation.

The bandwidth parameter for the combination load cases in the 0 Deg and 90 Deg heading may have to be analyzed using a different approach. This is because the excitation have been divided into three loading components resulting in three bandwidth parameter values while the corresponding fender response bandwidth parameter is single. It is easier comparing between two single excitation and response values. Hence an equivalent bandwidth value representing the three values of each component of the load combination could be computed. In general, the fender response for the 90 Deg combination case seems to be fairly narrow banded while components of its corresponding excitation are highly wide banded except the wave load component. The opposite occurs for the 0 Deg combination, because the fender response becomes wide banded.

Table 4.3 Bandwidth Comparison Between the Excitation and Fender Response.

Load Case and Heading		**Forcing**			**Response**		
		$T_{crest}\,(\text{sec})$	$\overline{T}_z\,(\text{sec})$	ε	$T_{crest}\,(\text{sec})$	$\overline{T}_z\,(\text{sec})$	ε
0 Deg Current Only		19.12	59.26	0.95	23.64	44.37	0.85
0 Deg Wave Only		13.90	14.67	0.32	14.81	17.22	0.51
0 Deg Wind Only		16.91	37.61	0.89	18.34	26.54	0.72
0 Deg Wind + Wave + Current	Wind	16.72	35.54	0.88	17.49	25.10	0.71
	Wave	13.99	14.92	0.35			
	Current	13.79	16.94	0.58			
90 Deg Wave Only		13.91	14.76	0.34	13.96	15.01	0.37
90 Deg Wind + Wave + Current	Wind	16.77	33.84	0.87	13.93	15.28	0.41
	Wave	13.93	14.93	0.36			
	Current	13.48	26.48	0.86			

4.4 Development of Two Parameter Model

It has been established in signal processing or data analysis of wave elevation time series record using the zero crossing method that the mean zero-upcrossing period is almost equal to the mean zero-downcrossing period. Analysis of our fender reaction response data confirmed that fact. However in practice, the mean zero-downcrossing is commonly adopted. Table 4.4 shows this comparison.

Table 4.4 Mean Zero-upcrossing and Mean Zero-downcrossing of Fender Reaction Response.

Load Case and Heading	$T_{upcros\sin g}\,(\sec)$	$T_{downcros\sin g}\,(\sec)$
0 Deg Current Only	44.37	44.37
0 Deg Wave Only	17.22	17.22
0 Deg Wind Only	26.54	26.55
0 Deg Wind + Wave + Current	25.09	25.07
90 Deg Wave Only	15.01	15.01
90 Deg Wind + Wave + Current	15.28	15.27

A study of the probability plots of extreme value in figures 4.4 to 4.11 lead to some notable observations. One of which was that the extreme values of the fender response data had a best fit with the Rayleigh distribution, which is a member of the Weibull family of distributions. The 3-parameter Weibull probability density function is given by equation 4.10, and can be transformed into a 2-parameter weibull probability density function by setting the location parameter equal to zero ($\gamma = 0$).

$$f_X(x) = \frac{\beta}{\eta}\left(\frac{x-\gamma}{\eta}\right)^{\beta-1} e^{-\left(\frac{x-\gamma}{\eta}\right)^{\beta}} \tag{4.10}$$

Interestingly, a few reliability engineering applications have modeled their extreme value random variable, mostly obtained from experiments, according to the Weibull distribution [12]. In the same light, we attempt to investigate how close our extreme value random variable adapts to the Weibull distribution by seeking to know how the distribution parameters obtained by the maximum likelihood method and the non-linear

least squares method converge for the 2-parameter weibull curve fit. A very close convergence or collapse of the parameters indicates that our extreme value random variable can be modeled by the 2-parameter weibull distribution using the converged parameters. Find in Table 4.5 a list of the parameters for these methods and figures 4.19-4.25 showing the same information as plots.

The plots show the curve of the extreme value exceedence probability based on the experimental data (EPdata), the curve-fit of the extreme value data using the maximum likelihood method (EPmlm), the non-linear least square curve-fit on the extreme value data (EPnls), and the logarithm of the non-linear least square curve-fit on the extreme value data (EPlog). The latter two fits are used to detect or suggest errors in the data.

The convergence of the parameters was very poor as seen by the comparison between parameters from the different methods, while noting that the parameters from the third method (logarithm of Extreme Value Exceedence Probability) were unrealistically high or showed a lot of errors. Also, the plots show the deviations for all the load cases.

At this point, the 2-parameter weibull fit was modified to a 3-parameter weibull fit by introducing initial vales of the location parameter to understand how it helps achieve convergence. This triggered some instability in the system of curves as result of overlapping.

Table 4.5 Weibull Parameters from Different Methods.

Load Case		Maximum Likelihood Method		Non-linear Least-square Curve fit	
		Scale Factor	Shape Factor	Scale Factor	Shape Factor
0 Deg, Current only		2.51	1.67	1.11	1.10
0 Deg, Wave only		2.12	1.68	1.29	1.55
0 Deg, Wind only		1.81	1.68	1.22	1.46
0 Deg, Wind+Wave+Current		1.87	1.67	1.25	1.48
90 Deg, Wave only		2.13	1.65	1.31	1.86
90 Deg, Wind+Wave+Current		2.38	1.66	1.24	1.62
0 Deg, Barge not Moored, Wind+Wave+Current	Realization 1	2.49	1.66	1.24	1.73
	Realization 2	2.04	1.65	1.29	1.73
90 Deg, Barge not Moored, Wind+Wave+Current	Realization 1	2.38	1.66	1.24	1.62
	Realization 2	3.22	1.66	1.24	1.63
	Realization 3	2.53	1.65	1.28	1.75

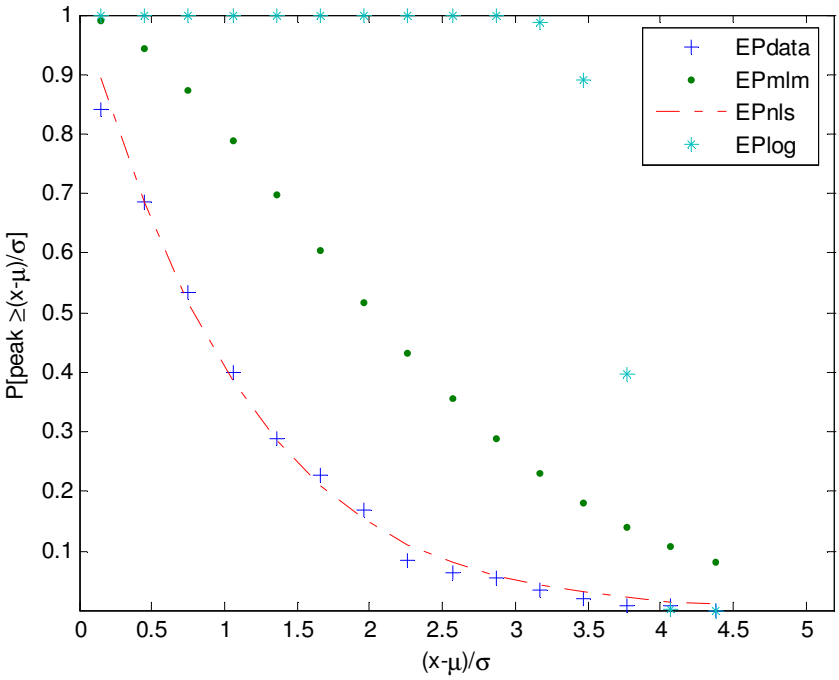

Fig 4.19 Convergence Testing for Weibull Parameters for Case 1.

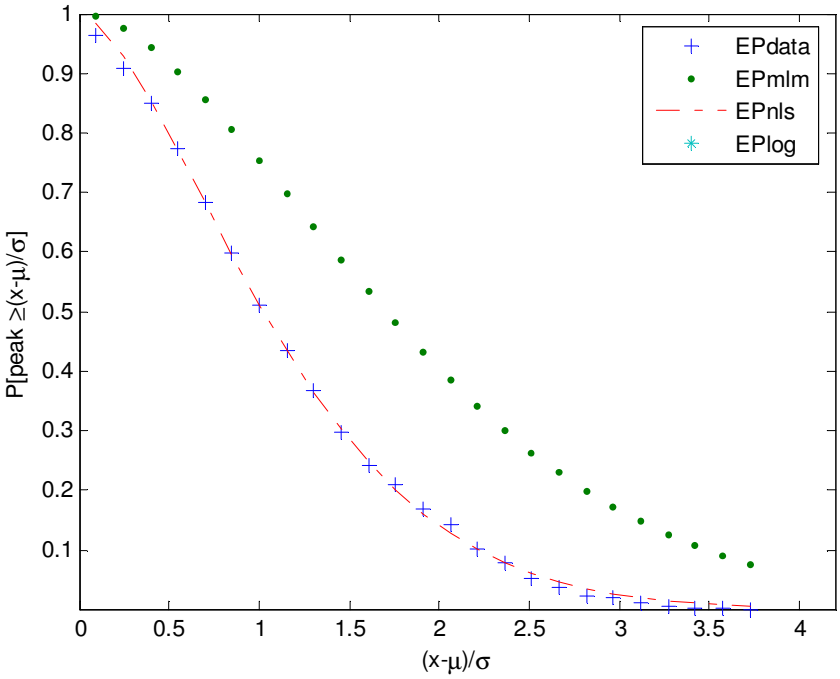

Fig 4.20 Convergence Testing for Weibull Parameters for Case 2.

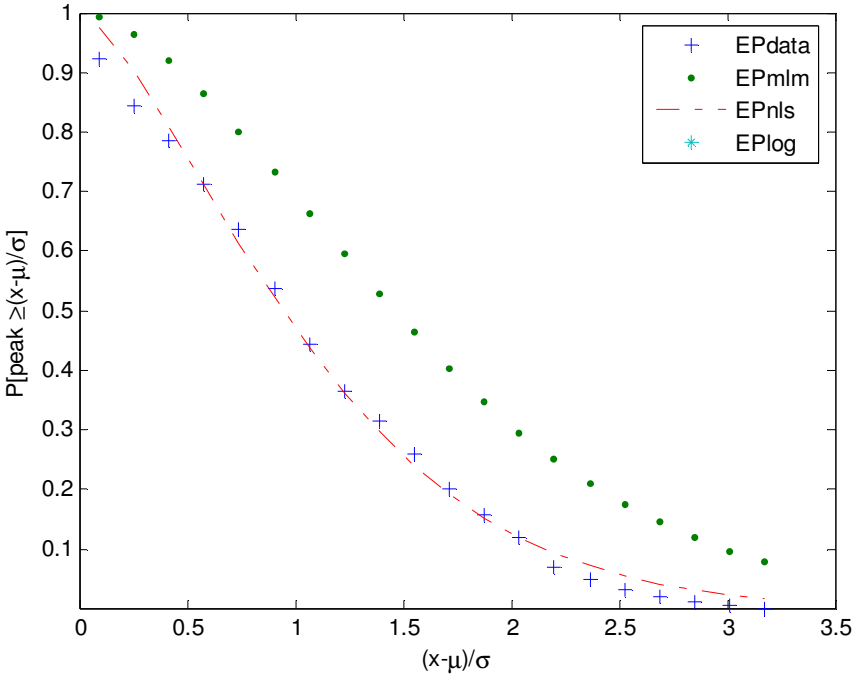

Fig 4.21 Convergence Testing for Weibull Parameters for Case 3.

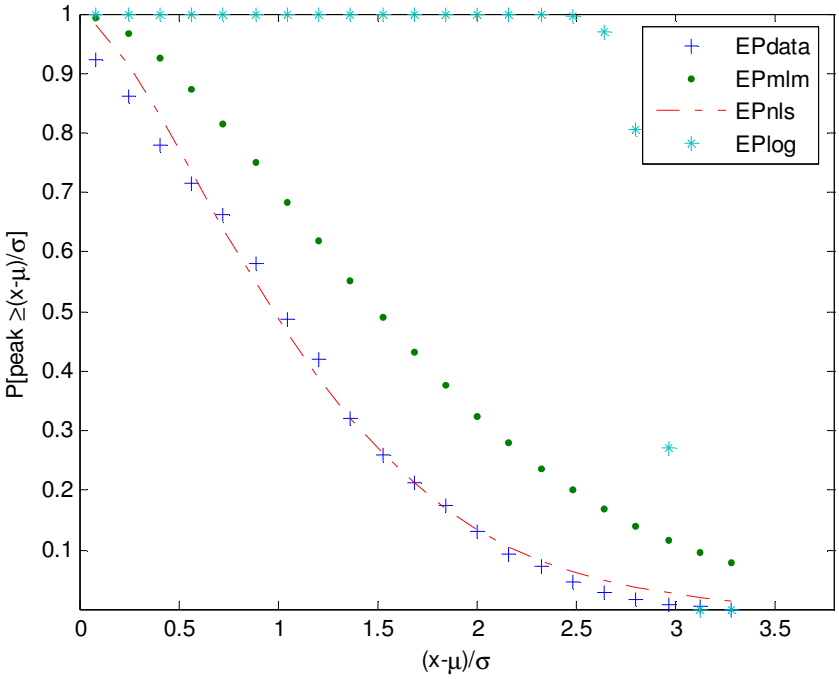

Fig 4.22 Convergence Testing for Weibull Parameters for Case 4.

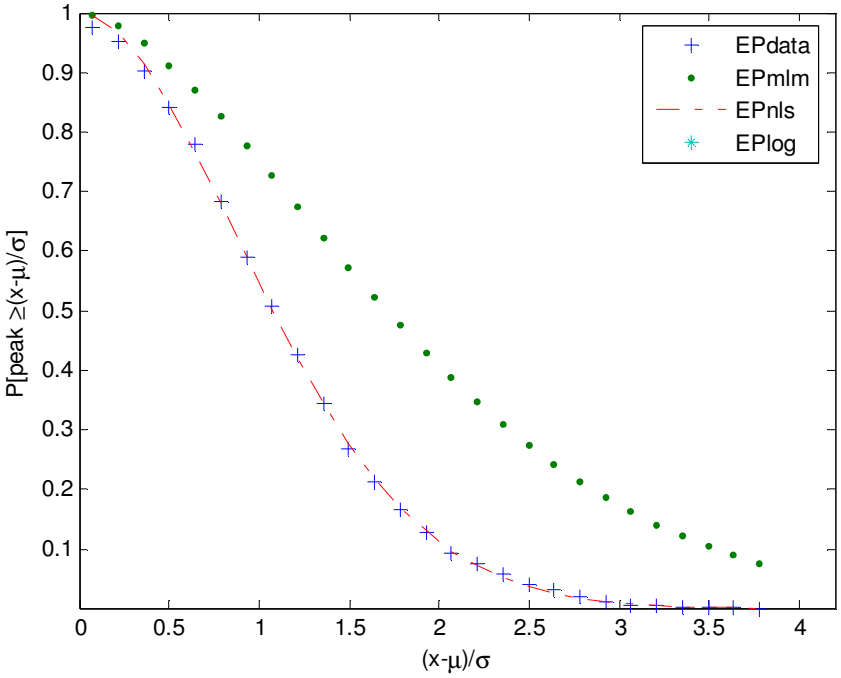

Fig 4.23 Convergence Testing for Weibull Parameters for Case 5.

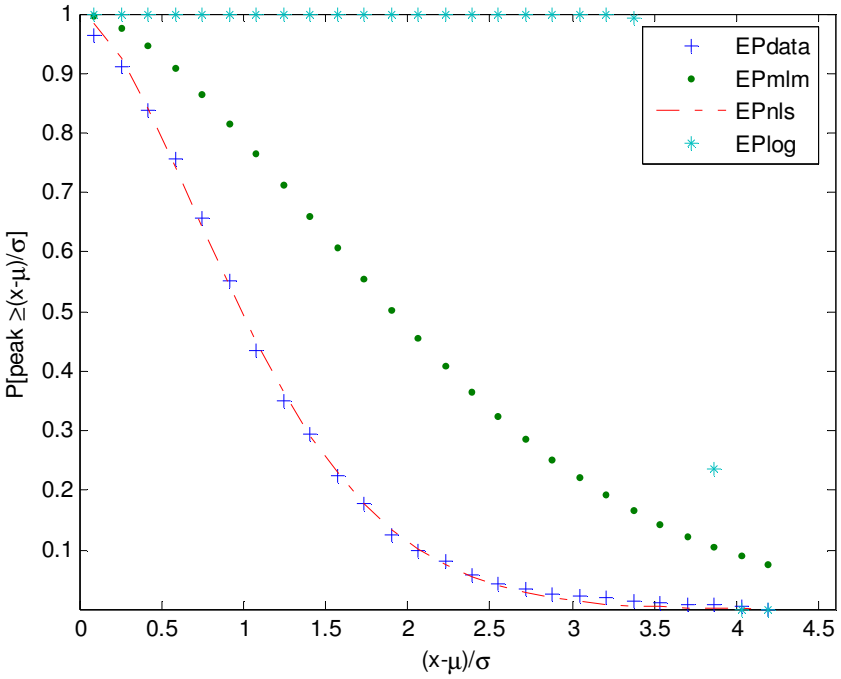

Fig 4.24 Convergence Testing for Weibull Parameters for Case 6.

From various functions investigated using the curve-fitting tool-kit in MATLAB, the Gaussian Polynomial was found to produce fewer coefficients yet maintaining very admirable goodness-of-fit statistics as shown in Equation 4.11, Table 4.6 and Figures 4.25 - 4.29. Also, the coefficients for the chosen function were obtained within 95% confidence bounds.

$$f(x) = A.e^{\left(-\left(\frac{x-B}{C}\right)^2\right)} \tag{4.11}$$

The goodness-of-fit statistics for the survivor function of the fender force are presented in Table 4.5. The estimation of error were obtained using the following standard definitions;

RMSE: - The root mean squared error.

A value closer to 0 indicates a better fit.

SSE: - The sum of squares due to error.

This statistic measures the deviation of the responses from the fitted values of the responses. A value closer to 0 indicates a better fit.

R-square: - The coefficient of multiple determination.

This statistic measures how successful the fit is in explaining the variation of the data. A value closer to 1 indicates a better fit.

Adj R-sq: - The degrees of freedom adjusted R-square.

A value closer to 1 indicates a better fit. It is generally the best indicator of the fit quality when you add additional coefficients to your model.

Based on the Figures 4.25 – 4.31, it is concluded that this two parameter model can be used for the data obtained in the experimental study.

Table 4.6 Coefficients and Goodness-of-fit for Gaussian Polynomial.

Load Case	Coefficients (A,B,C)	RMSE	SSE	R-square	Adj R-sq
0 Deg, Current only	1.474, -1.645, 2.386	0.010498	0.0013225	0.9987	0.99849
0 Deg, Wave only	1.101, -0.5159, 1.749	0.007949	0.0013901	0.99944	0.99939
0 Deg, Wind only	0.9913, -0.3649, 1.624	0.010439	0.0018524	0.999	0.99889
0 Deg, Wind+Wave+Current	0.9624, -0.282, 1.601	0.010562	0.002008	0.99899	0.99888
90 Deg, Wave only	0.9892, -0.05645, 1.382	0.005642	0.0007639	0.99975	0.99973
90 Deg, Wind+Wave+Current	1.06, -0.3479, 1.552	0.011849	0.0032291	0.99874	0.99863
0 Deg, Wind+Wave+Current (Barge not moored, R2)	0.9911, -0.144, 1.454	0.0079299	0.0014463	0.99949	0.99944

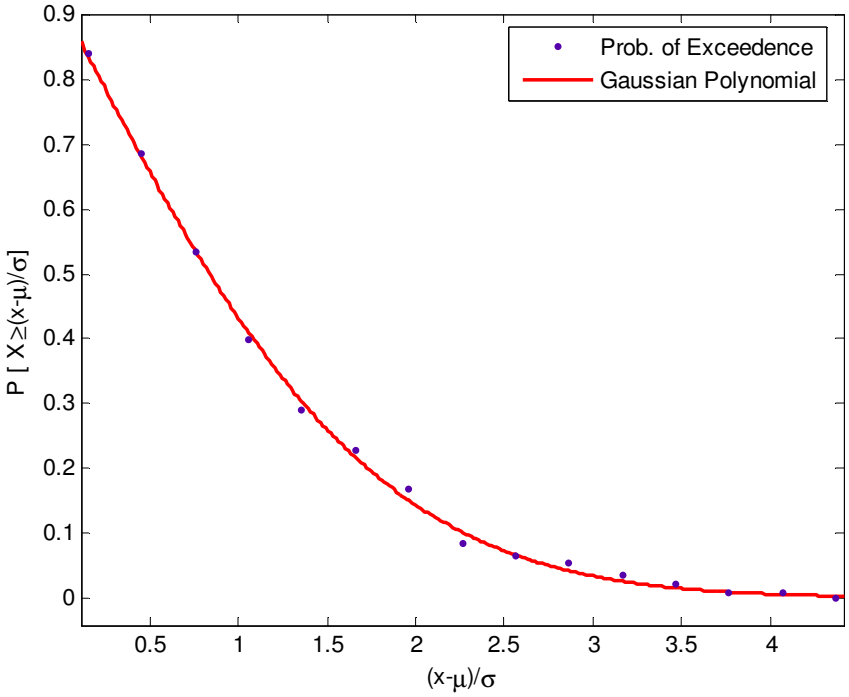

Fig. 4.25 Gaussian Polynomial Curve-fit for Case 1.

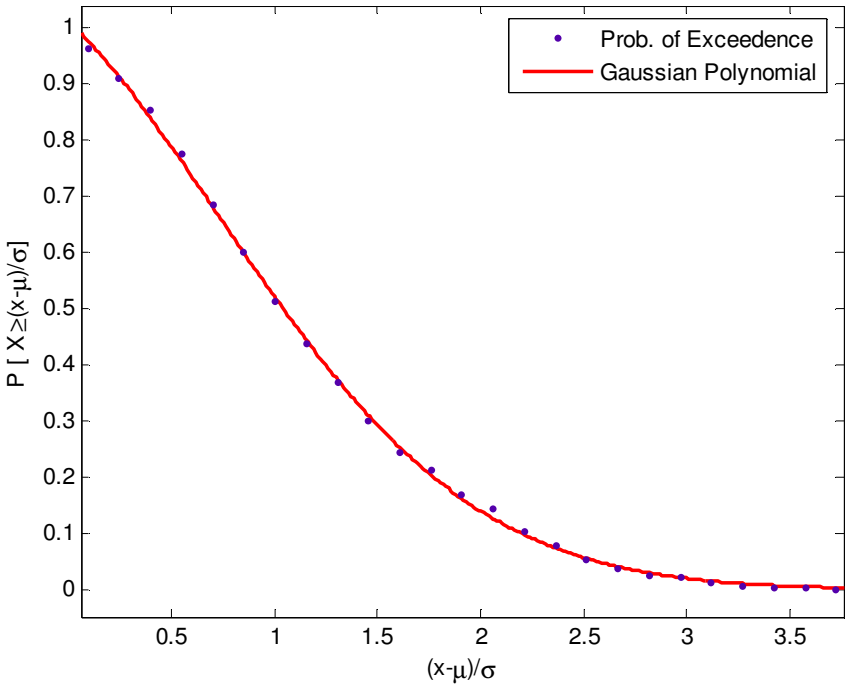

Fig. 4.26 Gaussian Polynomial Curve-fit for Case 2.

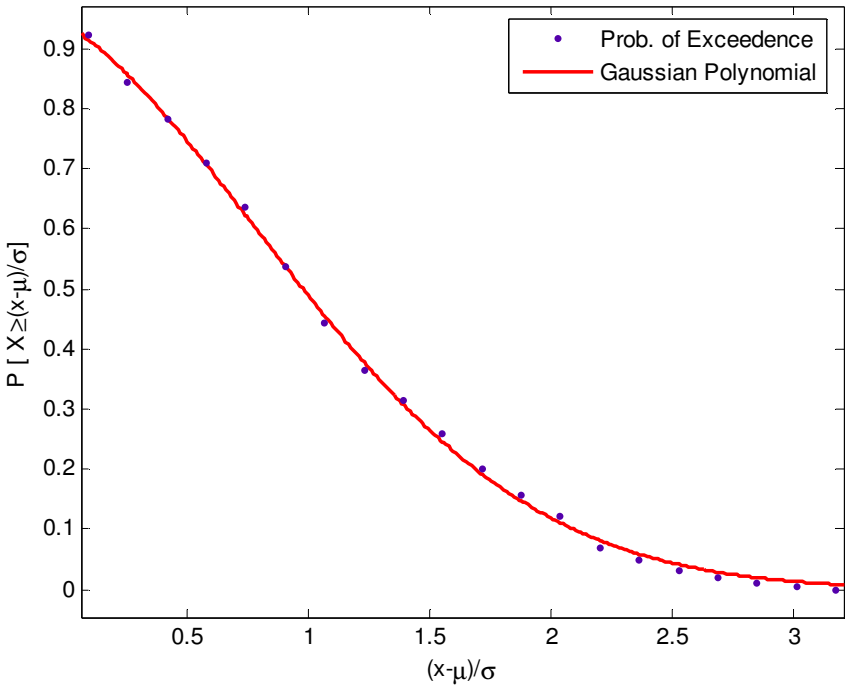

Fig. 4.27 Gaussian Polynomial Curve-fit for Case 3.

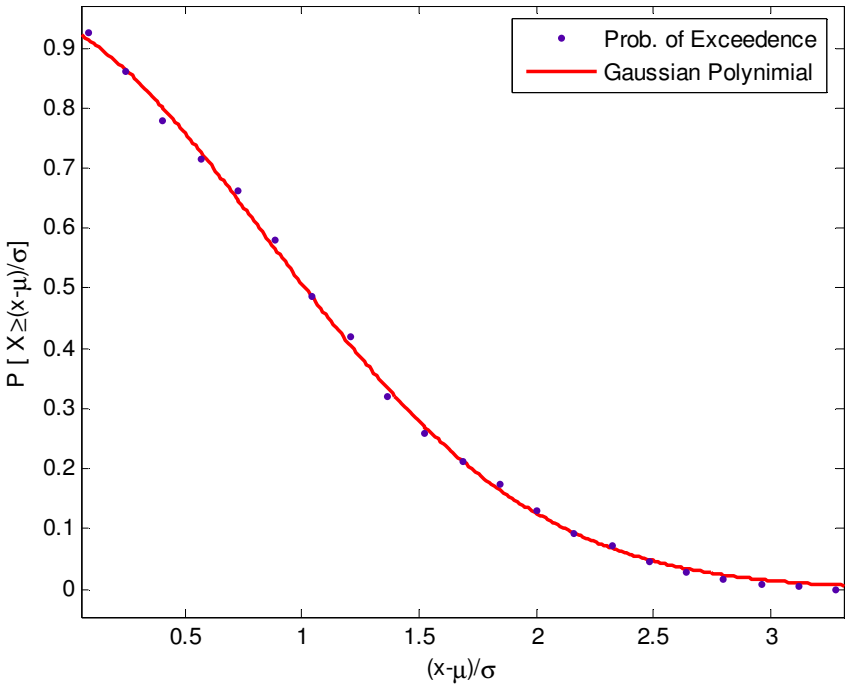

Fig. 4.28 Gaussian Polynomial Curve-fit for Case 4.

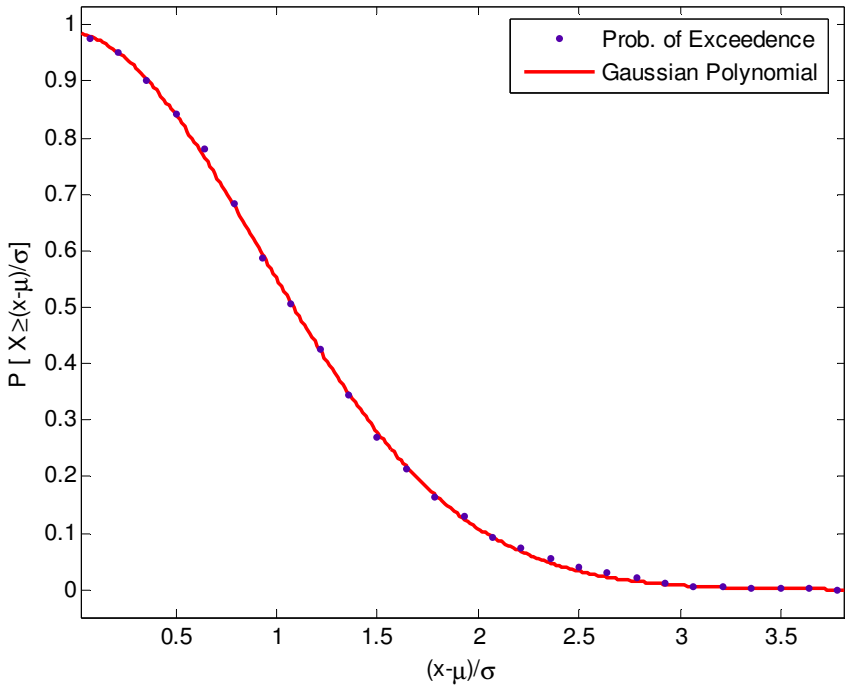

Fig. 4.29 Gaussian Polynomial Curve-fit for Case 5.

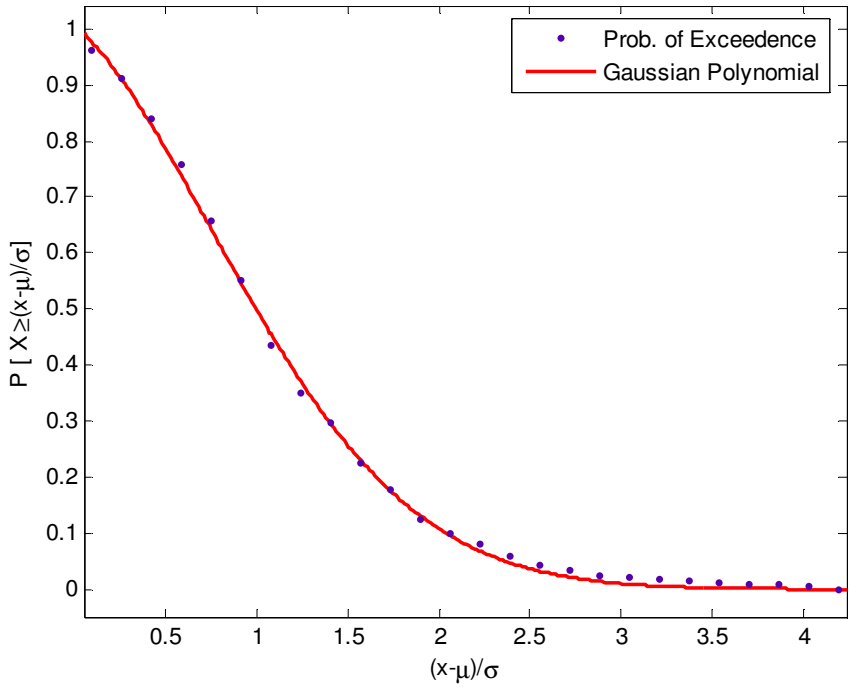

Fig. 4.30 Gaussian Polynomial Curve-fit for Case 6.

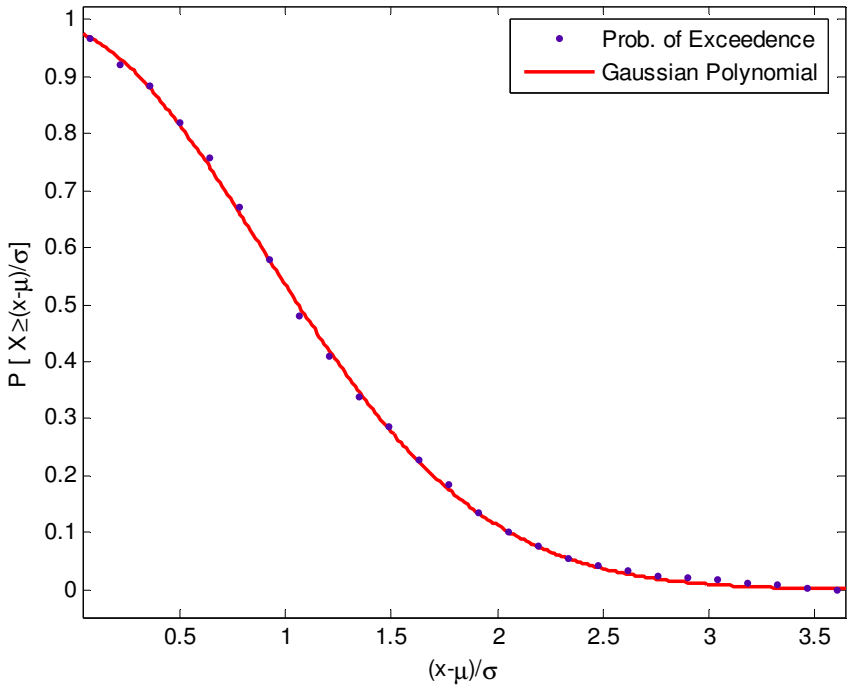

Fig. 4.31 Gaussian Polynomial Curve-fit for Case 7.

4.5 Comparative Example

An example was developed to provide a comparison of the regular wave and random sea approaches for fender system design. In order to calculate berthing energy for the mini-TLP/Tender Barge experiment in the regular wave approach, some assumptions were necessary to simplify the problem. In particular, the motion of the mini-TLP was minimal when compared to the mooring constraints of the tender barge. Further, the fender loading was shared equally by eight elastomeric fender units, see Figure 2.1. The random sea approach is treated considering the two load cases; Wind+Wave+Current in 0 Deg heading and Wind+Wave+Current in -90 Deg heading.

4.5.1 Regular Wave Approach

Displacement of Design Vessel (Tender Barge) = 8533 tonnes

Berthing condition is 'difficult berthing in exposed area'.

Berthing Velocity = 0.465m/s (Fig 4.2.1, PIANC 2002 Report)

Added Mass Coefficient, $C_M = 1 + \frac{2D}{B} = 1 + \frac{2 \times 3.7}{27.5} = 1.269$

Eccentricity Coefficient, $C_E = 1$

Berth Configuration Coefficient, $C_C = 1$

Softness Coefficient, $C_S = 1$

Berthing Energy, $E_f = \frac{1}{2} \times 8533 \times 0.465^2 \times 1.269 \times 1 \times 1 \times 1$

$= 1170.68 KN.m$

Energy absorbed for each fender unit for a system of 8 fender units attached to two legs of the mini-TLP = $\frac{1170.68}{8} = 146.335 KN.m$

Using 1.83m (6ft) DIA fender performance chart in figure 4.32, the percentage fender deflection and reaction force can be obtained below. For the fender size (6x12) selected, the following are read off from the chart;

Percentage fender deflection = 38%

Fender reaction = 480KN

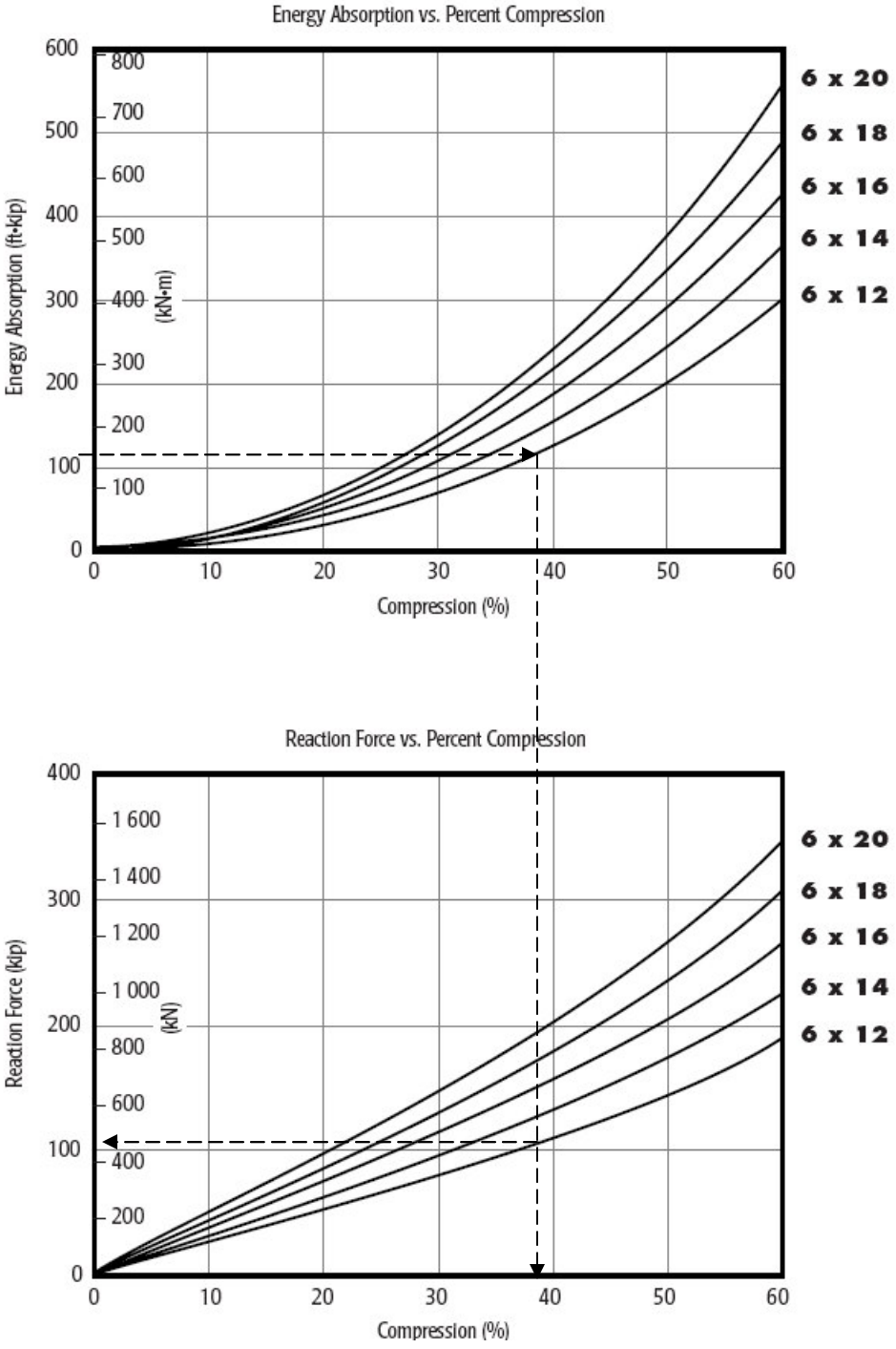

Fig. 4.32 Performance Curves for 6ft Dia Fender.

4.5.2 Random Sea Approach

Wind+Wave+Current, at -90 Deg Heading

From the Exceedence Probability curve, a probability of exceedence value is chosen. Let probability of exceedence, $P\left[X \geq \left(\frac{x-\mu}{\sigma}\right)\right] = 0.01$

Using the above load case, the extreme fender reaction standard normal value is obtained from either the Gaussian Polynomial curve or the expression below,

$$f(x) = 1.06 \times e^{\left(-\left(\frac{x-(-0.3479)}{1.552}\right)^2\right)} = 0.01$$

$$x = 3.00364$$

Where $\mu = 161.6$ and $\sigma = 24.44$ for the considered load case, the extreme fender reaction is

$$X = (3.00364 \times 24.44) + 161.6 = 235KN$$

Using 1.524m (5x12) DIA fender performance chart in figure 4.33, the percentage fender deflection and absorbed energy can be obtained from figure 4.33.

Percentage fender deflection = 24%

Fender absorbed energy = 60KN.m

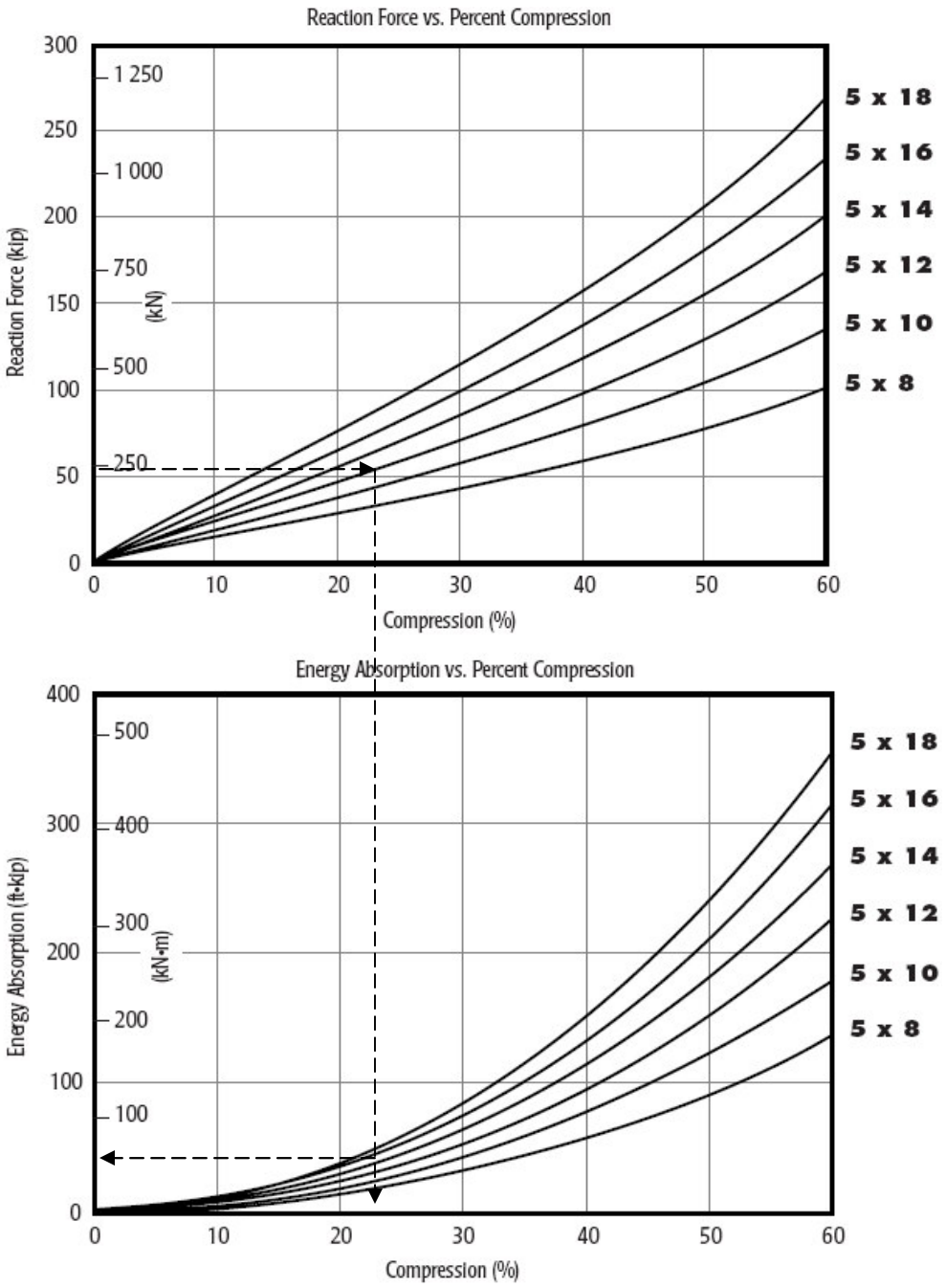

Fig. 4.33 Performance Curves for 5ft Dia Fender.

Wind+Wave+Current, at 0 Deg Heading

The computation for the above load case using the same probability of exceedence value equal to 0.01 is performed. This means the chances of exceeding an extreme fender reaction is set at 1 out of a 100. The extreme fender reaction standard normal value is obtained from either the Gaussian Polynomial curve or the expression below,

$$f(x) = 0.9624 \times e^{\left(-\left(\frac{x-(-0.282)}{1.601}\right)^2\right)} = 0.01$$
$$x = 3.1394$$

Where $\mu = 142.48$ and $\sigma = 4.73$ for the considered load case, the extreme fender reaction is

$$X = (3.1394 \times 4.73) + 142.48 = 157.33KN$$

Using 1.524m (5x12) DIA fender performance chart, the percentage fender deflection and absorbed energy can be obtained from charts as;

Percentage fender deflection =18%

Fender absorbed energy = 31KN.m

The above example clearly shows that the design fender reaction obtained from the random sea approach is less conservative and probability-based compared to the design fender reaction obtained from the regular wave approach. The conservative result obtained from the regular wave approach could be attributed to too many approximations in the Kinetic energy method, especially in the determination of the approach velocity. Although the data used for the random sea approach is based on model tests, it can be stated that the experiments were carried out under controlled conditions were most of the hydrodynamic parameters involved in the process can be determined. Also, it is important to note the order of estimation of variables in the two approaches. In the regular wave approach, the berthing energy is first obtained. From this, the deflection and the fender reaction are estimated. On the other hand, in the random sea approach, the design fender reaction is computed first by setting a desired exceedence probability and using the Gaussian Polynomial function with the supplied coefficients for each load combination

and heading. From this, the fender deflection and absorbed energy are estimated from fender performance curves.

Since, the random seas approach was based on model test results, we could also investigate the variability in the data for the two combined load cases. The combined load cases are a more realistic load condition because wave, wind and current never occur in an uncoupled state in reality, though studying them in an uncoupled state gives a better understanding of their behavior stand-alone. Table 4.7 shows the variability between the two combined load cases for fender reaction, which is measured, and fender deflection and energy absorbed, which are estimated numerically.

Table 4.7 Comparison of Data Characteristics for Combined Loading.

	Wind+Wave+Current, 0 Deg		Wind+Wave+Current, -90 Deg	
	Mean	Max	Mean	Max
F(t), KN	142.48	159.44	161.6	339.95
Δ(t), %	3.2	3.61	3.68	8.58
E(t), KN.m	24.19	26.59	27.14	67.18

5. SUMMARY AND CONCLUSION

An approach to incorporate empirical data and extend their interpretation to fender systems in random seas was achieved in two phases. The first was to understand fender system performance in a deterministic sense by studying the fender compression load test data produced by manufacturers for use in the industry. During this process, a review of current design practice and the vital considerations in the design process lead to the development of a flowchart to capture the critical steps in the design process. The use of dimensional analysis suggested that a more efficient and compact method of presenting the fender performance test data could be utilized in order to make fender sizing and selection an easier task for the design engineer. Secondly, the effect of loadings by virtue of the systems operating in a random sea environment was studied.

In the deterministic approach, a dimensional analysis approach was used to develop dimensionless groups. These groups comprised governing variables, which were carefully selected to represent the physics of the hydrodynamic coupling problem. The dimensionless groups are normalized functions of the absorbed energy, fender reaction force and fender deflection. For the fender system investigation in this study, the supplied manufacturer's fender performance test data is typically provided as a family of curves of fender reaction versus percentage deformation and absorbed energy versus percentage deformation for different diameters of elastomeric fenders. Data in these curves were extracted and the dimensionless groups were used to recast the data. It was presented in this form for several reasons. First, it provided a means to access the comparative accuracy of the data and secondly the nature of the non-linear material behaviour as a function of size could be seen.

Verification of the accuracy of the results from these recasted curves was performed by manually back-solving to see if initial values were obtainable. This test showed significant error, which suggested variations between data sets of ±15% error range used for the fender performance testing program. Also, there is a possibility that our initial list of variables for the dimensionless groups was not exhaustive to include variables affecting the fender material property. The phenomenon called 'hysteresis', which occurs in rubber materials subject to successive loading and unloading could also

have introduced some non-linearities in the fender rubber material that our approach did not capture.

Constraining our analysis to the linear regions of the absorbed energy-percentage deflection curve and reaction force-percentage deflection curve, a test of linearity was performed by plotting ratios absorbed energy against ratios of reaction force for similar deflection values. These showed significant linear behavior up to the prescribed limit of deflection equal to 60% of the fender diameter.

From the analysis of our model test data, we are able develop a tool-kit for transforming our measured response fender reaction time series to both absorbed energy time series and deflection time series. Although this tool-kit was adapted to the performance curves of a 10ft (3.04m) Diameter elastomeric fender, the size of the fender can be changed as long as its performance curves are changed to suit the new fender size. Characterization of the measured random variable (fender reaction) and simulated random variable (absorbed energy and percentage deflection) using stochastic tools in MATLAB showed Gaussian (linear) behaviour across the three variables for most of the load cases. This confirms that the fender behaves like a linear transfer function, which produces linear (Gaussian) response when subjected to a Gaussian load excitation. However, a few exceptions to this trend were the fender reaction response to current only loading in 0 Deg direction, wave only in 90 Deg direction and Wind+Wave+Current in 90 Deg direction. This is because, when these loads are uncoupled or act independently, the current loading does not seem to be Gaussian, hence the response of the fender system was non-Gaussian. But when the loads are coupled, especially in the 0 Deg, their behaviour is closer to Gaussian. An investigation into the effect of heading shows the responses in the 90 Deg heading to be generally higher than the 0 Deg heading due to the larger contact area of the tender barge perpendicular to the environmental loading. Also responses in the 90 Deg showed large deviations of the upper tail from the normal probability line indicating non-Gaussian behavior.

Since, extreme values govern designs, another tool-kit written with MATLAB codes was developed for obtaining the maximum values of the multiple peaks in each half-cycle of the fender response reaction data. This was after the data was filtered to remove high frequency noise. Using this tool-kit, the mean zero-crossing period and

mean crest period computed from the time series were used as input variables for calculating the most probable extreme value (theoretical) for risk parameters $\alpha = 0.01$ and $\alpha = 1$. The values of the most probable extreme value for the survival function $\alpha = 0.01$, shown in the exeedence curves, is greater than extreme values from our data or falls far from the range of our model test data.

Statistical characterization of the extreme values carried out to understand the underlying probability distributions governing their behavior showed at least two types of distributions closely describing it for some load cases. Hence, the 2-parameter weibull distribution and 3-parameter weibull distribution were tested on the extreme value data to determine a best fit distribution. This was achieved using the maximum likelihood method and a non-linear least-square fit to constrain the extreme value data to a weibull 2-parameter distribution and obtain its parameters. However, the parameters obtained using the two methods did not converge or yield the same value. A parametric Gaussian polynomial function was able to fit the extreme value while exhibiting minimal residual error as seen in the goodness-of-fit statistics for each curve. Its parameters will be useful to designers of fender systems subject to random loading against extreme impacts.

The modulation of the bandwidth of the loadings to the bandwidth of the fender response indicates that the energy in the system is either been stretched over a wide range of frequencies or concentrated over a smaller range of frequencies. This however does not give any indication of the order of magnitude of these energies. Load cases 1, 2, 3 & 5 show that the narrow-bandedness of the energy is conserved after modulation. The combination load case 4 reflects a mixture of narrow-banded and wide-banded signals for the forcing function, which transformed the response function to a wide-banded signal. The reverse is the case for combination load case 6, where the transformed signal of the response function is narrow-banded.

An example was presented that compared the regular wave approach with the random sea approach for fender system design. The results show that the random sea approach apart from been less conservative gives room for the designer to choose a desired probability of exceedence for the fender reaction. The higher values obtained in the regular wave approach could be as a result of too many approximations in the kinetic energy method, especially in the determination of the approach velocity. Also, a

comparison of the results obtained from the random sea approach with the model test data for the two combined load cases in 0 Deg heading and -90 Deg heading showed that it was within acceptable limits for specific exceedence probabilities.

REFERENCES

[1] PIANC, 2002, "Guidelines for the Design of Fender Systems", Report of Working Group 33 of the Maritime Navigation Commission, Brussels.

[2] Bruun P., 1989, *Port Engineering: Harbor Planning, Breakwaters and Marine Terminals Vol 1*, Gulf Publishing Co., Houston Texas, Chap. 4.

[3] Kirk M. D., 2007, "Floating Rubber Fenders for All-Tide Moorage of Vessels", Proc. 30th International Ports Conference, San Diego California.

[4] Louis K. A., 2007, "Flexible Steel Dolphins, System-Wide Performance Study", Proc. 30th International Ports Conference, San Diego California.

[5] Bradshaw A.S., Baxter C.D.P., Tsiatas G., Marinucci A., Ressler J., Morgan R., 2006, "Simple Dynamic Model for Fender Pile Analysis and Design", Journal of Waterway, Port, Coastal, and Ocean Engineering, 132, (5), pp 419-422.

[6] Fentek Marine Systems, 2001, "Catalogue of Fentek Marine Fendering Systems", Hamburg.

[7] Harish Girija S.P., 2005, "Analysis of Coupled Body Mooring and Fendering System", MSc Thesis, Texas A&M University, College Station Texas.

[8] Gaythwaite J. W., 2004, *Design of Marine Facilities for the Berthing Mooring and Repair of Vessel,* ASCE Press, Virginia, pp 133 – 174.

[9] BS 6349 Part 4, 1994, "Code of Practice for Design of Fendering and Mooring Systems", BSI, London.

[10] Munson B.R, Young D.F., Okiishi T.H., 2006, *Fundamental of Fluid Mechanics*, Wiley and Sons.

[11] Chen X., Niedzwecki J.M., Tiegen P., 2006, "Coupled Mini-TLP Barge Response in Random Seas", Proc. 16th International Society of Offshore and Polar Engineers Conference, San Francisco California.

[12] Ochi M.K., 1998, *Ocean Waves: The Stochastic Approach*, Cambridge University Press, Cambridge, Ch. 3 & 6.

[13] Davenport A.G., 1961, "The Application Of Statistical Concepts To The Wind Loading Of Structures", Conference Proc. of Institution of Civil Engineers, University of Bristol, Vol. 19, pp. 449-471.

VITA

Name:	James Ofoegbu
Address:	CE/TTI 201R , MS 3136 Zachry Civil Engineering Department Texas A&M University College Station, TX 77843
Email Address:	james_ofoegbu@tamu.edu

Education:	B.Eng., Civil Engineering, Federal University of Technology Owerri, 2004. M.S., Ocean Engineering, Texas A&M University, 2008.
Experience:	Texas A&M University, College Station, Texas (August 2006 – May 2008), Graduate Research Assistant to Dr. J.M. Niedzwecki. Emms Consulting Engineers, Lagos (June 2006 – August 2006), Structural Engineer. Cakasa Nig. Ltd., Lagos (April 2005 – May 2006), Junior Structural Engineer. Intercon Partnership, Ibadan (September 2004 – April 2005), Graduate Engineer. Dina Emms Partnership, Lagos (July 2002- April 2003), Intern.